KAUNAS UNIVERSITY OF TECHNOLOGY

EIGIRDAS SKUODIS

SYNTHESIS AND PROPERTIES OF BIPOLAR EMITTERS CONTAINING CYANO GROUPS

Doctoral Dissertation
Technological Sciences, Engineering of Materials (T 008)

2019, Kaunas

This doctoral dissertation was prepared at Kaunas University of Technology, Faculty of Chemical Technology, Department of Polymers Chemistry and Technology, during the period of 2014–2018.

Supervisor:

Dr. Aušra TOMKEVIČIENĖ (Kaunas University of Technology, Technological Sciences, Materials Engineering T 008)

Editor: Brigita Brasienė (Publishing house “Technologija”)

ISBN 978-609-02-1602-6

The bibliographical information of this issue is available at Martynas Mazvydas National Library of Lithuania National Bibliographic Database (NBD)

KAUNO TECHNOLOGIJOS UNIVERSITETAS

EIGIRDAS SKUODIS

CIANOGRUPES TURINČIŲ BIPOLINIŲ SPINDUOLIŲ SINTEZĖ IR SAVYBĖS

Daktaro disertacija
Technologijos mokslai, medžiagų inžinerija (T 008)

2019, Kaunas

Disertacija rengta 2014–2018 metais Kauno technologijos universiteto Cheminės technologijos fakulteto Polimerų chemijos ir technologijos katedroje.

Mokslinė vadovė:

Dr. Aušra TOMKEVIČIENĖ (Kauno technologijos universitetas, technologijos mokslai, medžiagų inžinerija, T 008)

Interneto svetainės, kurioje skelbiama disertacija, adresas:
http://ktu.edu

Redagavo:

Brigita Brasienė (leidykla „Technologija“)

ISBN 978-609-02-1602-6

Leidinio bibliografinė informacija pateikiama Lietuvos nacionalinės Martyno Mažvydo bibliotekos Nacionalinės bibliografijos duomenų banke (NBDB)

CONTENTS

LIST OF ABBREVIATIONS

3TPYMB – Tris-[3-(3-pyridyl)mesityl]borane;
AIEE – Aggregation-induced enhanced emission;
Al – Aliphatic;
Ar – Aromatic;
BmPyPb – 1,3-Bis(3,5-dipyrid-3-yl-phenyl)benzene;
Bpy-TP2 – 2,7-Di(2,2'-bipyridin-5-yl)triphenylene;
CBP – 4,4′-Bis(*N*-carbazolyl)-1,1′-biphenyl;
CELIV – Carrier extraction by linearly increasing voltage method;
CIE – International Commission on Illumination;
CV – Cyclic voltammetry;
CzSi – 9-(4-*Tert*-butylphenyl)-3,6-bis(triphenylsilyl)-9H-carbazole;
D – Deuterium;
D–A – Donor –acceptor;
DDCzTrz – 9,9'-(5-(4,6-Diphenyl-1,3,5-triazin-2-yl)-1,3-phenylene)bis(9H -carbazole);
DMFL-CBP – N-([1,1'-biphenyl]-4-yl)-9,9-dimethyl-N-(4-(9-phenyl-9H-carbazol-3-yl)phenyl)-9H-fluoren-2-amine;
DMSO – Dimethylsulphoxide;
DPDPO2A – 5,10-Diphenyl-phosphanthrene 5,10-dioxide;
DPEPO – Bis[2-(diphenylphosphino)phenyl] ether oxide;
$\mathbf{e^-}$ – Electron;
$\mathbf{E_A(CV)}$ – Electron affinity calculated from cyclic voltammetry;
Em – Emission;
EQE – Maximal external quantum efficiency of OLED;
$\mathbf{E_S}$ – Singlet energy;
$\mathbf{E_T}$ – Triplet energy;
Ex – Exitation;
Fc – Ferrocene (bis(η^5-cyclopentadienyl)iron);
FIrpic – bis-(2-(difluorophenyl)pyridyl-N,C'')-iridiumpicolinate;
$\mathbf{F_w}$ – Fraction of water;
$\mathbf{h^+}$ – Hole;
HATCN – Hexaazatriphenylenehexacarbonitrile;
HAT-CN6 – Dipyrazino[2,3-f:2',3'-h]quinoxaline-2,3,6,7,10,11-hexacarbonitrile;
HOMO – Highest occupied molecular orbital;
hν – Photon;
$\mathbf{I_{Ar}}$ – The intensity of photoluminescence at argon atmosphere;
$\mathbf{I_{Ox}}$ – The intensity of photoluminescence at ambient atmosphere;
$\mathbf{I_P(CV)}$ – Ionization potential calculated from cyclic voltammetry;
IR – Infrared spectroscopy;
$\mathbf{Ir(ppy)_3}$ – *fac*-tris-(2-phenylpyridine)-iridium;
ISC – Intersystem crossing;
ITO – Indium-tin oxide;
Liq – Lithium quinolate;

LUMO – Lowest unoccupied molecular orbital;
mCP – 9,9′-Dicarbazolyl-3,5-benzene;
mCPCN – [9-(3-(9H-carbazol-9-yl)-phenyl)-9Hcarbazole]-3-carbonitrile;
mMTDATA – 4,4′,4″-Tris[phenyl(*m*-tolyl)amino]triphenylamine;
MS – Mass spectroscopy;
NBS – N-bromosuccinimide;
NMR – Nuclear magnetic resonance;
NPB – N,N'-Bis- (1-naphthalenyl)-N,N'-bis-phenyl-(1,1'-biphenyl)-4,4'-diamine;
OLED – Organic light emitting diode;
PBO – Piperonyl butoxide;
PEDOT:PSS – Poly polystyrene sulfonate;
PL – Photoluminescence;
PO-01 – Iridium(III) bis-(4-phenylthieno-[3,2-c]-pyridinato-N,C2')-acetylacetonate;
PPBi – 4-Isopropyl-4'-methyldiphenyliodoniumtertakis-(pentafluorophenyl)-borate;
ppm – Parts per million;
PPT – 2,8-Bis(diphenylphosphoryl)dibenzo[b,d]thiophene;
PVCz – Polyvinylcarbazole;
PYM3 – 9,9',9"-(Pyrimidine-2,4,6-triyl)tris(9H-carbazole);
QY – Photoluminescence quantum yield;
$\mathbf{R_D}$ – Refractive index;
RISC – Reversible intersystem crossing;
$\mathbf{S_t}$ – The theoretical calculated singlet energy;
T2T – 2,4,6-Tris(biphenyl-3-yl)-1,3,5-triazine;
TADF – Thermally activated delayed fluorescence;
TAPC – 4,4′-Cyclohexylidenebis-*N,N*-bis(4-methylphenyl)benzenamine;
TCTA – Tris-(4-carbazoyl-9-ylphenyl)-amine;
TCz1 – 3,6-Bis(carbazol-9-yl)-9-(2-ethyl-hexyl)-9H-carbazole;
TDATA – 4-(Tris-N, N-diphenyl-amino)-triphenylamine;
THF – Tetrahydrofuran;
TmPyPB – 1,3,5-Tri(m-pyridin-3-ylphenyl)benzene;
ToF – Time of flight method of the measurement of charges mobility;
TPBi – 2,2′,2"-(1,3,5-Benzinetriyl)-tris(1-phenyl-1-H-benzimidazole);
T-PCz – 9.9′9″-Triphenyl-9H,9′H,9”H-3,3′:6′,3″-tercarbazole;
TSPO1 – Diphenyl-4-triphenylsilylphenyl-phosphineoxide;
$\mathbf{T_t}$ – The theoretical calculated triplet energy;
UV-vis – Ultraviolet and visible light;
$\mathbf{V_{on}}$ – Turn on voltage;
XRD – X-ray diffraction analysis;
α-NPD – *N,N*′-Di-(1-naphthyl)-*N,N*′-diphenyl-(1,1′-biphenyl)-4,4′-diamine;
δ – NMR shift;
$\mathbf{\Delta E_{ST}}$ – Splitting of singlet and triplet energies;
Δf – Orientation polarizability;
ΔT – The difference between host and guest triplet energies;
ε – Dielectric constant;
$\mathbf{\lambda_{OLED}}$ – The most intensive wavelength of electroluminescence;

λ_{Pl} – The most intensive wavelength of photoluminescence;
μ_{ToF} – Charges drift mobility measured by time of flight method.

1. INTRODUCTION

The science of physics and chemistry with engineering and industry have been developing intensively for the last hundred years as a result of modern technologies becoming an inseparable part of the world in modern times. The flame was the first source of man-made light until the time of accessible and affordable electric power, which superseded unhandy and danger flame. The first technologies of electric light as an incandescent bulbs and fluorescence lamps are becoming obsolete, and light emitting diodes are firmly entering into lighting the world. The inorganic light emitting diodes are effective and reliable technology for lighting, but its still expensive production is limiting the development, without it, the choice of colours is limited. The organic light emitting diodes are not as effective and reliable, but they have some advantages as inorganic analogues with flexible and wide choice of colours; thus, they are widely used for displays and give the possibility to make touchscreens and flexible displays. However, the efficiency, brightness and lifetime of OLED are clearly lower than inorganic devices. The manufacturing of multilayer OLEDs is a long and complicated process too. The biggest problems of OLEDs are efficiency of short wavelength devices, lifetime, expensive and complicated manufacturing of multilayer structure.

The improvements of OLEDs efficiency could be done by looking for perspective emitters, hosts. The perspective materials for the OLED emitters should have the following characteristics:

1) High photoluminescence quantum yields;
2) High charges mobility;
3) Eligible electroluminescence colour;
4) Stability by morphological and electrochemical;
5) Simple and cheap synthesis;
6) Compatibility with other materials in OLED structure.

The series of characteristics are influencing the efficiency and reliability of OLED device. One of the most important parts of multilayer structure making is equal thickness of layers in the area, which is one of the basic characteristic for the reliability of the device. It is possible to achieve that by vacuum sublimation or spin coating technique, which is cheaper, but the choice of handy materials is small. Another important task is the selection of materials for multilayer structure. The characteristics of all materials of layers and the interoperability have a huge influence on the device. The most important part is the characteristics of emitting material and the interoperability with host material.

There are three generations of OLEDs. The first and most ineffective generation devices are the devices with fluorescence emitters. The second type of OLEDs phosphorescence emitters is sufficiently effective technology, but the effective emitters of the devices are expensive organic complex of iridium or platinum. The devices with phosphorescence pure organic emitters are not effectively described in literature. The third generation OLEDs with thermally activated delayed fluorescence (TADF) emitters that are showing higher efficiency than the first generation OLEDs and materials can be made from pure organic materials without

rare metals. The structures of TADF materials are constructed of two basical parts of electron donating and electron withdrawing blocks, and this strategy is giving the possibility to plan wide diversity of structures and achieve desirable properties; thus, the investigations of TADF emitters for the OLEDs are perspective.

The electron donating chromophores are well known materials such as carbazole, phenothiazine, acridane, diphenylamine and others and have advantages and disadvantages that are widely described in literature. The materials that are exhibiting electron withdrawing properties are investigated further, and the intensive investigations are ongoing. The carbonitriles substituents are known as strong electrons acceptors and aa a stabile group of chemical and thermal actions. In this work, the three types of electron withdrawing blocks were used, and several electron donating parts were connected. The influence of structures on characteristics were investigated.

The aim of this work is to synthesize and investigate new donor and cyano acceptor derivatives to obtain perspective materials for the third generation OLEDs.

The following tasks were set to achieve the aim of the work:

1. To synthesize carbazolyl substituted derivatives containing cyano groups;
2. To synthesize isophtalonitrile-based derivatives;
3. To synthesize phenylpyridine dicarbonitrile-based derivatives;
4. To investigate the properties of synthesized compounds by using experimental and computational methods;
5. To investigate the applicability of synthesized compounds in organic light emitting diodes.

The main statements of the dissertation:

1) 4,6-Bis(9,9-dimethylacridan-10-yl)isophthalonitrile is a perspective material as an emitter of green organic light emitting diodes.
2) Isophtalonitrile-based derivatives exhibited low splitting of singlet and triplet energies of 0.06 – 0.02eV and exhibited properties of thermally activated delayed fluorescence.
3) Pyridine-dicarbonitrile based derivatives exhibited high triplet energies that are higher than 2.70eV.

The novelty of this work:

The three series of new organic structures based on carbazole, izophtalonitrile and phenylpyridinedicarbonitrile were synthesised, investigated, and the theoretical calculations were examined. The perspective materials 3-(2,7-dicyanocarbazol-9-yl)-9-ethylcarbazole, 4,6-bis (9,9-dimethylacridan-10-yl) isophthalonitrile, 4,6-Bis (3,6-dimetoxycarbazol-9H-yl) isophthalonitrile and 4,6-Bis (2,7-dimetoxycarbazol-9H-yl) isophthalonitrile were investigated in the OLED structures as emitters. The TADF emitter 4,6-Bis(9,9-dimethylacridan-10-yl)isophthalonitrile based organic light emitting diode exhibited 22.5% maximal external quantum efficiency of green light.

The practical valuation of work:

The investigations of materials showed that the synthesised derivatives 3-(2,7-dicyanocarbazol-9-yl)-9-ethylcarbazole, 4,6-dis (9,9-dimethylacridan-10-yl) isophthalonitrile, 4,6-Bis(3,6-dimetoxycarbazol-9H-yl) isophthalonitrile and 4,6-Bis

(2,7-dimetoxycarbazol-9H-yl)isophthalonitrile are useful for the OLEDs structures as TADF emitters. The 4,6-dis (9,9-dimethylacridan-10-yl) isophthalonitrile emitter based organic light emitting diode exhibited high efficiency.

The structure of doctoral dissertation:

The dissertation consists of an introduction, literature review, experimental part, results and discussion, conclusions, list of publications and acknowledgment; 147 sources of literature were cited, and 52 figures were included. The size of the dissertation is 110 pages.

The personal input of the author in the dissertation:

The author synthesised, purified and characterized the derivatives that were described in Chapter **4**. The optical, photophysical, electrochemical, melting point measurements were performed by the author, and the thermal characterization with the help of responsible person. The charge mobility, ionization potential measurements, X-ray diffraction analysis and fabrication with the characterization of OLEDs were performed by Dr. D. Volyniuk, O. Bezvikonyi, Dr. A. Bučinskas from the Department of Polymer Chemistry and Technology, Kaunas University of Technology, with the participation of the author. The theoretical calculations of the synthesized compounds were made with help of Dr. Gjergji Sini from Cergy-Pontoise University.

2. LITERATURE REVIEW

The phenomenon of electroluminescence was observed in silicon carbide by Round, and it was shortly described in 1907[1]. The crystal of silicon carbide was inserted by electrodes and showed yellow electroluminescence on the voltage of 10V. The first light emitting diode device that was based on the silicon carbide was investigated and described by Lossev[2] in 1928. The electroluminescence phenomenon of organic materials was observed in the acridine orange crystal at high voltage[3], but the first low voltage and efficiency organic light emitting diode was made by Tang and VanSlyke[4] in 1987. It was the first multilayer device that was made from two organic layers and as an emitter was used aluminium organic chelate, the device worked at voltages lower than 5V.
The organic light emitting diodes is a perspective technology because of possibility to take wide-area, and flexible devices (**Fig. 1**) such as flexible displays and touch screens are made widely at the moment. The possibility of printing on large area devices is used[5].

Fig. 1 The flexible OLED screen

The most complicated problems of OLED are low stability, brightness of devices and insufficiently effective blue devices[6]. It is important to search for effective and stabile structures of emitters and stabile structures of devices such as composition

with host and emitter in the layer[7]. As it was observed by Tang and VanSlyke[4], the most effective are multilayer structures, and the structure of OLED devices could be formed by some layers:

1) Anode;
2) Holes injection layer;
3) Holes transporting and electrons blocking layers;
4) Emitting layer;
5) Electrons transporting and holes blocking layers;
6) Electron injection layer;
7) Cathode.

It is possible not to use some of these layers such as injection layers or host, but they are improving the efficiency of the devices[8]. The host materials are helping to transfer energy because of the little difference of energy levels that the electrons, holes and excitons are transferring to the emitting material[8] (**Fig. 2**).

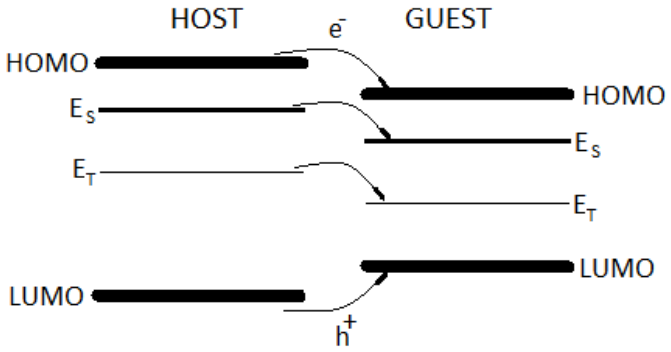

Fig. 2 The energy transfers diagram in host-guest system[8]

The holes transporting materials should exhibit these properties: high triplet energy (>2.9eV) and high holes mobility. The electron transporting layer should exhibit high electron mobility and should have high triplet energy as well. The host material is helping to transport charges in emitters layer, and it is doping the energy to guest material; thus, it should have well charges transporting properties for dissolving not sufficient charges transporting characteristics of emitter and should be characterized by high triplet energy for doping to guest (>2.8eV). The amount of the emitting material in host has sharply affected the efficiency of the device[9,10,11,12]. The HOMO and LUMO energies of layers' materials in the structure should be coordinated. The LUMO energy of host material should be lower than the emitting material, and HOMO energy level of the host should be higher than the emitter. It is improving the charges injection to layers in the structure[13]. The functions of layers of OLED structure were summarised in **table 1**. The scheme of organic light emitting diode is shown in **fig 3**. The working principle of OLED is based on the electronic excitation of molecules and photons generation from excited molecules during the relaxation. The most effective device structures are composed of host materials that are able to form excitons and doped emissive materials that can generate photons. It is not effective to use the same material which may generate excitons and photons [8,14].

Table 1 The functions of OLED layers[8,14]

Layer	Features and Requirements	Examples of materials
Cathode	The export of electrons to device structure. Should exhibit high electron affinity and low electron release energy.	Ca, Al, Mg, Ag
Electron injection layer	The facilitation of electrons injection from cathode to the transporting layer. It should show high electron affinity and high electron mobility.	Cs_2CO_3, LiF, Liq
Electron transporting layer	The acception of electrons from cathode and transporting to the emitting layer. It should exhibit high triplet state energy, high electron mobility.	TPBi, TSPO1, α-NPD etc.
Hole blocking layer	Blocks holes escaping from emissive layer to electron transporting layer or cathode. It should show higher electron affinity and higher ionization potential than the emissive layer materials.	Same as electron transporting materials
Host	The excitons forming material. It should exhibit high ambipolar charge mobility. It requires higher singlet and triplet state's energy than emitter materials, good morphological characteristics. Should show higher ionization potential and lower electron affinity than the emitter.	Should be chosen according to the emitter characteristics
Emitter	Converts excitons to photons. The main requirements are high luminescence quantum yields, desirable colour of luminescence.	FIrpic, Ir(ppy) etc.
Electrons blocking layer	Blocks electrons escaping from emissive layer to holes transporting layer or anode. It should exhibit lower electron affinity and lower ionization potential as emissive layer materials.	MTDATA, mCP, TAPC etc.
Holes transporting layer	Accepts holes from the anode and transports them to emitting layer. It should show high triplet state energy, high hole mobility.	PEDOT:PSS, PPBi etc.
Holes injection layer	The facilitation of holes injection from the anode to transporting layer.	TDATA, MoO_3 etc.
Anode	The export of holes in device structure. Should be transparent.	Indium tin oxide, polyaniline, polypyrrole

2.1. TADF phenomenon

The delayed fluorescence phenomenon was described by Perin in 1929, and the observation of delayed fluorescence in organic materials was observed by Lewis

from the fluorescein solution in 1941, but the phenomenon of TADF was explained by Wilkinson and Horrocks only in 1968. The first TADF emitter based on OLED was described in 2012[15].

The newest, cheap and effective third-generation organic light emitting diodes are devices with thermally activated delayed fluorescence emitters. The first-generation OLEDs with simple fluorescence phenomena exhibiting materials emitters show low efficiency because of electrical excitation that results in 25% of singlet excitons (S_1) and 75% of triplet excitons (T_1)[16]. The second-generation phosphorescent emitters are showing very high efficiency, nearby 100%, but the most effective materials are iridium, platinum or other rare and expensive and toxic metal complexes[17], and organic metals-free phosphorescence materials exhibit much lower efficiency. The first third-generation OLED with TADF emitter that was made from simple organic metals-free construction was described by Endo with co-authors[18].

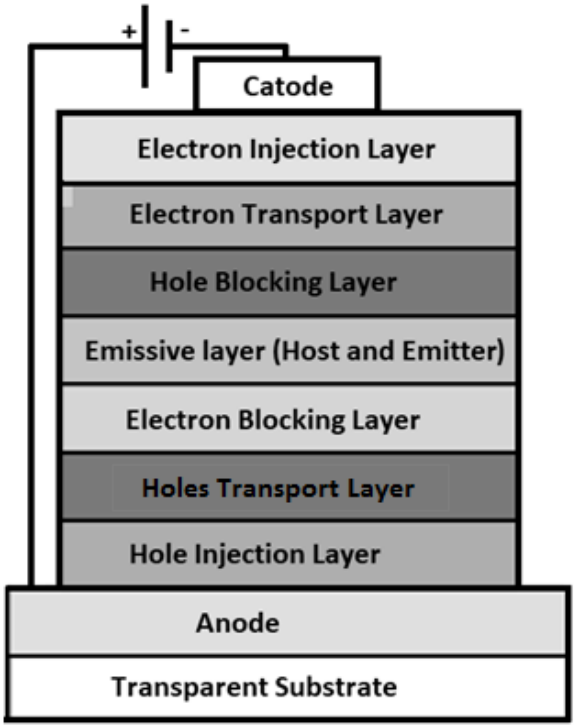

Fig. 3 The principal structure of OLED

A TADF phenomenon (**Fig. 4**) of materials is explained by very low splitting of singlet and triplet energies, there is a possibility to cross from T_1 energy state to S_1 by thermal action[19].

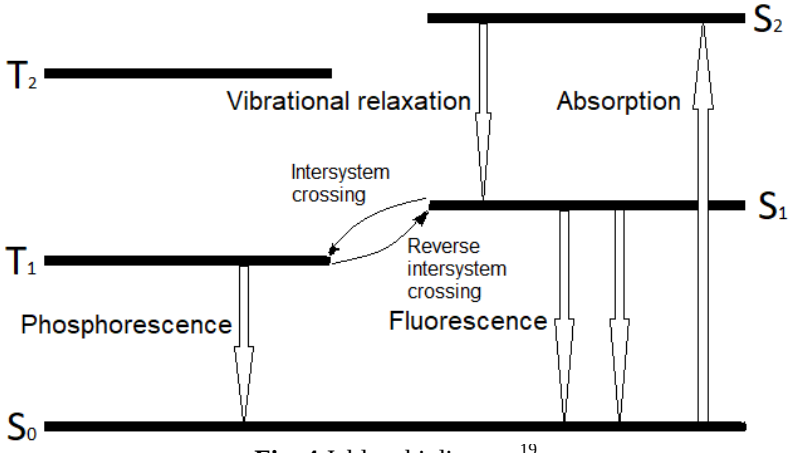

Fig. 4 Jablonski diagram[19]

The process is practically too low to affect the fluorescence quantum yield; then, the splitting is higher than 0.4eV[18,20]. As the reverse intersystem crossing process is excited by thermal influence, the fluorescence intensity and delaying time are depending on the temperature[21,22]. The dependence[23] of reverse intersystem crossing by temperature is described in formula (1):

$$k_{RISC} \propto exp^{-\frac{\Delta E_{ST}}{k_B T}} \qquad (1)$$

where k_{RISC} is rate constant of reverse intersystem crossing, k_B – Boltzmann constant, T – absolute temperature.

Because of the possibility of reversible intersystem crossing from triplet to singlet energies, the TADF materials are perspectives to be used as hosts. The TADF host is a perspective by more effective Förster resonance energy transfer from singlet to singlet energy levels of the host-guest system, because more energy of the singlet state exists at TADF molecules. The Dexter type exited electrons' transfers are not effective in triplet energy states in organic materials by the low density of materials, and low distance energy transfer and Förster transfer is not possible from the triplet state of host material to a triplet state of the guest. The intersystem energy crossing from the singlet state of energy to singlet state of the guest or the transfer from the singlet state of the host to the triplet state to guest by Förster resonance energy transfer and the intersystem crossing from triplet state to singlet energy state in guest are increasing the efficiency of luminescence (**Fig. 5**)[24, 25, 26].

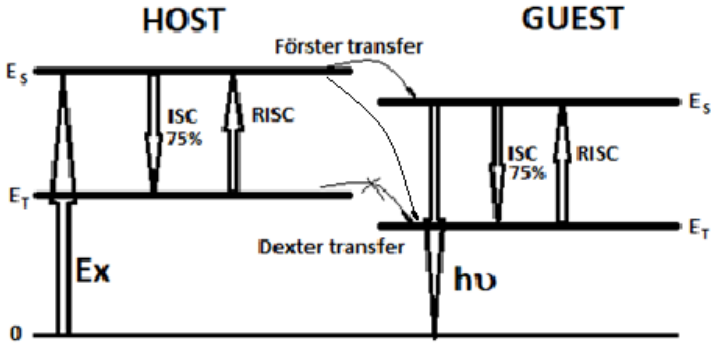

Fig. 5 The energy transfers in host-guest system of TADF materials[24-26]

2. 2. TADF emitters

2.2.1. Nitrogen-acceptor based derivatives

The structures of TADF exhibiting derivatives are formed by the donor-acceptor system because the separation between HOMO and LUMO orbitals minimizing exchanges of energy and minimizing the splitting of singlet and triplet energies; thus, TADF materials are used as emitters and is a perspective to use as host materials[27, 28].

The chromophore of carbazole is used for electroluminescence materials because of balanced charges mobility, moderate or high PL quantum yields and good thermal properties[29]. Cyanobenzene or other carbonitrile substituted structures are known as strong electron acceptors which are improving electron mobility and optical properties[30, 31].

The first high efficiency TADF OLED emitters that are made from the simple structures of carbazole substituted dicyanobenzene derivatives were published by Uoyama and co-authors[32]. The cyanobenzene and carbazole based structures were chosen because of well theoretical crystalline structure of molecule and good electron withdrawing properties of cyanobenzene part. Derivatives **L1**-**L3**, **L6** and **L7** (**Fig. 6**) were synthesized by the simple nucleophilic coupling method and got yields from 9% to 79%. Derivatives **L2**, **L3** and **L7** were investigated as the emissive layer in OLED structures: ITO/α-NPD/5% **L3** or **L7**: CBP/TPBi/LiF/Al and ITO/ α-NPD/5% **L2** and PPT/PPT/LiF/Al. The quantum yield of 507 nm maxima wavelength fluorescence of derivative **L3** was 94%, and the device of **L3** exhibited 19.3% maximum EQE of green light. The devices of **L7** and **L2** showed 11.2% efficiency of orange light and 8.0% efficiency of blue sky light. Derivative **L4** was described by Cho and co-workers[33]. The splitting of singlet and triplet energies of derivative is 0.05eV, and the quantum yield of PL was 67%. The structure of blue and yellow OLEDs devices was ITO /PEDOT:PSS /TAPC /mCP /mCP:**L4** or PO-01:**L4** /TSPO1 /LiF /Al and achieved 0.87% of blue light and 16.4% maximum external quantum efficiencies of exciplex yellow light. The properties and OLED preparation from **L5**, **L13** and **L14** was published by Park and coworkers[34]. The fluorescence analyses of derivatives were made in toluene solution in air and

oxygen free atmosphere. Derivative **L5** exhibited 39% of 472nm fluorescence quantum yield in air and oxygen atmosphere, and there was observed 20ns fluorescence decay time. **L13** has lower fluorescence quantum yield and the same characteristics, but **L14** exhibited high influence of oxygen in fluorescence measurements by quantum yields of 15 and 49% in air and oxygen atmosphere[35] with 31ns fluorescence decay time.

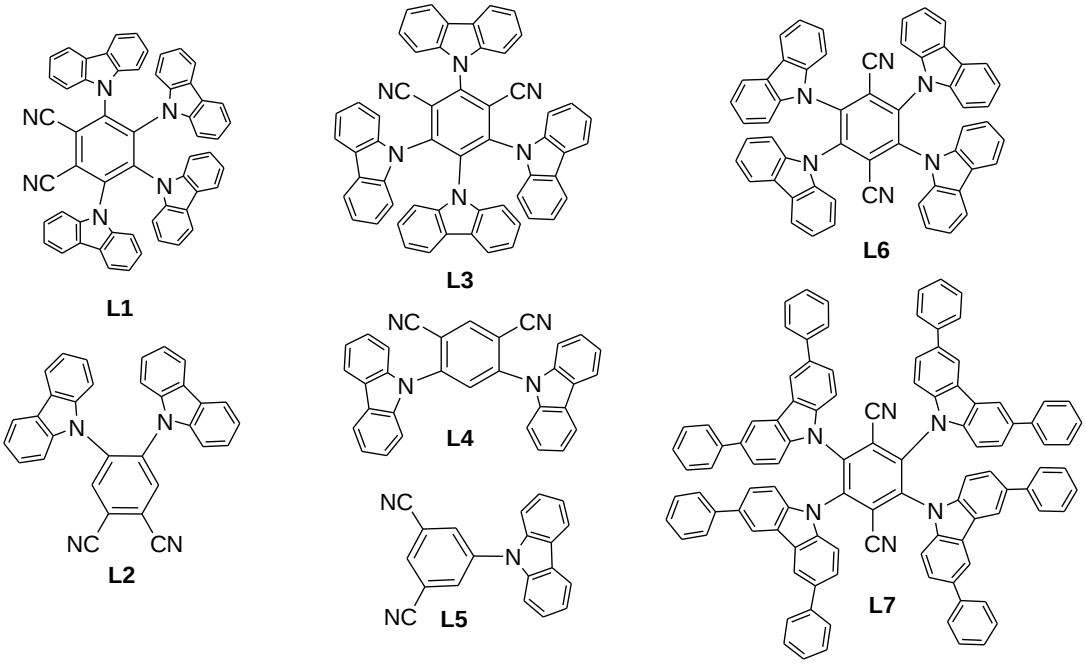

Fig. 6 Structures of derivatives **L1-L7**[32,33,34]

Materials **L8-L11** were described by Zhang[36] and co-authors (**Fig. 7**), and the compound **L12** was investigated by Tanaka et al.[37]. All compounds were synthesised by nucleophilic coupling reaction, which were catalysed by NaH or t-BuOK and obtained as white materials. The devices were made by structures of ITO /HAT-CN /NPB /TCTA /mCP /**L8-L11** /DPEPO /Bphen /LiF /Al or ITO /HAT-CN /T-PCz /mCP /10% **L3**:**L12** /T2T /Bpy-TP2 /LiF /Al. The characteristics of derivatives and devices are summarised in **table 2**. The derivatives **L8-L12** showed high triplet energy and blue-region PL with sufficiently high quantum yield.
The dimer **L15** (**Fig. 8**) was prepared by lithium diisopropylamide-catalyst reaction[38] from derivative **L4** as the starting material. Dimer shown 91% photoliumenescence quantum yield which is higher than **L4,** but the photoliumencescence maxima are 447nm, and it is 30 nm longer than **L4**. The singlet and triplet energies are 2.60 and 2.47eV. The device was formed by structure ITO/ PEDOT:PSS/ TAPC/ mCP/ mCP: BmPyPb: 1% **L15** /TSPO1/ TPBi/ LiF/ Al and achieved 18.9% maximal EQE of blue-greenish device.

Table 2 Characteristics of derivatives **L8–L12**

	E_T,eV	ΔE_{ST}, eV	λ^{Pl}, nm	QY_{PL}, %	EQE_{max}, %	Ref. No
L8	2.95	0.17	404	77	13	36
L9	2.88	0.27	405	72	21.5	
L10	2.97	0.32	396	75	20	
L11	2.83	0.21	431	50	29.5	
L12	2.92	0.34	420	39	17	37

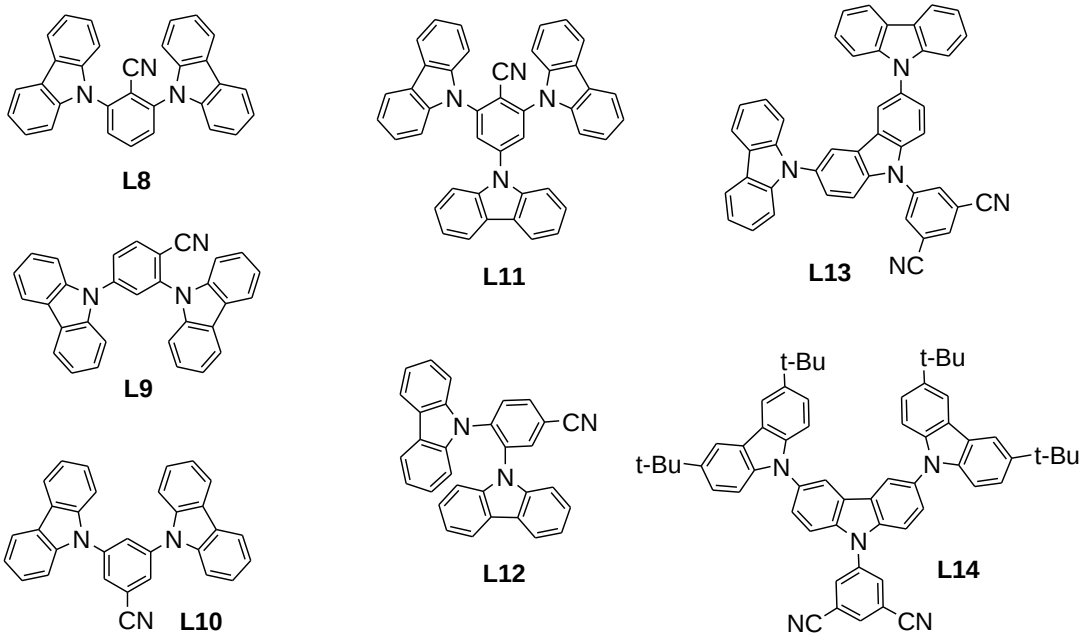

Fig. 7 Structures of derivatives **L8**-**L14**[34,36,37]

Derivatives **L16** and **L17** were investigated by Li and co-workers[39]. The synthesis was made from bicarbazole by K_2CO_3 catalysed nucleophilic coupling reaction. The physical measurements were investigated, and the devices were made by the scheme: ITO/α-NPD/mCP/**L16** or **L17**/TPBi /LiF/Al. The derivatives **L18–L20** were described by Kim et al[40]. The devices of materials **L18–L20** were made by the structure: ITO/ PEDOT:PSS/ TAPC/ TCTA/ mCP/ DPEPO: **L18–L20**/TSPO1/TPBi/LiF/Al. The characteristics of derivatives **L16–L20** and the properties of devices were summarized in **table 3**. It is possible to see that PL maxima are shorter than maxima of electroluminescence of devices. The 3,6'-bicarbazole –substituted derivative **L18** exhibited higher PL quantum yield than 4,6'-bicarbazole or 4,5'-bicarbazole-based derivatives **L19** and **L20**, but the electroluminescence quantum yields were higher for derivatives **L19** and **L20**. The PL maxima of 3,6'-bicarbazole dimer **L18** is longer than the acceptor-connected dimer **L15,** but the differents between the quantum yields and the splitting of singlet

and triplet energies are little. 3,4 and 4,4 bicarbazole-substituted derivatives exhibited shorter PL maxima, but the quantum yields were lower.

Table 3 Characteristics of derivatives **L16–L20**

	λ_{PL},nm	QY, %		ΔE_{ST}	EQE, %	λ^{OLED}, nm	Ref. No.
		In air	Oxygen free				
L16	488	12	72	0.06	9.6	501	39
L17	470	15	50	0.14	9.2	487	
L18	470	87	-	0.11	17.9	510	40
L19	448	66	-	0.16	21.8	475	
L20	444	61	-	0.21	19.5	473	

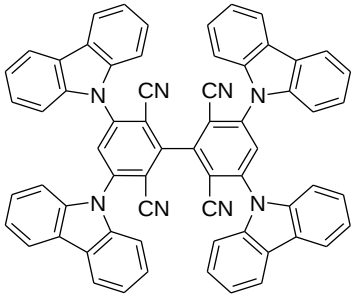

L15

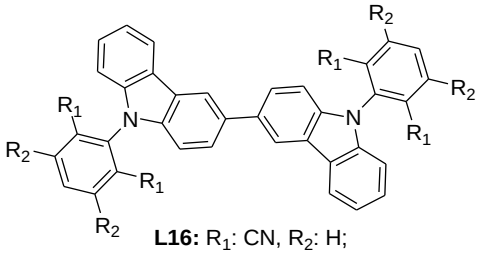

L16: R_1: CN, R_2: H;
L17: R_1: H, R_2: CN;

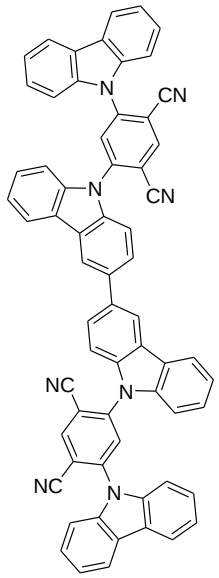

L18

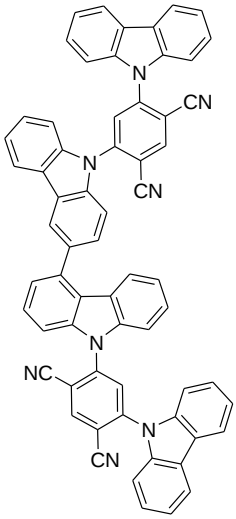

L19

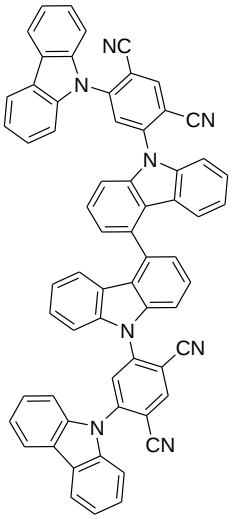

L20

Fig. 8 Structures of derivatives **L15–L20**[39,40]

Pyridine, pyrazine, pyrimidine or triazine are strong electron withdrawing groups that are widely investigated and described in literature for TADF molecules[23].
The cyanopyridine and phenylacridane based emitters **L21**–**23** were synthesized and investigated by Pan and co-workers[41] (**Fig. 9**). The derivatives were synthesized from *p*-(N-acrydanyl)-phenylboronic acid and respective acceptor by Suzuki coupling and got high yields of products. The derivatives are stable at temperatures higher than 273 °C. The PL measurements were recorded from toluene solutions and solid state in matrix of mCPCN. The PL maxima of degassed toluene solutions were 488, 504 and 652nm, and 490, 459 and 550nm were observed from solid state with mCPCN for derivatives **L21–L23** respectively. The PL quantum yields of derivatives were 34.5, 30.6 and 48.9% that were measured from degassed toluene solution and 91.6, 83.5 and 90.4% from matrix in mCPCN for derivatives **L21–L23** respectively. The phosphorescence maxima of derivatives were observed at 538, 516 and 550nm, and the calculated splitting of singlet and triplet energies were 0.19, 0.18 and 0.032eV for derivatives **L21–L23** respectively. The OLED devices containing emitters **L21–L23** were made by scheme ITO/ PEDOT:PSS/ TAPC/mCP/mCPCN:8% emitter of **L21**-**L23**/3TPYMB/LiF/Al. The device of **L21** emitter exhibited 23.9% maximal EQE of sky-blue light. The devices of emitters **L22** and **L23** exhibited 23.1 and 29.2% maximal EQE with green and yellow light.

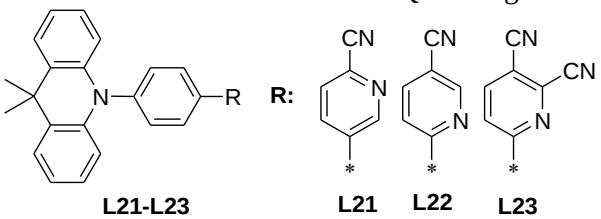

Fig. 9 Cyanopyridine-based derivatives **L21–L23**[41]

Di-*tert*-butylcarbazolyl and 9,9-dimethylacridanyl substituted dicyanopyrazine derivatives **L24** and **L25** (**Fig. 10**) were investigated by Cai and co-authors[42]. The mass lost temperatures of derivatives were higher than 400 °C. The fluorescence maxima of thin films were observed at 534 and 618nm for derivatives **L24** and **L25** respectively. Derivative **L25** exhibited higher fluorescence quantum yield (39.8%) than derivative **L24** (28.6%). The investigations of the influence of fluorescence quantum yield from solution in air and oxygen-free conditions were made as well. The measurements of PL quantum yield from thin films showed higher values in nitrogen atmosphere (38 and 43% respectively). The quantum yield of derivative **L24** was higher in hexane solution in oxygen-free atmosphere (62.9 and 53.8% in air). Acridane substituted derivative **L25** is exhibiting twice higher fluorescence quantum yield in oxygen-free atmosphere (16.4 and 8.6% respectively). The OLED most effective structures were formed with 5% **L24** and 1% **L25** as emitter in the CBP host by structure: ITO/HATCN/TAPC/emitter/TmPyPB/LiF/Al. The maximum quantum efficiency of devices was 8.1% and 15.6% and PL maxima of devices were 546 and 572nm for **L24** and **L25** respectively.

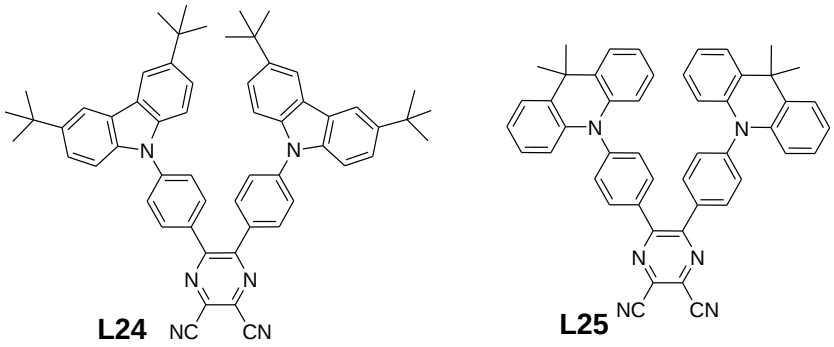

Fig. 10 Derivatives **L24** and **L25**[42]

The quinoxaline acceptor-based materials **L26–29 (Fig. 11**) were synthesized and explored by Yu and co-workers[43]. The derivatives were synthesized by Buchwald-Hartwig (**L23**), Ullman-coupling (**L27** and **L28**) and Suzuki-coupling (**L29**) reactions with high yields. The physical properties of derivatives are summarized in **table 3**. The derivatives showed high thermal stability and high glass transition temperature. The OLED device was made by scheme: ITO/MoO_3:TAPC/TAPC/mCP/10% **L26**:CBP/TmPyPB/LiF/Al. The device showed 7.4% maximum quantum efficiency by 580nm PL maxima. The physical properties of derivatives **L26–L29** were summarized in **table 4**. The lowest splitting of singlet and triplet energies exhibited acridane-substituted derivative **L26**. However, it showed the longest PL maxima and the lowest PL quantum yield from the series of derivatives **L26–L29**.

Table 4 Structures of derivatives **L26–L29**

	$T_{-5\%}$, °C	T_G, °C	λ_{max}, nm	QY, %	E_S, eV	E_T, eV	ΔE_{ST}, eV	Ref. No
L26	394	134	603	14	2.06	1.99	0.07	43
L27	414	150	537	47.8	2.31	2.11	0.20	
L28	419	194	557	42.7	2.23	2.05	0.18	
L29	471	157	502	67.3	2.47	2.14	0.33	

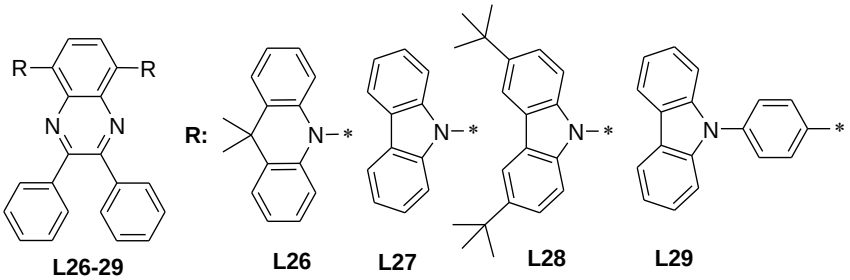

Fig. 11 Structures of derivatives **L26–L29**[43]

The pyrimidine based derivatives **L30–L33** were investigated by Ganesan and co-workers[44], and derivative **L34** (**Fig. 12**) was investigated and described by Nakao and co-authors[45]. The derivatives **L30**–**L33** exhibited high thermal stability in the range of 357–382 °C, and the derivative **L34** exhibited 453 °C 5% mass lost temperature, but the glass transition of derivatives **L30**–**L34** were in the range 90–95 °C, only then, **L34** exhibited 181 °C glass transition. The OLED devices containing emitters of **L30**–**L33** were made by the scheme: ITO/TAPC/ host: 10% emitter **L30**–**L33**/ TmPyPB/LiF/Al. The mCP was used as host for devices containing emitters of **L30**–**L33**, and DPEPO was used with **L32** emitter. The device with **L34** emitter was prepared by the scheme: ITO/PPBi/TAPC/10% **L34**: DPEPO/B3PyPB/LiF/Al. The OLEDs with mCP hosts showed 7.2% of blue colour, 12.6% of green colour maximal EQE for emitters **L30** and **L32** and 11.8% of blue sky light for **L31** and **L33** emitters equally. The devices with **L32** emitter and DPEPO host showed 14.2% EQE of green light emitting, and OLED with dicarbazolyl substituted **L34** emitter exhibited noticeable higher 23.7% maximal EQE of shorter wavelength blue sky light.

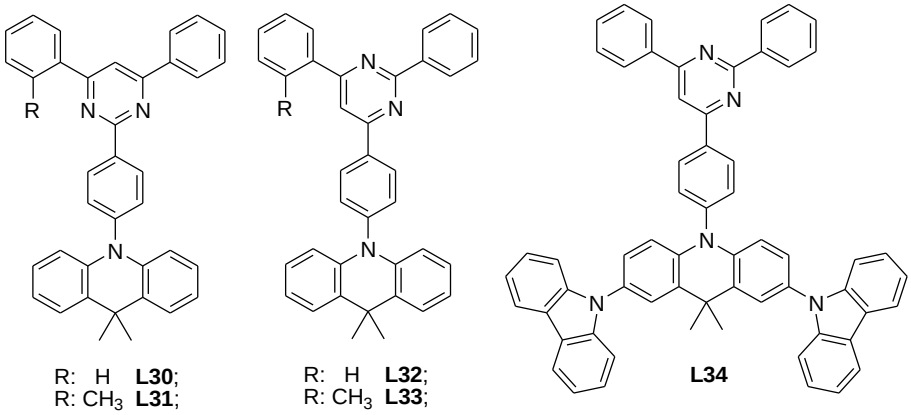

Fig. 12 Pyrimidine-based derivatives **L30–L34**[44,45]

The derivatives **L35**–**L37** that were based on triazine ring acceptor were synthesized by Ullman coupling and Myiaura-Suzuki coupling tree steps reaction[46]. All materials (**Fig. 13**) were obtained as a yellow powder. The derivative **L37** showed the highest mass lost and glass transition temperatures (372 and 127 °C respectively). All materials exhibited enough low splitting of singlet and triplet energies with the biggest value of 0.17eV. The OLEDs devices with derivatives emitters were formed by the structure: ITO/PEDOT:PSS/TAPC/mCP/mCP:5% **L35**–**37**/TSPO1/LiF/Al. The bicarbazolyl and tricarbazolyl substituted biphenyltriazine derivatives **L38**–**L40** were synthesized and characterized by Kim and co-workers[47]. OLED were formed according to the scheme: ITO/PEDOT:PSS/TAPC/mCP/DPEPO:10% **L38**–**L40**/TSPO1/TPBi/LiF/Al. The derivatives **L41** and **L42** were described by Kim and co-authors[48]. The device was made by the structure: ITO/α-NPD/TCTA/mCP/6%

L41–**L42**:DPEPO/DPEPO/TPBi/LiF/Al. Derivative **L43** was synthesized from N-phenylbicarbazole and difluorotriphenyltriazine by NaH catalysed nucleophilic coupling reaction[49] (**Fig. 13**).

Table 5 The physical characteristics of derivatives **L35–L43**

	E_S, eV	E_T, eV	ΔE_{ST}, eV	λ_{max}, nm	QY, %	λ^{OLED}_{max}, nm	EQE, %	Ref. No.
L35	2.76	2.66	0.10	455	16.7	470	9.3	46
L36	2.61	2.58	0.03	481	50.5	484	14.7	
L37	2.60	2.59	0.01	477	43	480	12.3	
L38	3.00	2.79	0.03	460	82	473	15.7	47
L39	2.92	2.80	0.01	465	62	488	12.4	
L40	2.98	2.97	0.12	502	85	476	15.7	
L41	2.98	2.84	0.14	499	61.3*	504	10.3	48
L42	2.79	2.70	0.09	505	60.5*	531	11.6	
L43	2.69	2.52	0.17	465	30**	493	23.5	49

* - measured from film of 6% of derivative in DPEPO; ** - the quantum yield in thin film with DPEPO that was 40%.

The optimized amount of emitter was 20% in DPEPO host, and the best structure of the device was formed by the scheme: ITO/PEDOT:PSS/ TAPC/ **L43**: DPEPO/ TSPO1/TPBi/LiF/Al. The physical characteristics and properties of OLED devices of derivatives **L35**–**L43** were summarized in **table 5**. As shown in the table, triazine-based derivatives **L35**–**L43** are exhibiting low splitting of singlet and triplet energies, but PL maxima of derivatives were longer than 455nm. The characteristics of derivatives **L35**–**L37** indicate that alkyl-substituted carbazole substituent improved the characteristics of higher PL quantum yield, and the bathochromical shifts were observed as well. The photophysical properties of derivative **L38** are higher than **L40**, but the characteristics of the devices are quite similar. The 1,3-biscarbazol-9-yl-carbazole substituted derivative **L39** showed lower splitting of singlet and triplet energies, but all other properties were worse than in **L38** and **L40**. The PL maxima of diphenylamine-substituted derivative **L41** was shorter by 6nm than di-(biphenyl)amine-substituted derivative **L42**, and the quantum yields were quite similar, but the difference of electroluminescence maxima of devices was 27nm, and the maximal EQE was higher than **L41**. The photophysical characteristics of dibicarbazole-substituted derivative **L43** was lower than other triazine-based derivatives **L35**–**L42**, but the efficiency of electroluminescence was the highest. It is possible to explain by well exploring the best optimized structure of OLED.

2.2.2. Sulphone-based materials

Thiantrene tetroxide and diphenylsulfoxide are strong electron accepting parts which are used to make D-A or D-A-D structures because of the interruption of conjugation at diphenylsuphoxide part[23].

The series of four thiantrene-tetraoxide-based derivatives **L44**–**L47** (**Fig. 14**) were synthesized and investigated by Sun et al[50]. The derivatives were synthesized by Suzuki coupling reaction from bromothiantrene-tetraoxide and respective boronic acid pinacol ester with higher than 60% of yields. The derivatives have high thermal stability that is higher than 360 °C, but **L47** showed lower glass transition at 110 °C temperature. The splitting of singlet and triplet energies of derivatives were 0.28, 0.30, 0.38 and 0.21eV for derivatives **L44**–**L47** respectively. The PL characteristics of derivatives were measured from thin films and are 487, 501, 558 and 610nm maxima of emission wavelength with 71, 65, 72 and 50% of PL quantum yield for derivatives **L44**, **L45**, **L46** and **L47** respectively. It is possible to see that metoxi-substituted derivative **L47** exhibited lower splitting of singlet and triplet energies, but PL characteristics was much lower. The quantum yield of triphenylamino-substituted derivative **L46** exhibited higher than phenylcarbazole-substituted derivative **L45** and similar to 9-phenyl-carbazol-3-yl-substituted derivative **L44**, but there was observed a wide bathochromical shift. The electroliumenescence properties of materials were investigated by device structure: ITO/PEDOT:PSS/10% emitter:host/ TPBi/Cs_2CO_3/Al. Where host for **L44** was mCP and CBP for the others. The device with **L44** emitter emitted blue sky light and achieved 4% maximum EQE. The best properties had emitter **L45**, and there was achieved 9.1% EQE with 502nm maxima of wavelength light. The electroluminescence properties of **L46** and **L47** devices were 5.1 and 3.3% maximal EQE and 521 and 570nm wavelength maxima of emitting respectively.

For comparison with thianthrene tetraoxide based derivative **L46**, there are presented properties of anthraquinone based derivative **L48** with triphenylamino chromophores. The anthraquinone - triphenylamine derivative **L48** was described by Bin Huang and co-authors[51]. The derivative was synthesized by Suzuki coupling reaction and is exhibiting thermal stability of 367 °C. The splitting of singlet – triplet energies was very low as 0.05eV, and PL quantum yield was 52% of red light. The OLED was formed by the structure: ITO/ PEDOT:PSS/ 10% **L48**:CBP/ TPBi/ Cs_2CO_3/ Al. The device emitted red light (612nm maxima) with 7.5% maximal EQE.

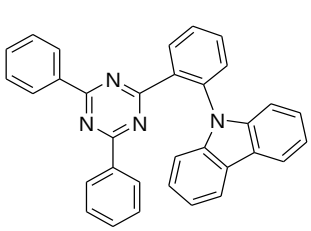

L35

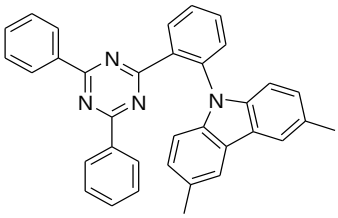

L36

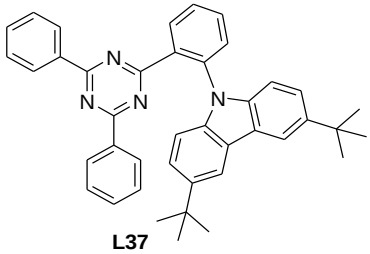

L37

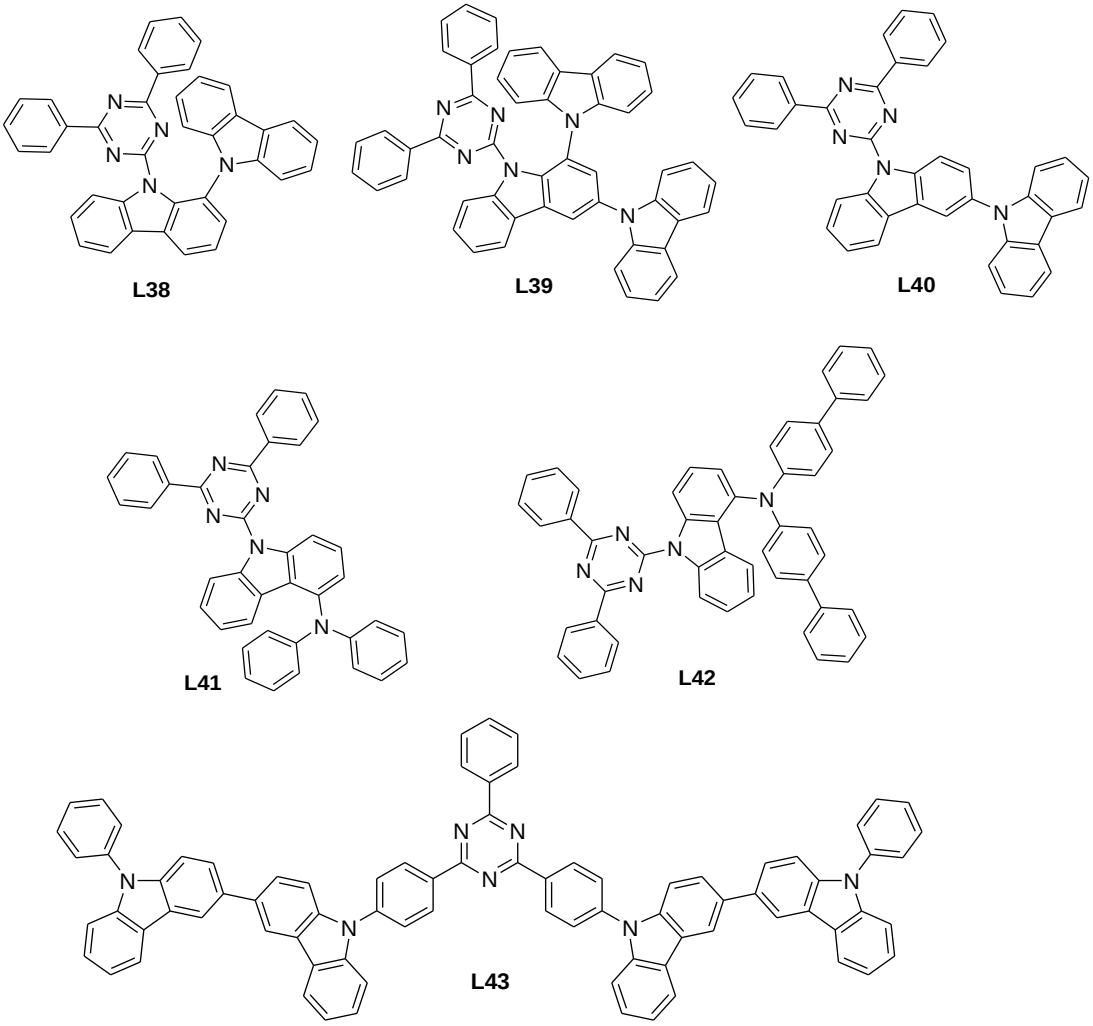

Fig. 13 Structures of derivatives **L35–L43** [46-49]

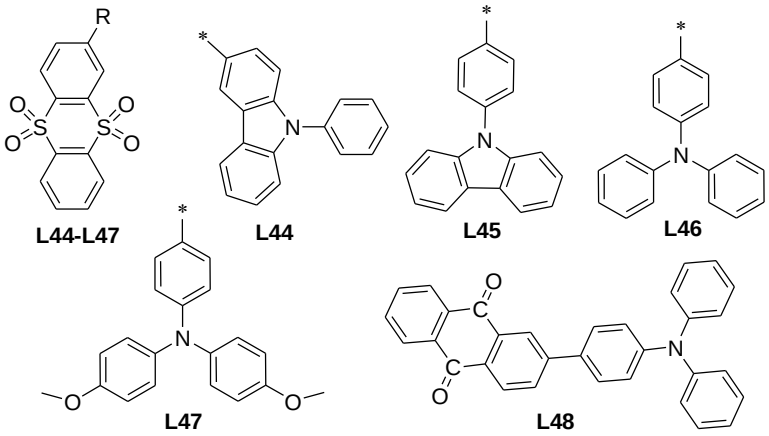

Fig. 14 Derivatives **L44–L48**[50,51]

Derivatives **L49**–**L53** (**Fig. 15**) were investigated for physical characteristics and OLED structures by several authors, and they were described in series of papers[52-61]. Derivatives **L49** and **L54** emitted blue light on 419 and 408nm with 32.1 and 25.4% PL quantum yield from solid state respectively[52]. Derivative **L50** characteristics were as follows: E_S=2.80eV, E_T=2.66eV, ΔE_{ST}=0.14eV, QY=71%. The OLED structure was[53] ITO/PEDOT:PSS/TAPC/TCTA/mCP/**L50** (20%):DPEPO/TSPO1/TPBi/LiF/Al. The device showed 20.7% EQE of blue light. One more investigated OLED structure was ITO/PEDOT:PSS/mCP/**L50**/TSPO1/TPBi/LiF/Al. The device emitted blue light, and the maximal EQE was 15.7%. The different substituted derivative **L51** with carbazolyl and phenthiazinyl chromophores and diphenothiazinyl substituted derivative **L51** exhibited 518 and 510nm emission. The PL measurement of **L51** showed 66.3 and 93.3% quantum yield from thin film in air and argon atmosphere. Quantum yields of **L52** were 30.2 and 52.8% respectively. The higher PL quantum yield of **L51** is explained by fluorescence from two different parts of molecule[52]. Derivative **L53** was used by several authors for OLED structure investigations[54]: ITO/α-NPD/DPEPO/**L53**/TPBi/LiF/Al. The device showed 16% EQE of blue light. Another structure[55] was ITO/ PEDOT:PSS/ TAPC/ mCP/ DDCzTrz/ **L53**/ TSPO1/ TPBi/ LiF/ Al. The exciplex was formed in structure from diphenyl-(3,4,5-tris(carbazole-9-yl)-phenyl)-triazine and **L53**. The exciplex consisting OLED showed 15.3% EQE of green light. Without it, there was made OLED by structure[56]: ITO /PEDOT:PSS /TAPC /TCTA /mCP /**L53**(50%):DPEPO/ DPEPO/TSPO1/TPBi/LiF/Al. The EQE of the device was 22.6% of blue light (λ_{max}=470nm). The device with 5,10-diphenyl-phosphanthrene 5,10-dioxide host was formed by structure[57]: ITO/MoO_3/NPB/mCP/**L53**:DPDPO2A/DPDPO2A /BPhen/LiF/Al. The device emitted blue light with EQE of 17.9%. Zhang and co-authors[61] described the investigation of the influence of layers for the characteristics of the device. The structures of devices and characteristics are summarized in **table 6**. The results show that holes and electrons transporting layers are increasing the

EQE of the device, but the little bathochromic shift of electroluminescent is observed.

Derivatives **L54**–**L56** were described in two papers[58, 59,61,].The fluorescence measurements of derivative **L54** showed 69% quantum yield with 402nm emission maxima. The singlet-triplet splitting of derivative is 0.32eV. The OLED was formed by the scheme: ITO/α-NPD/TCTA/CzSi/**L54**/DPEPO/TPBi/LiF/Al. The device exhibited 9.9% maximal EQE of near standard blue light. The derivatives have high thermal stability and high glass transition temperatures. The singlet and triplet energies of **L55** and **L56** are 3.25; 3.15eV and 3.00; 2.98eV respectively. The splitting of singlet and triplet energies are 0.25 and 0.17eV. The blue OLEDs were made by simple structure: ITO/PEDOT:PSS/**L55** or **L56**/TPBi/LiF/Al.

Table 6 The characteristics of OLEDs with **L53** emitter

Structure	**EQE_{max}, %**	**λ^{OLED}, nm**	**Ref. No.**
ITO/MoO_3/**L53**/LiF/Al	0.11	476	61
ITO/ MoO_3/**L53**/PO15/LiF/Al	14.4	481	
ITO/MoO_3/mCP/**L53**/PO15/LiF/Al	11.8	479	
ITO/MoO_3/mCP/**L53**/DPEPO/LiF/Al	19.5	480	

Derivatives **L57**–**L59** were synthesized and investigated by Gong et al[62]. The thermogravimetric analysis showed high thermal stability of derivatives that are higher than 372 °C. The glass transition of derivatives was observed at the interval 143–194 °C. PL properties of derivatives were investigated from solution in toluene on argon atmosphere and from thin films with mCP. The PL quantum yields of derivatives **L57**–**L59** solutions were 8.3, 12.4 and 6.3% with 490, 549 and 498nm emission respectively.

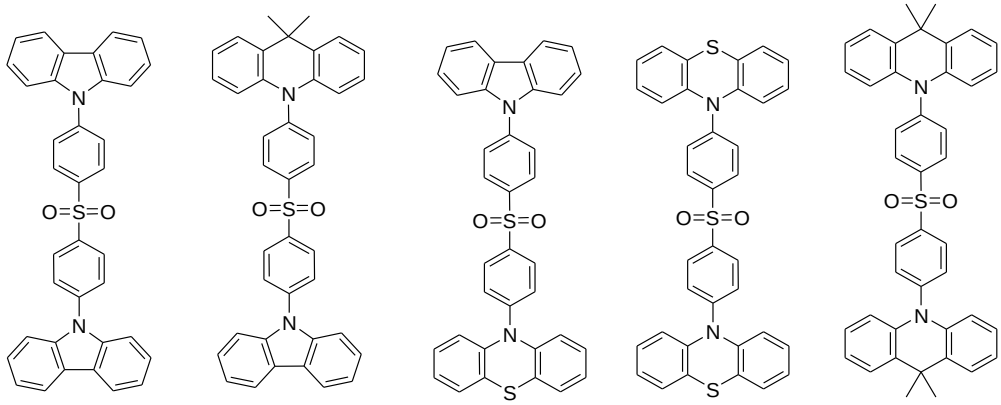

Fig. 15 Derivatives **L49**–**L53**[52-59]

The quantum yield of thin films with mCP were 87, 45 and 27%. The singlet and triplet energies were calculated from fluorescence (300K) and phosphorescence spectra (77K). The singlet energies of derivatives **L57**–**L59** are in the range 2.56–2.87eV, the triplet energies are in the interval 2.52–2.65eV, and ΔE_{ST} are 0.22, 0.04 and 0.29eV respectively. The devices were made by the scheme: ITO/PEDOT:PSS/mCP:15% **L57**–**L59**/TPBi/Liq/Al. The blue sky light (λ_{OLED}=496nm) device of compound **L57** showed 3.8% EQE, yellow light emitting device **L58** had 8.1% EQE, and the device with **L59** emitter showed luminescence of green light (λ_{OLED}=522nm) with 1.3% EQE.

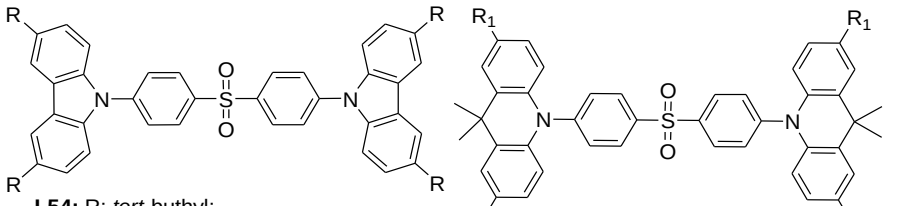

L54: R: *tert*-buthyl;
L55: R: 3,6-di(tert-buthyl)-carbazol-9H-yl;
L56: R: 3,6-di(3,6-ditert-buthylcarbazol-9 H-yl)carbazol-9H-yl-cabazol-9Hyl;

L57: R_1: phenyl;
L58: R_1: N-diphenylamino;
L59: R_1: 4-(N-phenylbenzoamine)-phenyl;

Fig. 16 Derivatives **L54-L59**[58-62]

The compounds **L60**, **L61**[63] and **L62**, **L63**[64] were synthesized and described by Liu with co-authors in two papers (**Fig. 17**). All these derivatives have high thermal stability that is higher than 400 °C. The fluorescence measurements of derivatives were recorded from films. The PL maxima of derivatives **L60**, **L61** and **L63** were fixed in the range from 444 to 474nm and 521nm for **L62**. The PL quantum yields of chloroform solution of derivatives **L60** and **L61** were 39.3 and 48.5% in air and 56.3 and 69.3% under argon atmosphere. The singlet-triplet splitting of derivatives are 0.14, 0.12, 0.19 and 0.26eV for derivatives **L59–L62** respectively. The OLED with **L60** and **L61** emitters were made by the structure: ITO/NPB/TCTA/CzSi/10% **L60** or **L61**:DPEPO/DPEPO/TPBi/LiF/Al. The sky-blue device with **L60** emitter had 11.7% maximal EQE, and blue OLED with **L61** emitter showed 5.5% EQE. Derivatives **L62** and **L63** were investigated as emitters in OLED structure: ITO/triphenylamine-containing polymer[65]: PPBi/TAPC/mCP/20% **L62** or **L63**: DPEPO/ DPEPO/B3PyPB/LiF/Al. The green device with **L62** emitter showed 13.5% EQE, and the device with derivative **L63** emitter had 24.5% maximum EQE of blue light luminescence with CIE light colour coordinates (0.16:0.21).

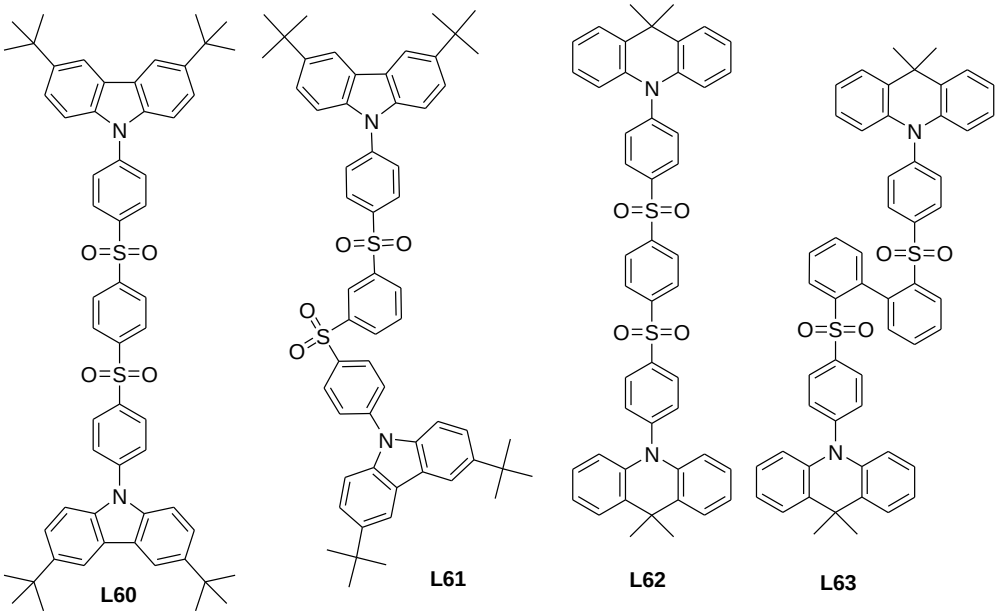

Fig. 17 Derivatives **L60–L63**[63,64]

2.2.3. Dendrimers and polymers

The dendrimer-form molecules are known as derivatives with excellent thermal stability characteristics[66], dendrimers are using as holes transporting and emitting single layer in devices because-off good holes transporting properties[67] and were investigated as organometallic complexes for phosphorescent host-free emitters layer in OLED[68]. Polymeric materials are perspective for the OLED devices because of easy layers' making from the solutions by spin-coating process possibility, and it is enabling to make the devices by cheap printing technology[69].

The triphenyltriazine and carbazole-based dendrimers **L64–L66** (**Fig. 18**) were synthesized and described by Albrecht with co-authors[70]. The thermogravimetric analysis showed very high thermal stability of dendrimers about 600 °C. The quantum yields of green and sky-blue PL from thin films were 52, 31, 8.5% for dendrimers **L64**, **L65** and **L66** in nitrogen atmosphere respectively. The PL quantum yields were measured from solutions in toluene. The air and oxygen-free conditions were made, and the derivatives showed 76, 59 and 6.4% PL quantum yield in the air and 94, 100 and 94% QY in nitrogen atmosphere. The singlet-triplet energies splitting of dendrimer **L64** was 0.03eV and 0.06eV for dendrimers **L65** and **L66**. There were made non-optimized structure OLED by the scheme: ITO/PEDOT:PSS/**L64**-**L66**/TPBi/Ca/Al and achieved 2.4, 3.4 and 1.5% maximal external quantum efficiencies of blue light.

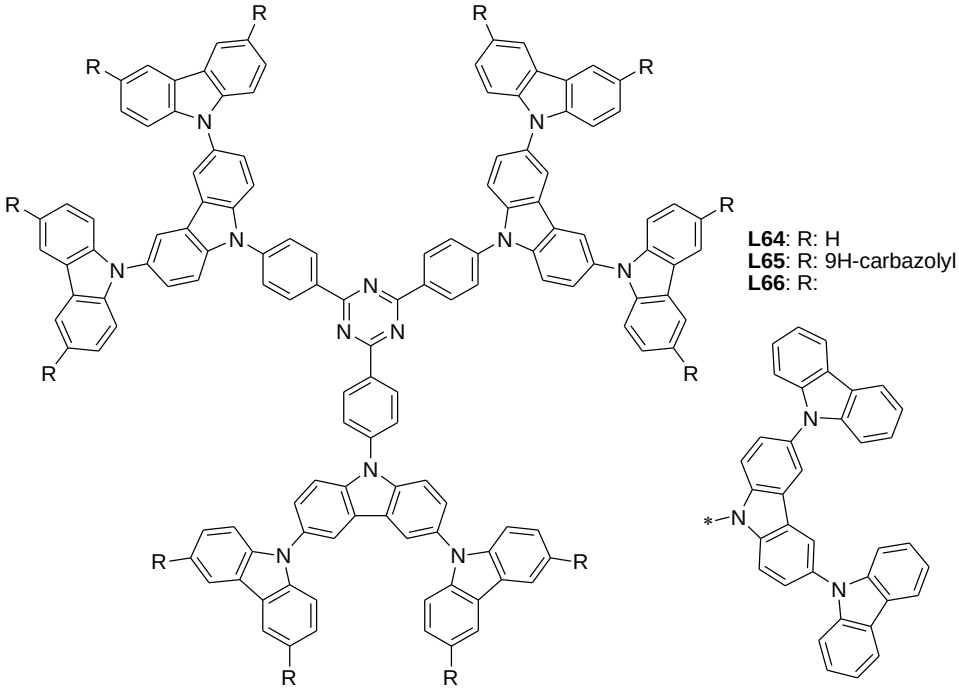

Fig. 18 Dendrimers **L64–L66**[70]

The dendrimers **L67–L69** (**Fig. 19**) were described by Sun with co-authors[71]. The compounds are stable at temperature higher than 388 °C but not consisting molecular glasses. The triplet energies of derivatives **L67** and **L68** are 2.33eV, but in the case of tricarbazolyl-substituted dendrimer **L69**, the energy is decreasing to 2.29eV. The singlet energies are 2.51, 2.50, 2.49, and a splitting of singlet-triplet energies are 0.18, 0.17, 0.20eV for derivatives **L67–L69** respectively. The maxima of PL were observed in the range 541–553nm with the quantum yield of 44, 56 and 71% for dendrimers **L67–L69** respectively. The devices were formed by simple structure: ITO/ PEDOT:PSS/ **L67–L69**/ TPBi/ Cs_2CO_3/ Al. The OLEDs showed green electroluminescence with maximum external quantum efficiencies 1.2, 6.5 and 11.8% for emitters **L67–L69** respectively.

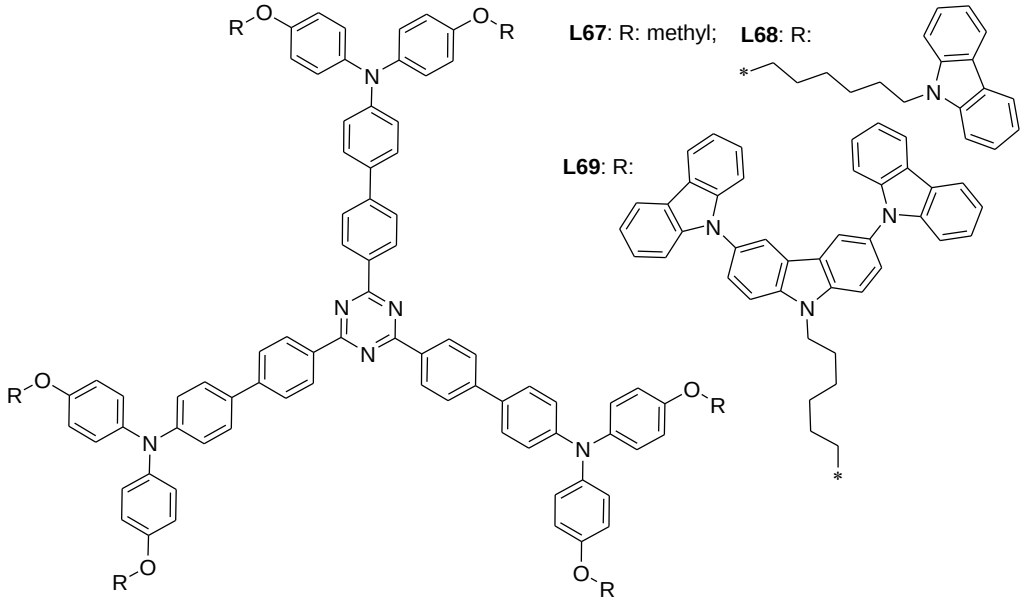

Fig. 19 Dendrimers **L67–L69**[71]

The derivative **L70** was investigated by Zhang with co-workers[61], and dendrimers **L71** and **L72** were described by Li and co-authors[72]. The derivative **L70** was investigated as an emitter for different structures of OLED devices. The simplest structure was ITO/ MoO_3/ **L70**/ LiF/ AL. There was observed 508nm emission maxima and 0.06% maximal EQE only. The best investigated structure with **L69** emitter was ITO/MoO_3/mCP/**L70**/TPBi/LiF/AL. The maximum EQE of this structure was 18.9% with 510nm electroluminescence maxima. The influence of temperature of efficiency for TADF emitters was investigated with derivatives **L71** and **L72** in the OLED structures. There were used no holes transporting layers. The structures of OLED were ITO/PEDOT:PSS/**L71** or **L72**/TPBi/Liq/Al.

Table 7 The thermal behaviour of OLED characteristics

Emitter	Temperature, °C	λ_{OLED}, nm	EQE_{max}, %	Ref. No.
L71	Ambient	546	9.7	72
	80		12.0	
	120		8.8	
	160		8.3	
L72	Ambient	522	3.3	
	80	522	5.2	
	120	528	5.2	
	160	528	4.7	

As the results are indicating in **table 7**, the highest EQE of OLEDs were observed at temperatures of 80 °C. The exciplex emitter structure of OLED was formed by the structure: ITO/PEDOT:PSS/**L71**/TmPyPB/Liq/Al. There was achieved 13.8% maximal EQE with 552nm electroluminescence maxima. The dendrimers **L73** and **L74** were investigated by Luo et al[73]. The derivatives exhibited high mass loss temperature of 459 and 479 °C and very high glass transition point of 272 and 274 °C for derivatives **L73** and **L74**. The PL wavelength maxima of dendrimers are 492 and 464nm. The PL quantum yield of derivative **L74** is 48.2%. The singlet and triplet energies of dendrimers are similar: 2.52, 2.58 and 2.51, 2.50eV for **L73** and **L74** respectively, but singlet-triplet energies splitting are 0.01 and 0.08eV. The OLED devices containing dendrimeric emitters were made by scheme ITO/PEDOT:PSS/**L73** or **L74**/TPBi/Liq/Al. The OLED with L72 emitter light sky-blue light with 12.2% maximal EQE and **L74** OLED made blue light electroluminescence with 2.2% maximal EQE.

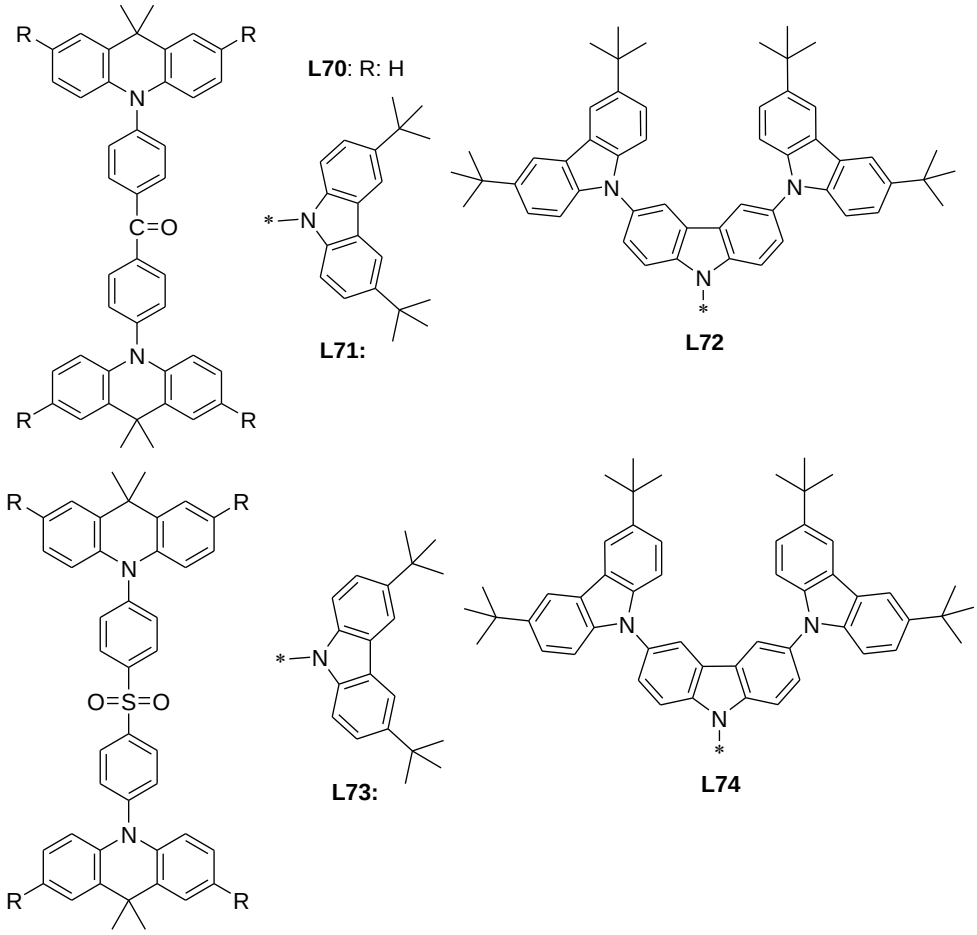

Fig. 20 Dendrimers **L70–L74**[61,72,73]

Copolymers **L75**–**L77** and polymer **L78** were investigated by Ren and co-workers[74]. The compositions of copolymers were confirmed by elemental analysis exactly. The

molecular weight of polymers was higher than 11500. The thermal investigations showed that polymers have high thermal stability higher than 400 °C, and it were consisting glasses at temperature higher than 217 °C. The narrowest splitting of singlet–triplet energies showed polymers **L75** and **L78** as 0.35 and 0.4eV respectively. The PL maxima of polymers are in the range from 535 for **L75** to 556nm for **L78** polymers. These polymers were used for OLED forming by the scheme: ITO/PEDOT:PSS/10% **L75**–**L79**:mCP/TPBi/LiF/Al. The devices exhibited electroluminescence with 533–539nm maxima for copolymers **L75**–**L77** and 556nm for **L78** polymer. The maximum external quantum efficiencies were 20.1, 15.2, 1.8 and 1.4% for polymers **L75**–**L78** respectively. Polymer **L79** was described by Nobuyasu with co-authors[75]. The device was made by the structure: ITO/PEDOT:PSS/10% **L79**, 40% PBO, 50% PVCz/TPBi/LiF/Al, and there was achieved 11.05% maximal EQE. The copolymers **L80** and **L81** were described by Zhu and co-authors[76]. The PL spectra of copolymers were investigated from films, and there was observed 487 and 507nm maxima of peaks for copolymers **L80** and **L81** respectively with quantum yields of PL that were 8 and 28% respectively. Triazine-substituted copolymer **L81** exhibited lower singlet-triplet energies splitting (0.13eV) than **L80** (0.37eV). The devices were formed by the scheme: ITO/ PEDOT:PSS /**L80** or **L81**/ TmPyPB/ LiF/ Al. The characteristics of devices were 1.3% maximal EQE of 521nm maxima light for **L80** emitter and 12.6% maximal EQE of 508nm for **L81** emitter device (**Fig. 21**).

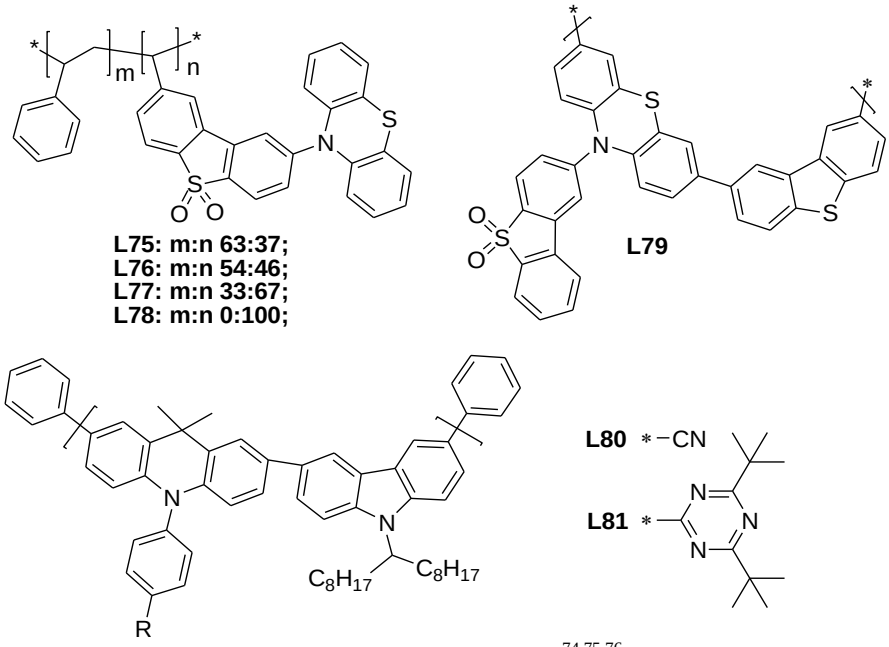

Fig. 21 Polymers **L75**–**L81**[74,75,76]

2.3. Summary of literature review

The best results of OLED investigations that were described in the literature review were summarised in **table 8**. As seen in table, the devices based on emitters with nitrogen acceptor exhibit maximum EQE at approximately 29%. It is significant that emitters are forming exciplexes with host materials, and large bathochromic shifts were observed. It is worth noting that the synthesis of these materials is usually difficult and have low yields. Sulfone based derivatives are not that effective emitters, but the wavelength of PL maxima is short. It should be noted that sulfone-based derivatives exhibit higher thermal stability. The OLED structures based on dendrimeric and polymeric emitters exhibit remarkably lower efficiency.
The main advantages of TADF materials are relatively cheap raw materials for the synthesis, wide possibilities of the design of the structures of compounds with desirable characteristics and high enough efficiencies of electroluminescent devices. The main raw-materials for the synthesis are well-known compounds, such as carbazole, and wide range of electron accepting compounds. The most widely used electron accepting moieties are carbonitriles, sulphones, nitrogen-containing aromatic rings, ketones. The carbazole, cyanobenzene and cyanopyridine based derivatives are exhibiting high photoluminescence quantum yields with blue emission and other desirable characteristics. Due to the possibilities to use cheap raw materials and select simple synthetic routes, TADF materials are promising in comparison to the expensive organic metal chelates, which are used in phosphorescent organic light emitting diodes.

Table 8 The most perspective reviewd materials

Class of compounds	**No. of derivative**	**λ_{max}, nm**	**QY, %**	**EQE_{max}, %**	**OLED colour**	**Ref. No.**
Cyanobenzene	**L11**	431	50	29.5	blue	35
Dicyanobenzene:	**L3**	507	94	19.3	green	32
dimer	**L15**	477	91	18.9	sky-blue	38
dimer	**L19**	448	66	21.8	sky-blue	40
Cyanopyridine	**L21**	488	91.6	23.9	sky-blue	41
Dicyanopyridine	**L23**	550	90	29.2	yellow	41
Cyanopyrazine	**L25**	572	16	15.6	yellow	42
Pyrimidine	**L34**	not described		23.7	sky-blue	45
Triazine	**L38**	460	82	15.7	sky-blue	47
Thianthrene tetraoxide	**L44**	487	71	4	sky-blue	50
	L46	558	72	5.1	yellow	50
Diphenylsulfone	**L53**	not described		22.6	blue	55
Tetraphenyldisulfone	**L63**	not described		24.5	sky-blue	64

The main disadvantages of TADF-based OLEDs are short lifetime, still too low efficiency of blue devices, long and difficult manufacturing of multilayer structures by vacuum evaporation. The fabrication of OLEDs by solution processing is much simpler, but the efficiencies of polymeric devices are usually low. Blue OLEDs showing maximum external quantum efficiency higher than 20% were reported, but their stability was low. Yellow and red TADF based OLEDs exhibit high efficiencies and much better stability. The stock of inexpensive, easily preparable

OLED emitters is still not sufficient. In addition, structure-properties relationship of organic emitters intended for OLEDs has not been sufficiently explored yet.

3. EXPERIMENTAL SECTION
3.1. Instrumentation

Nuclear magnetic resonance spectra were recorded by *Bruker Avance III* (400 MHz – ^{1}H, 100MHz – ^{13}C spectra) or *Bruker Avance III* (700 MHz – ^{1}H, 176 MHz – ^{13}C) equipment. All measurements were recorded from the solutions in deuterated chloroform, acetone or DMSO with tetramethylsilane as internal standard.

Infrared spectra were recorded from KBr pellets with 1% of the exploring material by *Perkin Elmer Spectrum BX II FT-IR System equipment.*

Mass spectra were recorded by *Waters SQ Detector 2* equipment. The samples were prepared as diluted solutions in methanol.

Ultraviolet-visible light absorption spectra were recorded by *Perkin Elmer lambda 25* equipment from diluted solutions or thin films on quartz plates at ambient temperature. The experimental error of measurements is 1nm. The optical band gaps were calculated by Planck hypothesis formula **2**[77]:

$$E = h\nu = \frac{hc}{\lambda} = \frac{4.136\times10^{-15}eVs\times2.998\times10^{8}ms^{-1}}{\lambda\times10^{-9}m} \approx \frac{1240}{\lambda_{edge}(nm)}eV \qquad (2),$$

where h is Planck's constant, ν – frequency, c – speed of light, λ – wavelength.

Fluorescence and **phosphorescence** (77K) spectra, **fluorescence quantum yields** and **fluorescence decay times** were recorded and calculated by *Edinburg instruments FLS980* equipment from diluted solutions or thin films. The declared signal and noise ration is higher than 35000:1. The excitation of photoluminescence was exited by a 450W xenon arc lamp with *TMS300* monochromator or *PicoQuant LDH-D-C-375* picosecond laser (374nm), and the emission was detected by a red cooled detector *Hamamatsu R928P*. The manufacturer declared accuracy of the wavelength is ±0.2nm. The quantum yields of photoluminescence were measured by using a special calibrated sphere. The manufacturer declared that the experimental error of measurements of PL quantum yields is ±2%. The photoluminescence measurements at different temperatures were investigated by using liquid nitrogen cooled cryostat *Optistat DN2* under inert N_2 atmosphere. The accuracy of temperature measurements is ±0.1K.
The singlet and triplet energies were calculated from the onset of fluorescence or phosphorescence spectra by Planck hypothesis.

The colour coordinates of photoluminescence were calculated according to the International Commission on Illumination (CIE) recommended formulas[78].

The noisy curves of photoluminescence were **smoothed**, or the fitting curves were calculated by adjacent-averaging method according to formula **3** by Origin 8.1 software[79].

$$w_j = 1 - \left(\frac{(j-i)}{\left(\frac{(N+1)}{2}\right)} \right)^2 \qquad (3),$$

where w is the average value, N – points on the window (50), j, i – values.

Differential scanning calorimetry measurements were carried out by using Perkin Elmer DSC 8500 equipment at a heating rate of 10°C/min. The manufacturer declared accuracy of measurements is ±0.05 °C. The energy flow was recorded. The energy flow change, which depends from temperature, shows the structural transformations.

Thermogravimetric analysis measurements were recorded by *Perkin Elmer TGA 4000* equipment. The measurements of mass were recorded at heating rate of 20 °C per minute at nitrogen atmosphere. The declared accuracy of measurements is ±0.5 °C of temperature and ±0.02% of sample mass. Mass changes were registered by raising temperature, and the mass lost curves were recorded.

Cyclic voltammetry measurements were carried out by using *micro-AUTOLAB III equipment* with Ag/Ag^+, Pt and working carbon electrode of a glassy carbon of 0.12 cm^2 surface. The measurements were investigated from tetrabutylamonium hexfluorophosphate 0.1M solutions in dichloromethane or acetonitrile in inert argon atmosphere. The measurements were calibrated by using an internal ferrocene standard. The investigations were recorded at voltage rate of 50mV/s. The current was recorded. The declared accuracy of measurements is ±0.2%. The current peaks are shown as electrochemical transformations. The ionization potentials and electron affinities were calculated from the oxidation-reduction or reduction-oxidation potentials according to formulas **4** and **5**[80]:

$$-I_p(CV)=U_{ox}+4.8 \qquad (4),$$
$$-E_A(CV)=U_{red}+4.8 \qquad (5),$$

where U_{ox} is ionization potential by oxidation-reduction conditions, Fc - ferocene ionization potential, U_{red} - ionization potentials by reduction-oxidation conditions.

X-ray diffraction analyses were investigated by *Rigaku Xtalab mini* equipment from the single crystal of derivatives. The calculations of crystal characteristics were calculated by Mercury 3.8 software[81]. The method is based on electromagnetic waves diffraction of crystals, and the slopes of beams were recorded. The distances between atoms were calculated according to Bregs law (**6**):

$$n\lambda = d \sin 2\Theta \qquad (6),$$

where n is 1,2…, λ - wavelength of X-ray, d - spacing of the crystal layers, Θ – angle.

Melting points were investigated by *Electrothermal MEL-TEMP* melting point equipment. The measurements were explored in the capillary at air conditions. The measurments heating rate 1°C/min and the processes were observed visually.

Elemental analysis was measured by *Exeter Analytical CE-440 Elemental Analyzer* equipment. The manufacturer declared error of measurements is ±0.15%.

Charge mobilities were recorded by the time of flight (ToF) method[82,83].
The structures ITO/material/Al were formed by vacuum deposition, and the charges mobility was generated by Nd: YAG pulsing laser (*EXPLA NL300*) with 355nm wavelength, and the pulse period was 3-6ns. The declared pulse stability of equipment is ±3%. The mobility's were calculated from the transit photocurrent curves. The measurements were observed by *Keithley 6517B* electrometer, and a *Tektronix TDS 3052C* oscilloscope. The accuracy of voltage is ±1%, and the accuracy of the oscilloscope is ±21%. The principle of measurement is the determination of time crossing charges till excitation of a laser beam to the stopping of conductivity of the prepared device. The conductivity is excitated by picosecond laser beam to make electron and hole pairs. The different charges move to different electrodes with fixed voltage which not initiate conductivity. The conductivity is stopped; than, the free charges go out from semiconductor layer. ITO and aliuminium were used as electrodes. The thickness of semiconductors layers were measured by CELIV method. The mobility charges were calculated by formula **7**:

$$\mu = \frac{d^2}{Ut_t} \qquad (7),$$

where d is the thickness of the cell, U – voltage, t – time.

Carrier extraction by linearly increasing the voltage method[84,85] (CELIV) was used to estimate the thickness of OLEDs layers[86]. The charge carriers were excited by Nd:YAG laser pulses (355nm, pulse duration – 25ps). The results were recorded by *Tektronix AFG 3011* delay generator and a digital storage oscilloscope *Tektronix DPO 4032*. The declared accuracy of equipments are ±1%. The method of CELIV is similar to ToF, but the conductivity of layer is excitating by the raising of voltage with a light beam or without. The thickness of layers was calculated from photocurrent curves by formula **7** as ToF.

Ionization potentials were measured by the electron photoemission method that is described in literature[87, 88]. The materials were coated on Al plates from solutions at THF, and the layers were prepared by spin-coating with methylmethacrylate and

methacrylic acid as adhesive materials. The accuracy of measurements is ±1%. The electrode voltage was 300V, and the samples were illuminated by monochromatic light from *SBN-D130-CM and CM110 1/8 m* monochromator. The photocurrent were measured by *Keithley 6517B* electrometer. The photoelectrons were excited by UV light, and the photoelectrons energy were measured.

OLEDs were prepared from the purchased materials of host and transporting layers with synthesized emitters. The purchased materials were used:
1) Indium thin oxide (ITO) was used as electrode;
2) Molybdenum trioxide, m-MTDATA were used as holes injection layer;
3) TCTA, NPB were used as holes transportation and electrons blocking layer;
4) For hosts were used mCP, DPEPO, TCTA, TCz, m-MTDATA;
5) BPhen and TPBi were used as holes blocking and electrons transporting layer;
6) Ca and Al were used as electrode;
The layers were formed by vacuum evaporation at vacuum lower than $2 \cdot 10^{-6}$mBar. All layers were about 6mm^2 working area. The host-materials and transporting layers were chosen by experimental results that were calculated from fluorescence measurements. The properties of devices were measured by a *Keithley 6517B* electrometer and a *Keithley 2400C* sourcemeter in air conditions. The devices were not passive after the made measurements. The brightness measurements were measured by calibrated photodiode. The calibrating mistake of photodiode is ±2%. The seven samples of same structure devices were made and the best sample measurements were fixed.

3.2. Materials

2,2,6,6-Tetramethylheptane-3,5-dione (98% Sigma-Aldrich), 2-bromo-5-methoxynitrobenzene (98% Sigma-Aldrich), 3,4-difluoro-bromobenzene (99% Sigma-Aldrich), 3-amino-9H-ethylcarbazole (98% Sigma-Aldrich), 4-(*tert*-butyl)-aniline (98% Sigma-Aldrich), 4,4'-dibromobiphenyl (95% Aldrich), 4-bromobiphenyl (95% Aldrich), 4-iodobenzonitrile (99% Sigma-Aldrich), 4-methoxyiodobenzene (99% Sigma-Aldrich), 6-crown-18 (99% Sigma-Aldrich), acetic acid (99% Eurochemicals), bis-(triphenylphosphine)-palladium (II) dichloride (95% Sigma-Aldrich), bromoethane (95% Aldrich), carbazole (95% Reakim), copper (99% Sigma-Aldrich), copper cyanide (98% Sigma-Aldrich), copper dichloride dihydrate (95% Reakim), diphenylamine (99% Reakim), hydrochloric acid (36% Eurochemicals), iodobenzene (99% Sigma-Aldrich), malononitrile (95% Sigma-Aldrich), methylanthranilate (98% Sigma-Aldrich), methylmagnesiumiodide (3M in hexane Acros), N-bromosuccinimide (98% Sigma-Aldrich), nitric acid (65% Eurochemicals), *ortho*-phosphoric acid (98% Eurochemicals), paladium (II) acetate (98% Sigma-Aldrich), phenothiazine (99% Acros), phenoxazine (97% Sigma-Aldrich), phenylboronic acid (95% Sigma-Aldrich), potasium carbonate (98% Eurochemicals), potassium iodate (95% Reakim), potassium iodide (95% Reakim), potassium *tert*-butoxide (99% Sigma-Aldrich), pyridine (95% Reakim), sodium (95% Reakim), sodium hydride (60% in mineral oil Sigma-Aldrich), sodium *tert*-

butoxide (99% Sigma-Aldrich), *tert*-butylnitrite (98% Sigma-Aldrich), tri-(*tert*-butyl)-phosphine (1M in toluene Sigma-Aldrich), trimethylorthobenzoate (99% Sigma-Aldrich), triphenylphosphine (95% Sigma-Aldrich).

All solvents were purchased from *Sigma-Aldrich*, *Eurochemicals* or *Fluka*. The solvents were distilled before fluorescence spectra measurements.
The copper dichloride anhydrate was prepared by heating copper dichloride dihydrate at 200 °C temperature in a vacuum, and other chemicals were used as received.

3.3. Synthesis

3-Iodo-9H-carbazole (M1, FW=293 g/mol, m.p.=238–239 °C , lit. 238 °C) was synthesized as described in literature source [89]. The off-white solids were obtained.

9H-Ethyl-3-iodocarbazole (M2, FW=321 g/mol, m.p.=84–85 °C , lit. 83 °C [89])
The material was as described in literature procedure[90]. The product was isolated as light brown needles.

3,6-Dibromocarbazole (M3, FW=325 g/mol, m.p.=211–213 °C , lit. 209–210 °C) was synthesized as described in literature[91]. The product was obtained as white crystals.

3-Cyano-9H-carbazole (M4):
3-Iodocarbazole (4.50 g, 15.4 mmol), copper (I) cyanide (2.79 g, 30.8 mmol) and N-methyl-2-pyrrolidone (50 ml) were mixed in a flask. The reaction mixture was heated at 155 °C under nitrogen atmosphere for 22 h. The reaction mixture was then cooled to room temperature and poured into the solution of cold water (500 ml), hydrochloric acid (80 ml) and $FeCl_3$ (16 g). The reaction mixture was heated at 80 °C for 1 h, and then cooled to room temperature. The precipitate which had formed was filtered off. The product was crystallized from methanol and was obtained as light brown crystals (mp = 187–188 °C, lit.: 189–190 °C [92]) in 30% (0.89 g) yield.
^{1}H NMR (400 MHz, DMSO-d_6) δ (ppm): 10.50 (s, 1H, NH), 7.33 (s, 1H, Ar), 6.87 (d, J = 7.7 Hz, 1H, Ar), 6.38 (d, J = 8.3 Hz, 1H, Ar), 6.26 (d, J = 8.4 Hz, 1H, Ar), 6.20 (d, J = 8.0 Hz, 1H, Ar), 6.11 (t, J = 7.4 Hz, 1H, Ar), 5.88 (t, J = 7.3 Hz, 1H, Ar).
^{13}C NMR (100 MHz, DMSO-d_6) δ (ppm):142.1, 140.7, 129.0, 127.4, 126.0, 123.0, 122.0, 121.4, 121.0, 120.3, 112.4, 112.0, 100.7.

4,4'-Dibromo-2-nitro-1,1'-biphenyl (**M5**, FW=357 g/mol, m.p.=126–127 °C, lit. 125–127 °C) was synthesized as described in literature[93]. The yellow crystals were obtained.

2,7-Dibromo-9H-carbazole (**M6**, FW=325 g/mol, m.p.=234–235 °C, lit. 236–238 °C)
was synthesized as described in literature[93]. The off-white crystals were obtained.

2,7-Dicyanocarbazole (**M7**, FW=217 g/mol, m.p.=279–280 °C, lit. 279–281 °C) was prepared according to the published procedure[94].

3,6-Dimethoxy-9H-carbazole (**M8**, FW=227 g/mol, m. p.=133–134 °C, lit. 131–133 °C) was prepared according to the published procedure[95]. The light brown crystals were obtained.

3,6-Diphenyl-9H-carbazole (M9, FW=319 g/mol, m.p.=184–185 °C, lit. 186–187 °C) was synthesized as described in literature[96]. The product was isolated as white needles.

4-Bromo-2-nitrobiphenyl (M10, FW=278 g/mol, m.p.=126–127 °C, lit. 125–127 °C)
The synthesis of derivative was made by literature method[97]. The material was received as yellow crystals.

2-Bromo-9H-carbazole (**M11**, FW=246 g/mol, m.p.=251–253 °C, lit. 250–251 °C) was synthesized by reported procedure[98]. The product was isolated as white crystals.

2-Bromo-9H-ethylcarbazole (**M12**, FW=274 g/mol, m.p.=79–80 °C, lit. 77–79 °C). The material was prepared from **M11** by alkylation as described early[99]. The material was obtained as white needles.

Methyl-2-(phenylamino)-benzoate (**M13**, FW=227 g/mol) was synthesized from methylanthranilate and iodobenzene by Ullman coupling reaction as described in literature[100]. The product was isolated as the yellow oil.

2-(2-(Phenylamino)phenyl)-propan-2-ol (**M14**, FW=227 g/mol) was prepared by Grignard reaction from M13 and methyl magnesium iodide as described in literature [101]. The product was isolated as the orange oil.

9,9-Dimethyl-10H-acridane (**M15**, FW=209 g/mol) was prepared as described in literature[101.] and obtained as transparent crystals.

4,4'-Dimethoxi-2-nitrobiphenyl: (**M16**, FW=259 g/mol, m.p.=138–140 °C) was prepared by the reported procedure[102].

2,7-Dimethoxi-9H-carbazole (**M17**, FW=227 g/mol, m.p.=275–277 °C, lit. 271–272 °C). The preparation of derivative was described in literature[103]

1,3-Dibromo-4,6-difluorobenzene (**M18**, FW=272 g/mol, m.p.= 205–207 °C (subl.)) was synthesized as described in literature[104]. The material was obtained as white needles form crystals.

1,3-Dicyano-4,6-difluorobenzene (M19 FW=164 g/mol, m.p.= 107–109 °C (exp.)) was prepared from Rosendmund-von Brown reaction as described in literature[104]. The material was obtained as transparent crystals with 38% of yield.

2-Amino-6-chloro-4-phenylpyridine-3,5-dicarbonitrile (**M20**, FW=255 g/mol) was prepared according to the publicized procedure[105]. The yellow crystals were obtained with 60% of yield.

2,6-Dichloro-4-phenylpyridine-3,5-dicarbonitrile (**M21**, FW=274 g/mol, mp=203–204 °C(exp.)) was prepared from **M20** and anhydrous copper dichloride with t-butylnitrite in acetonitrile as described in literature[106]. The product was obtained as transparent crystals with 38% of yield.

N-Biphenyl-N-(4-*tert*-butylphenyl)-amine (M22):
The 4-*t*-butylaniline (2.5g, 16.75mmol), 4-bromobiphenyl (3.9g, 16.75mmol), sodium tert-butoxide (3.2g, 33.5mmol), tri-*t*-butylphosphine (1.7ml, 1M), and dry toluene (20ml) were charged. The mixture was degassed, and palladium (II) acetate (0.2g, 0.9mmol) was added. The reaction mixture was refluxed under argon atmosphere overnight. After cooling to room temperature, the reaction mixture was poured into water, extracted with ethyl acetate. After being dried over sodium sulfate and filtered, the solvent was removed, and the crude product was purified by silica gel column chromatography by using ethyl acetate/hexane 1:20 as an eluent. The product was recrystallized from methanol and toluene mixture and was obtained as white crystals (FM=301 g/mol, mp=96–97°C, mp=90–92 °C (lit.[107])) in 14% (0.7g) yield.
1H NMR (400 MHz, $CDCl_3$) δ (ppm): 7.55 (d, J = 7.6 Hz, 2H), 7.49 (d, J = 8.2 Hz, 2H), 7.40 (t, J = 7.6 Hz, 2H), 7.33–7.23 (m, 3H), 7.09 (s, 4H), 5.93 (s, 1H, NH), 1.32 (s, 9H, CH_3).

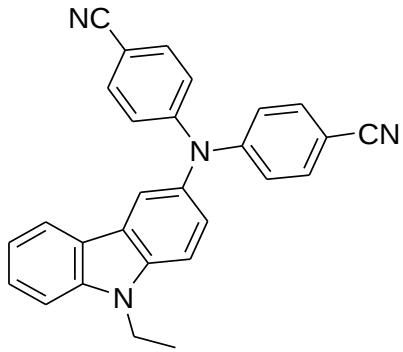

N,N-(bis(4-cyanophenyl))-N-(9-ethylcarbazol-3-yl)-amine* (C1):
The 3-amino-9H-ethylcarbazole (0.7g, 3.3mmol), 4-cyanoiodobenzene (3g, 13.2mmol), 18-crown-6 (0.3g), copper (1.47g, 23mmol) and potassium carbonate (5.46 g, 39.6 mmol) were added to three necks flask, and o-dichlorobenzene (15 ml) was filled. The reaction mixture was stirred for 24h under N_2. After reaction, the mixture was filtered, the filtrate was evaporated and adsorbed on SiO_2. The product was separated by column chromatography (eluent EtOAc: hexane 1:20), (fw = 412 g/mol, mp = 168-171 °C) in 32% (0.45 g) yield.

* The synthesis of derivatives **C1–C4** was described in reference: SKUODIS, E. et al. OLEDs based on the emission of interface and bulk exciplexes formed by cyano-substituted carbazole derivative. *Dyes and Pigments* **2017**, *vol. 139*, 795–807; eISSN 1873-3743.

^{1}H NMR (400 MHz, DMSO-d_6) δ (ppm): 8.15 (d, J = 7.8 Hz, 1H, Ar), 8.11 (s, 1H, Ar), 7.74–7.69 (m, 5H, Ar), 7.65 (d, J = 8.2 Hz, 1H, Ar), 7.48 (t, J = 8.3 Hz, 1H, Ar), 7.30 (dd, J =8.6 Hz, 2.1 Hz, 1H, Ar), 7.21–7.14 (m, 5H, Ar), 4.47 (q, J = 7.1 Hz, 2H, NCH2), 1.35 (t, J = 7 Hz, 3H, CH_3).
^{13}C NMR (100 MHz, DMSO-d_6) δ (ppm): 150.9, 140.6, 138.6, 136.2, 134.1, 133.4, 128.5, 126.8, 126.4, 124.0, 122.3, 121.3, 120.8, 119.6, 111.4, 109.8, 104.1, 37.1 (NCH_2), 13.8 (CH_3).
MS (ESI) m/z (%) = 411 (M^+-H, 100).
FTIR ν_{max} in cm^{-1} (KBr): (C-H Ar) 3046; (C-H Al) 2975; (-CN) 2219; (C=C Ar) 1592, 1498; (C-H Ar) 747.

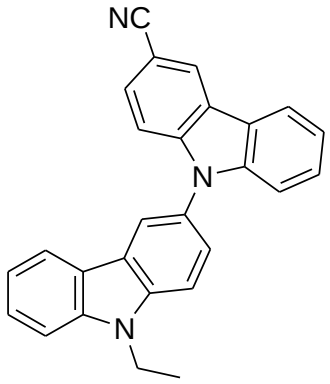

3-(3-Cyanocarbazol-9-yl)-9-ethylcarbazole (C2):
The **C2** was synthesized by the same Ullman-coupling procedure as **C1**. 3-Iodo-9-ethylcarbazole (0.72 g, 2.25 mmol), 3-cyanocarbazole (0.3 g, 1.5 mmol), potassium carbonate (0.62 g, 4.5 mmol), copper (0.19 g, 3 mmol), 18-crown-6 (0.04 g) were used, and 10 ml of o-DCB was used as a solvent. The reaction mixture was stirred at 180 °C temperature under nitrogen atmosphere for 24 h. The product was purified by silica gel column chromatography (eluent ethyl acetate: hexane) as an eluent. The target compound was obtained as yellow crystals (fw = 385 g/mol, mp = 214–216 °C) with 0.45 g (78%) yield.
^{1}H NMR (400 MHz, $CDCl_3$) δ (ppm): 8.50 (s, 1H, Ar), 8.23–8.21 (m, 2H, Ar), 8.11 (d, J = 7.8 Hz, 1H, Ar), 7.67–7.64 (m, 2H, Ar), 7.60–7.48 (m, 4H, Ar), 7.42–7.38 (m, 3H, Ar), 7.31 (t, J = 8.0 Hz, 1H, Ar), 4.52 (q, J = 7.2 Hz, 2H, NCH2), 1.57 (t, J = 7.2 Hz, 3H, CH3).
^{13}C NMR (100 MHz, $CDCl_3$) δ (ppm): 143.6, 142.8, 140.7, 139.5, 129.1, 127.4, 127.3, 126.7, 125.3, 124.8, 124.0, 123.2, 123.0, 122.4, 122.0, 120.9, 119.6, 119.5, 110.7, 110.6, 109.7, 108.9, 102.2, 37.9 (NCH_2), 13.9 (CH_3).
MS (ESI) m/z (%) = 386 (M^+-H, 30).
FTIR ν_{max} in cm^{-1} (KBr): (C-H Ar) 3047; (C-H Al) 2972, 2929; (-CN) 2214; (C=C Ar) 1595, 1472; (C-H Ar) 807, 747.

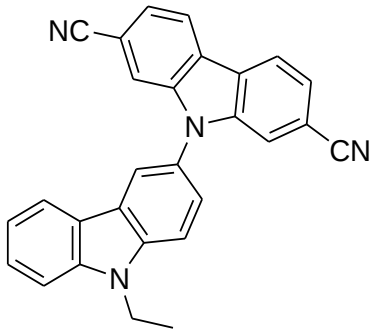

3-(2,7-Dicyanocarbazol-9-yl)-9-ethylcarbazole (C3):

The derivative was prepared by **C1** method. 3-Iodo-9-ethylcarbazole (2.2 g, 6.9 mmol), 2,7- dicyanocarbazole (1.5 g, 6.9 mmol), potassium carbonate (7.62 g, 55.2 mmol), copper (1.75 g, 27.6 mmol), 18-crown-6 (0.73 g) and 30 ml of ortho-dichlorobenzene were used. The reaction mixture was refluxed under nitrogen atmosphere for 72 h. The product was separated by column chromatography (eluent THF: hexane 1:9). The product was obtained as greenish crystals (fw = 410 g/ mol, mp =270–272 °C) in 20% (0.55 g) yield.

^{1}H NMR (700 MHz, $CDCl_3$) δ (ppm): 8.17 (d, J = 8.0 Hz, 2H, Ar), 8.08 (s,1H, Ar), 8.00 (d, J = 7.8 Hz,1H, Ar), 7.60 (s, 2H, Ar), 7.56 (d, J = 8.1 Hz, 1H, Ar), 7.50–7.46 (m, 3H, Ar), 7.45–7.40 (m, 2H, Ar), 7.20 (t, J = 7.5 Hz, 2H, Ar), 4.41 (q, J = 7.5 Hz, 1H, NCH_2), 1.46 (t, J = 7.3 Hz, 3H, CH_3).

^{13}C NMR (176 MHz, $CDCl_3$) δ (ppm): 141.1, 139.7, 138.7, 125.9, 125.1, 124.0, 123.4, 123.2, 122.4, 121.1, 120.9, 119.8, 118.7, 118.4, 113.9, 109.4, 109.0, 108.0, 36.9 (NCH_2), 12.9 (CH_3).

MS (ESI) m/z (%) = 411 (M^++H, 35).

FTIR ν_{max} in cm^{-1} (KBr): (C-H Ar) 3053; (C-H Al) 2978, 2924; (-CN) 2227; (C=C Ar) 1496; (C-H Ar) 806.

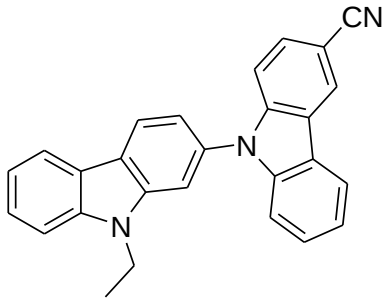

2-(3-Cyanocarbazol-9-yl)-9-ethylcarbazole (C4):

The 2-bromo-9-ethylcarbazole (1 g, 3.6 mmol), 3-cyano-9H-carbazole (1.04 g, 5.4 mmol), potassium *tert*-butoxide (2 g, 18 mmol), copper iodide (1.4 g, 7.2 mmol), 2,2,6,6-tetramethyl-3,5- heptanedione (TMHDO, 0.4 ml) and anhydrous DMF (20 ml) were charged to round bottom flask. The mixture was refluxed under nitrogen atmosphere for 24 h. After it, the reaction mixture was poured into water, extracted with ethyl acetate, washed with 2 N HCl and water. After being dried over Na_2SO_4

and filtered, the solvent was removed, and the crude product was purified by column chromatography (eluent THF: hexane 9: 1). The product was crystallized from methanol and was obtained as yellowish crystals (fw = 385 g/mol, mp = 187−188 °C) in 47% (0.65 g) yield.
^{1}H NMR (700 MHz, $CDCl_3$) δ (ppm): 8.39 (s, 1H, Ar), 8.21 (d, J = 8.0 Hz, 1H, Ar), 8.10 (d, J = 7.8 Hz, 2H, Ar), 7.56 (dd, J = 8.5, 1.5 Hz, 1H, Ar), 7.48−7.37 (m, 6H, Ar), 7.30 (t, J = 7.4 Hz, 1H, Ar), 7.24 (m, 2H, Ar), 4.29 (q, J = 7.2 Hz, 2H, NCH_2), 1.36 (t, J = 7.2 Hz, 3H, CH_3).
^{13}C NMR (176 MHz, $CDCl_3$) δ (ppm): 142.1, 141.2, 139.7, 139.5, 132.8, 128.2, 126.4, 125.4, 124.3, 122.4, 122.0, 121.4, 121.1, 120.7, 120.1, 119.7, 119.6, 119.5, 118.6, 116.8, 109.7, 109.5, 107.8, 106.2, 101.5, 36.8 (NCH_2), 12.8 (CH_3).
MS (ESI) m/z (%) = 386 (M^++H, 100).
FTIR ν_{max} in cm^{-1} (KBr): (C-H Ar) 3060; (C-H Al) 2972, 2932; (-CN) 2220; (C=C Ar) 1597; (C-H Ar) 810, 739.

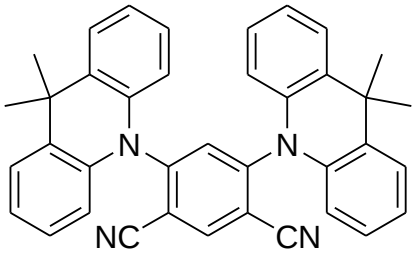

4,6-Bis(9,9-dimethylacridan-10-yl)isophthalonitrile* (N1):
Potassium *tert*-butoxide (0.75g, 6.7 mmol) was added to a stirred solution of 9,9-dimethyl-10H-acridane (1g, 4.78 mmol) in dry DMF (20 ml) under argon atmosphere at room temperature. After stirring for 30 min, 4,6-difluoroisophthalnitrile (0.3g, 1.91 mmol) was added. The reaction mixture was stirred at 30 °C temperature for 3 hours. The reaction mixture was quenched with water and neutralized by 2M HCl. After extraction by using ethyl acetate, the mixture was purified by column chromatography on silica gel by using acetone/hexane (1/5) as an eluent and recrystallized from the mixture of dichloromethane and methanol. The target compound was obtained as yellow needles-form crystals (fw = 542 g/mol, mp = 291–292 °C) in 27% (0.28g) yield.
MS (ESI) *m/z* (%) = 543 (M^++H, 21).
^{1}H NMR (400 MHz, $CDCl_3$) δ (ppm): 8.51 (s, 1H, Ar), 7.77 (s, 1H, Ar), 7.52 (dd, J_1 = 7.5, J_2 = 1.8 Hz, 4H, Ar), 7.10–7.02 (m, 8H, Ar), 6.23 (dd, J_1 = 7.9, J_2 = 1.4 Hz, 4H, Ar), 1.71 (s, 12H, CH_3).
^{13}C NMR (101 MHz, $CDCl_3$) δ (ppm): 150.7, 141.6, 139.8, 139.0, 131.0, 126.8, 126.2, 122.5, 117.9, 114.0, 113.0, 36.1 ($\underline{C}H_3$), 31.2 ($\underline{C}$–$(CH_3)_2$).
FTIR ν_{max} in cm^{-1} (KBr): 3066, 3032 (C–H Ar); 2972, 2957 (C–H Al); 2235 (–C≡N); 1587, 1498, 1474, 1447 (C=C); 744 (C–H Ar).

* The synthesthesis of derivative was published in reference: SKUODIS, E. et al. Aggregation, thermal annealing, and hosting effects on performances of an acridan-based TADF emitter. *Organic Electronics* **2018**, *vol. 63*, 29–40; eISSN 1878-5530.

Elemental analysis: calculated for $C_{38}H_{30}N_4$ (%): C 84.10, H 5.57, N 10.32; found (%): C 84.15, H 5.59, N 10.35.

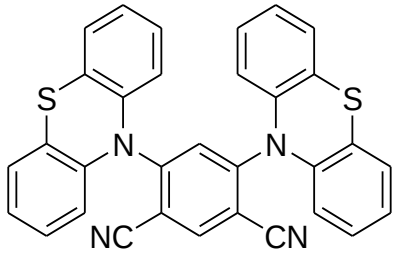

4,6-Bisphenothiazin-10-yl-isophtalonitrile (N2) was prepared according to the procedure similar to that described for the synthesis of N1. 10H-phenothiazine (1.43 g, 7.2 mmol), 4,6-difluoroisophthalnitrile (0.4 g, 2.4 mmol), t-BuONa (1.15 g, 12 mmol), and 20 ml of dry DMF were used. The reaction mixture was stirred at 30 °C for 30 min. The crude product was purified by silica gel column chromatography by using hexane/ethyl acetate with the volume ratio of 5/1 as an eluent and recrystallized from toluene. The target compound was obtained as red crystals (fw=522 g/mol, mp=279–281 °C) in 16% (0.2 g) yield.
MS (ESI) m/z (%) = 540 (M++18, 100).
1H NMR (400 MHz, $CDCl_3$) δ (ppm): 8.05 (s, 1H), 7.60 (s, 1H), 7.33 (dd, J = 7.4, 1.5 Hz, 4H), 7.21–7.07 (m, 8H), 6.79 (d, J = 7.8 Hz, 4H).
13C NMR (100 MHz, $CDCl_3$) δ (ppm): δ 150.2, 143.1, 141.3, 128.4, 128.3, 127.5, 125.7, 124.0, 120.8, 114.4, 105.5.
FTIR νmax in cm-1: 3033 (C–H Ar); 2235 (–C≡N); 1580, 1492, 1466, 1440 (C=C Ar).

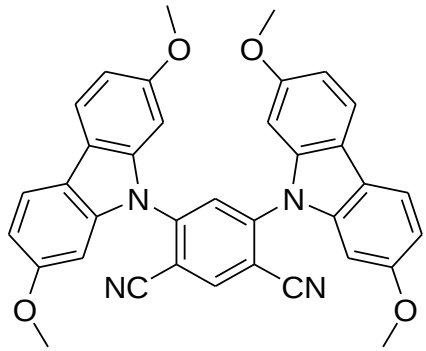

4,6-Bis(2,7-dimethoxycarbazol-9-yl)-isophthalonitrile (N3) was prepared according to the procedure similar to that described for the synthesis of N1. 2,7-Dimethoxycarbazole (0.5 g, 2.2 mmol), 4,6-difluoroisophthalnitrile (0.12 g, 0.73 mmol), *t*-BuONa (0.35 g, 3.6 mmol), and 10 ml of dry DMF were used. The reaction mixture was stirred at 30 °C for 2 hours. The crude product was purified by silica gel column chromatography by using hexane/acetone with the volume ratio of 2/1 as an eluent and recrystallized from toluene. The target compound was obtained as orange crystals (fw=578 g/mol, mp=237–240 °C) in 86% (0.36 g) yield.

MS (ESI) *m/z* (%) = 601 (M^++23, 100).
^{1}H NMR (400 MHz, $CDCl_3$) δ (ppm): 8.38 (s, 1H), 7.84 (s, 1H), 7.51 (d, *J* = 2.2 Hz, 5H), 7.25 (dd, *J* = 12.1, 9.6 Hz, 6H), 7.07 (dd, *J* = 8.9, 2.4 Hz, 5H), 3.93 (s, 16H).
^{13}C NMR (100 MHz, $CDCl_3$) δ (ppm): 155.6, 146.1, 140.9, 134.9, 128.1, 125.5, 115.4, 114.6, 110.9, 109.8, 103.7, 56.0 (OMe).
FTIR ν_{max} in cm^{-1}: 3061 (C–H Ar); 2996 (C–H Al); 2233 (–C≡N); 1462, 1431 (C=C); 1325 (C–N Ar); 835, 812, 788, 742 (C–H Ar).

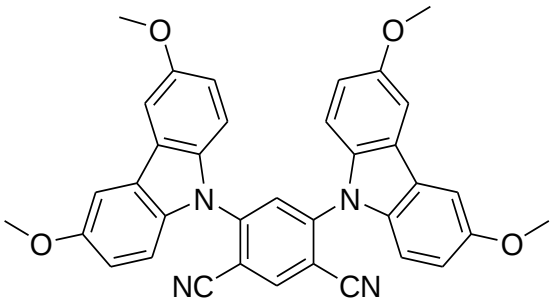

4,6-Bis(3,6-dimethoxycarbazol-9-yl)-isophthalonitrile (N4) was prepared according to the procedure similar to that described for the synthesis of N1. 3,6-Dimethoxycarbazole (0.82 g, 3.6 mmol), 4,6-difluoroisophthalnitrile (0.2 g, 1.2 mmol), *t*-BuONa (0.58 g, 6 mmol), and 20 ml of dry DMF were used. The reaction mixture was stirred at 30 °C for 2 hours. The crude product was purified by silica gel column chromatography by using hexane/acetone with the volume ratio of 3/1 as an eluent and recrystallized from toluene and methanol. The target compound was obtained as the yellow crystals (fw=578 g/mol, mp=279–281 °C) in 16% (0.2 g) yield.
MS (ESI) *m/z* (%) = 601 (M^++23, 100).
^{1}H NMR (400 MHz, Acetone-d_6) δ (ppm): 8.90 (s, *J* = 8.0 Hz, 1H), 8.16 (s, 1H), 7.77 (s, 1H), 7.49 (d, *J* = 8.9 Hz, 1H), 7.10 (d, *J* = 7.3 Hz, 1H), 3.91 (s, 1H).
^{13}C NMR (100 MHz, Acetone-d_6) δ (ppm): 156.51, 147.06, 142.61, 136.47, 130.34, 126.19, 116.37, 115.82, 112.37, 111.93, 104.47, 56.31 (OMe).
FTIR ν_{max} in cm^{-1}: 3044 (C–H Ar); 2833 (C–H Al); 2236 (–C≡N); 1462, 1432 (C=C Ar); 1323 (C–N Ar); 834, 811, 791 (C–H Ar).

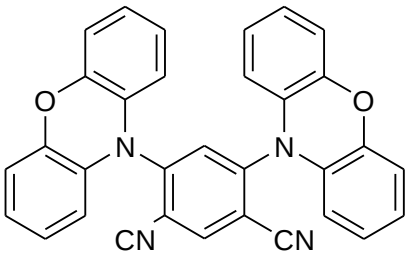

4,6-Diphenoxazin-10-yl-isophthalonitrile (N5) was prepared according to the procedure similar to that described for the synthesis of N1. Phenoxazine (0.88 g, 4.8 mmol), 4,6-difluoroisophthalnitrile (0.27 g, 1.6 mmol), *t*-BuONa (0.77 g, 8.0 mmol),

and 10 ml of dry DMF were used. The reaction mixture was stirred at 30 °C for 2 hours. The crude product was recrystallized from dichloromethane and methanol mixture 2 times. The target compound was obtained as the red crystals (fw=490 g/mol, mp=347–348 °C) in 43% (0.35 g) yield.
MS (ESI) *m/z* (%) = 513 (M^++23, 100).
^{1}H NMR (400 MHz, Acetone-d_6) δ (ppm): 8.98(s, 1H), 8.34 (s, 1H), 6.89–6.67 (m, 12H), 6.31 (d, *J* = 7.5 Hz, 4H).
^{13}C NMR (101 MHz, Acetone-d_6) δ (ppm): 149.5, 144.5, 143.9, 138.6, 133.2, 124.7, 124.0, 118.8, 116.9, 115.0, 114.6.
FTIR ν_{max} in cm^{-1}: 3043 (C–H Ar); 2984 (C–H Al); 2363 (–C≡N); 1589, 1486 (C=C Ar); 1328, 1271 (C–N Ar); 924, 857, 738 (C–H Ar).

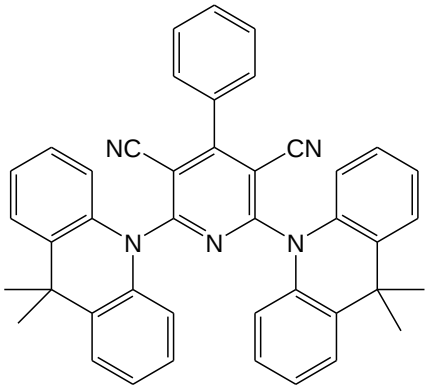

2,6-Bis(9,9-dimethylacridan-10-yl)-4-phenylpyridine-3,5-dicarbonitrile (P1)
Sodium *tert*-butoxide (0.35g, 3.65mmol) was added to the stirred solution of 9,9-dimethyl-10H-acridane (0.46g, 2.19mmol) in dry DMF (5ml) under the nitrogen atmosphere at room temperature. After stirring for 15 min, 2,6-dichloro-3,5-dicyano-4-phenylpyridine (0.46g, 2.19mmol) was added. The reaction mixture was stirred for 15 min at room temperature. The reaction mixture was quenched with water. After extraction with ethyl acetate, the mixture was purified by silica gel column chromatography by using hexane/isopropanol with the volume ratio of 20/1 as an eluent and recrystallized from toluene and hexane mixture. The product was obtained as yellow crystals (FM=619g/mol, mp=266–267 °C) in 40% (0.18g) yield.
MS (ESI): m/z(%)=642 [M+Na+, 100].
^{1}H NMR (400 MHz, Acetone-d_6) δ (ppm): 7.69–7.67 (m, 2H, Ar), 7.62–7.55 (m, 7H, Ar), 7.46–7.40 (m, 4H, Ar), 7.18–7.11 (m, 8H, Ar), 1.73 (s, 12H, CH3).
^{13}C NMR (100 MHz, Acetone-d_6) δ (ppm): 165.5, 159.1, 140.5, 136.50, 135.0, 131.7, 130.1, 129.6, 127.5, 125.8, 125.0, 119.0, 114.6, 104.2, 37.8 (CH3), 29.5 (C–(CH3)2).
FTIR ν_{max} in cm^{-1}: 3035, 3029 (C–H Ar), 2967 (C–H Al), 2217 (–C≡N), 1546, 1495, 1474 (C=C Ar), 1400C–C Ar)1268 (C–N Ar), 760, 744, 714 (C–H Ar).

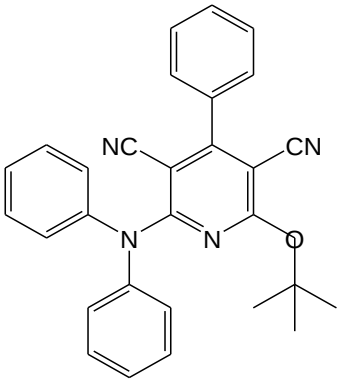

2-(*tert*-butoxy)-6-(diphenylamino)-4-phenylpyridine-3,5-dicarbonitrile (P2)

Potassium *tert*-butoxide (1.02g, 9.1mmol) was added to the stirred solution of diphenylamine (0.91g, 5.5mmol) in 20ml of dry dioxane. The reaction mixture was heated at 50 °C for 30 min under nitrogen atmosphere. 2,6-Dichloro-3,5-dicyano-4-phenylpyridine (0.5g, 1.82mmol) was added to the reaction mixture and stirred at ambient temperature for 2 hours. Then, the reaction mixture was poured into water and extracted with ethyl acetate. After being dried over Na_2SO_4 and filtered, the solvent was removed and the crude product was purified by silica gel column chromatography by using hexane/ethyl acetate (4/1) as eluent. The product was recrystallized from methanol and was obtained as transparent needles-form crystals (FM=444g/mol, mp=308–309 °C) in 41% (0.33g) yield.

MS (ESI) m/z(%)=467 [M+Na] 15%

^{1}H NMR (400 MHz, DMSO-d_6) δ (ppm): 7.62–7.56 (m, 3H, Ar), 7.55–7.45 (m, 6H, Ar), 7.43 (dd, *J* = 8.4, 1.3 Hz, 4H, Ar), 7.35 (t, *J* = 7.2 Hz, 2H, Ar), 1.26 (s, 9H, CH_3).

^{13}C NMR (101 MHz, DMSO-d_6) δ (ppm): 164.6, 159.1, 158.7, 145.2, 135.0, 130.3, 129.4, 129.0, 128.7, 127.0, 126.9, 126.3, 117.8, 115.0, 86.9, 83.5, 50.9, 40.2.

FTIR ν_{max} in cm^{-1}: 3062 (C–H Ar), 2984 (CH_3, Al), 2217 (–C≡N), 1584, 1555, 1538, 1491 (C=C Ar), 1435 (CH_3 Al), 1399 (C-C Ar), 1257 (Ar-O-C), 1131 (N-Ar), 754, 695 (C-H Ar).

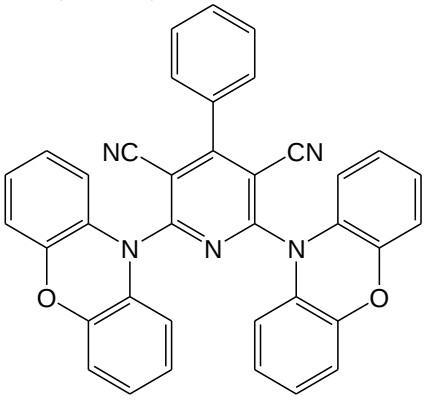

2,6-Bis(phenoxazin-10-yl)-4-phenylpyridine-3,5-dicarbonitrile (P3) was prepared according to the procedure similar to that described for the synthesis of **P2**. Phenoxazine (1g, 5.46mmol), 2,6-dichloro-3,5-dicyano-4-phenylpyridine (0.5g, 1.82mmol), potassium *tert*-butoxide (1.02g, 9.10mmol) and dry dioxane (30ml) were used. The reaction mixture was stirred at 50 °C for 20 min. The crude product was purified by silica gel column chromatography by using hexane/ethyl acetate (4/1) as eluent, and additionally it was washed with methanol. The product was obtained as orange crystals (FM=567g/mol, mp=258–259 °C) in 22% (0.22g) yield.
MS (ESI): m/z(%)=590 [M+Na+, 100].
^{1}H NMR (400 MHz, Acetone-d_6) δ (ppm): 7.69–7.59 (m, 5H, Ar), 7.28 (d, J = 7.6 Hz, 4H, Ar), 7.08–6.98 (m, 8H, Ar), 6.97–6.87 (m, 4H, Ar).
^{13}C NMR (101 MHz, Acetone-d_6) δ (ppm): 164.4, 157.5, 146.5, 133.6, 131.6, 131.1, 129.1, 128.9, 125.0, 124.0, 117.1, 116.7, 113.2, 105.7.
FTIR νmax in cm^{-1}: 3049 (C–H Ar), 2225 (–C≡N), 1538, 1484, 1392 (C=C Ar), 1207 (Ar-O-Ar), 745 (C–H Ar).

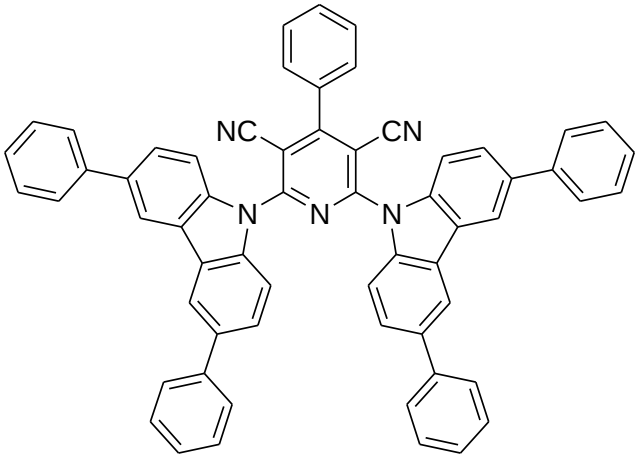

2,6-Bis(3,6-diphenylcarbazol-9-yl)-4-phenylpyridine-3,5-dicarbonitrile (P4):
A flask was charged with the mixture of 3,6-diphenyl-9H-carbazole (0.7g, 2.2mmol), 2,6-dichloro-3,5-dicyano-4-phenylpyridine (0.2g, 0.73mmol), sodium *tert*-butoxide (0.35g, 3.7mmol), triphenylphosphine solution (0.1ml, 1M in toluene) and dry toluene (10ml) . The flask was degassed and purged with argon. Then, palladium acetate (0.01g, 0.03mmol) was added to the reaction mixture at inert atmosphere and stirred at 100 °C for 20 hours. After cooling, the reaction mixture was poured into water and extracted with ethyl acetate. After being dried over Na_2SO_4 and filtered, the solvent was removed, and the crude product was purified by silica gel column chromatography by using hexane/ethyl acetate (4/1) as eluent. The product was crystallized from eluent and recrystallized from toluene and hexane mixture. The product was obtained as yellow crystals (FM=839g/mol, mp=210–241 °C) in 38% (0.23g) yield.
MS (ESI): m/z(%)=862 [M+Na^+, 100].

^{1}H NMR (400 MHz, $CDCl_3$) δ (ppm): 8.37 (d, *J* = 1.2 Hz, 4H, Ar), 7.97–7.85 (m, *J* = 7.0 Hz, 5H, Ar), 7.79–7.67 (m, 14H, Ar), 7.48 (t, *J* = 7.6 Hz, 7H, Ar), 7.37 (t, *J* = 7.3 Hz, 4H, Ar), 7.24 (t, *J* = 3.6 Hz, 1H, Ar), 7.20–7.12 (m, 2H, Ar).
^{13}C NMR (101 MHz, $CDCl_3$) δ (ppm): 167.7, 158.0, 143.9, 142.2, 138.7, 132.9, 132.6, 132.5, 131.9, 130.8, 130.5, 129.3, 129.0, 128.8, 122.8, 117.9, 116.6, 107.7.
FTIR ν_{max} in cm^{-1}: 3067 (C–H Ar), 2226 (–C≡N), 1527, 1475, 1445, 1417 (C=C Ar), 760, 695 (C–H Ar).

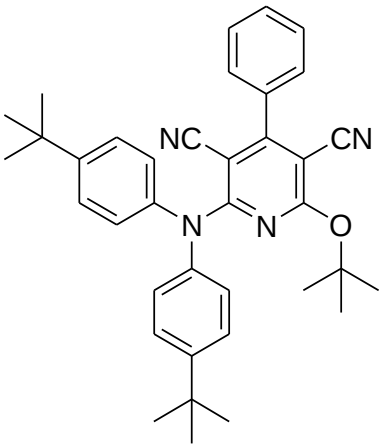

2-((4-*tert*-butylphenyl)amino)-6-(*tert*-butoxy)-4-phenylpyridine-3,5-dicarbonitrile (P5) was synthesized according to the procedure similar to that described for the synthesis of P4. Bis-(4-*tert*-butylphenyl)-amine (1.54g, 5.47mmol), 2,6-dichloro-3,5-dicyano-4-phenylpyridine (0.5g, 1.82mmol), sodium *tert*-butoxide (0.87g, 9.1mmol), triphenylphosphine solution (0.2ml, 1M in toluene), palladium acetate (0.02g, 0.1mmol) and dry toluene (20ml) were used. The reaction mixture was stirred at 110 °C overnight. After being dried over Na_2SO_4 and filtered, the solvent was removed, and the crude product was purified by silica gel column chromatography by using hexane/tetrahydrofuran (7/1) as eluent. The product was obtained as yellow crystals (FM=556g/mol, mp=272–273 °C) in 17% (0.17g) yield.
MS (ESI): m/z(%)=579 [$M+Na^+$, 100].
^{1}H NMR (400 MHz, DMSO-d_6) (ppm): δ 7.55–7.49 (m, 3H, Ar), 7.48–7.40 (m, 6H, Ar), 7.31 (d, *J* = 8.6 Hz, 4H, Ar), 1.27 (s, 18H, CH_3), 1.17 (s, 9H, OCH_3).
^{13}C NMR (101 MHz, DMSO-d_6) δ (ppm): 163.5, 159.6, 150.2, 142.4, 130.5, 129.0, 128.9, 127.4, 126.9, 88.5, 87.6, 84.4, 34.8, 31.6, 31.5, 28.0.
FTIR ν_{max} in cm^{-1}: 3057, 3036 (C-H Ar), 2964, 2903, 2868 (C-H Al), 2221 (C≡N), 1584, 1556, 1529, 1509 (C=C), 1401 (C≡$(CH_3)_3$ Al), 1149 (N-Ar), 932, 832, 752, 703 (C-H Ar).

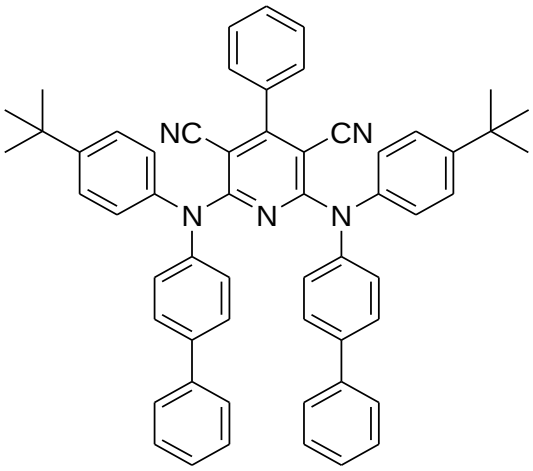

2,6-Bis((4-*tert*-butylphenyl)-(4-biphenyl)-amino)-4-phenylpyridine-3,5-dicarbonitrile (P6) was synthesized according to the procedure similar to that described for the synthesis of P4. N-biphenyl-N-(4-*tert*-butylphenyl)-amine (1.4g, 4.6mmol), 2,6-dichloro-3,5-dicyano-4-phenylpyridine (0.42g, 1.55mmol), sodium *tert*-butoxide (0.75g, 7.75mmol), tri-(*tert*-butyl)phosphine (0.16ml, 1M in toluene), palladium acetate (0.02g, 0.08mmol) and 20ml of dry toluene were used. After being dried over Na_2SO_4 and filtered, the solvent was removed, and the crude product was purified by silica gel column chromatography by using hexane/tetrahydrofuran/acetone (20/2/1) as eluent. The product was obtained as yellow crystals (FW=804g/mol, mp=275–276 °C) in 8% (0.1g) yield.

MS (ESI): m/z(%)=826 [M+Na^+, 100].

^{1}H NMR (400 MHz, $CDCl_3$) δ (ppm): 7.43–7.36 (m, 13H, Ar), 7.32–7.26 (m, 10H, Ar), 7.11 (dd, *J* = 9.7, 8.7 Hz, 8H, Ar), 1.23 (s, 18H, CH_3).

^{13}C NMR (101 MHz, $CDCl_3$) δ (ppm): 164.4, 159.0, 149.9, 144.0, 141.4, 140.0, 138.4, 134.7, 130.1, 128.7, 128.7, 128.6, 127.4, 127.2, 126.8, 126.8, 126.5, 126.4, 114.3, 90.1, 34.5, 31.2.

FTIR ν_{max} in cm^{-1}: 3032 (C-H Ar), 2961 (C-H Al), 2216 (C≡N), 1546, 1523, 1487 (C=C), 1392 (C≡$(CH_3)_3$ Al), 1294 (N-Ar), 829, 764, 736, 696 (C-H Al).

4. RESULTS AND DISCUSION

4.1. Cyanocarbazole-based derivatives

One of the most explored chromophore for TADF materials is carbazole[27]. The possibility to use different substituted carbazole helps to synthesize the large diversity of carbazole compounds[108]. The multicarbazole blocks are exhibiting some well characteristics such as high ambipolar charge mobility[109] or high triplet state energies[110, 111]. Due to strong electron-accepting characteristics, cyanogroup or dicyanodiphenylamine were chosen to make classical donor-acceptor structure[32] of molecules to achieve TADF characteristics. The differently connected bicarbazole chromophores were described as high PL quantum yield exhibiting material[34,40], but cyano-substituted N-bicarbazoles were not investigated and described in literature.

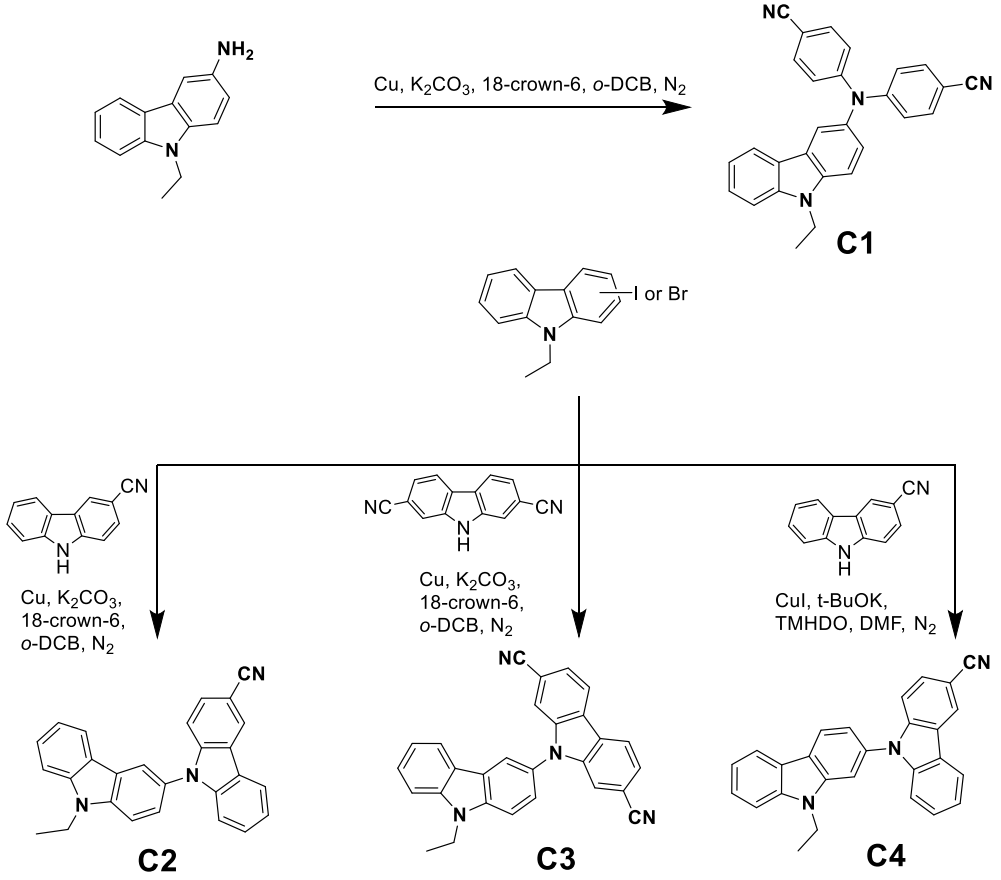

Scheme 1 Cyanocarbazole-based derivatives **C1–C4**

The derivatives **C1–C4*** were synthesized by copper or copper iodide catalysed C-N Ullman coupling, and the yields of 20–78% were obtained (**Scheme 1**). The structures of derivatives were confirmed by ^{1}H and ^{13}C NMR, FTIR, mass spectra, and all materials were obtained as yellow crystalline materials. The thermal characteristics of derivatives were explored by DSC and TGA methods under N_2 atmosphere. All synthesized derivatives were obtained as crystalline materials, but these derivatives were formed as molecular glasses; then, the samples were cooled down at DSC measurement. The thermal properties are highly dependant on the positions of substituents. The derivative **C3** substituted by two carbonitrile substituents exhibited higher thermal stability and higher glass transition and melting point. The **C1** showed lower melting point and glass transition due to more flexible dicarbonitrilediphenylamino substituent. The derivatives exhibited moderate thermal stability in the range of 302–359 °C. The thermal characteristics of derivatives **C1–C4** were summarized in **table 9**. The DSC thermogram of **C2** is shown in **fig. 22**.

Table 9 Thermal characteristics of **C1–C4**

Derivative	T_m, °C	T_g, °C	$T_{-5\%}$, °C
C1	176	77	333
C2	224	79	302
C3	261	111	359
C4	191	93	320

The reversible oxidation processes were found for dicarbonitrilediphenylamino-substituted derivative **C1** only. The carbonitrile-carbazolyl substituted derivatives **C2–C4** with unstable C-3 or C-6 positions of carbazole rings exhibited irreversible oxidation due to higher electron spin density at free C-3 and C-6 positions at carbazole rigs and possibility to form radical cations or new carbazole-based compounds[112, 113]. The reduction potentials were not observed for single carbonitrile-substituted derivative **C2**. The dicarbonitrilediphenylamino-substituted derivative **C1** showed higher electron affinity then 2,7-dicarbonitrilecarbazolyl-substituted derivative **C3**. The ionization potentials are important characteristics for the application of derivatives for optoelectronic devices, which is showing electrons' releasing work under excitation. The electrons photoemission spectra are shown in **fig. 23**. The values of ionization potentials are in the range of 5.58–5.75eV, and it has shown good stability of derivatives in the air. The electrochemical characteristics of derivatives **C1–C4** are summarized in **table 10**.

* The synthesis and investigations of derivatives **C1–C4** were described in reference: SKUODIS, E. et al. OLEDs based on the emission of interface and bulk exciplexes formed by cyano-substituted carbazole derivative. *Dyes and Pigments* **2017**, *vol. 139*, 795–807; eISSN 1873-3743.

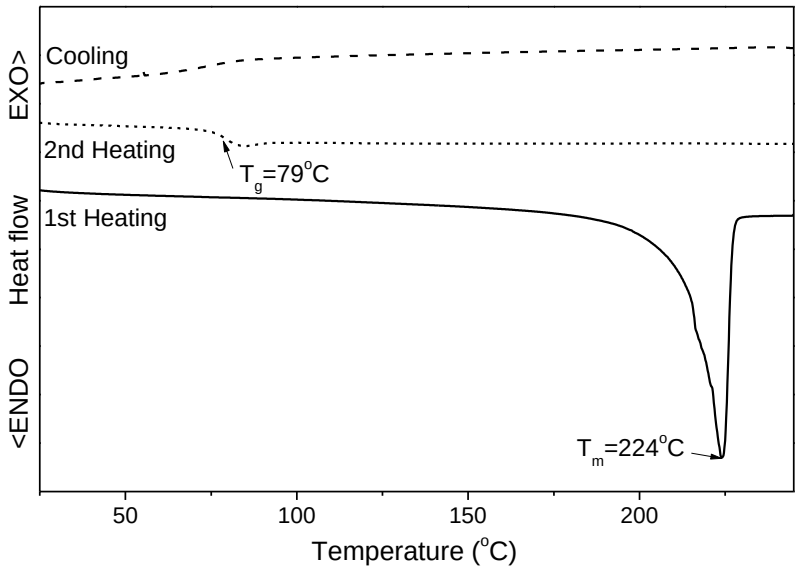

Fig. 22 DSC measurements of **C2**

Table 10 Electrochemical characteristics of derivatives **C1–C4**

	U_{red}, V	U_{ox}, V	I_p(CV), eV	E_A(CV), eV	I_P(Ph), eV
C1	-2.07	0.54	5.34	-2.73	5.60
C2	Not fixed	0.84	5.64	-	5.63
C3	-1.97	0.77	5.57	-2.83	5.58
C4	Not fixed	0.89	5.69	-	5.75

The quantum chemistry calculations of the values of HOMO and LUMO energies were estimated by the density functional theory (DFT) with the B3LYP energy functional and the 6-31G(d,p) basis set in vacuum. The calculations were calculated by Spartan 14 software[114]. The structures of derivatives were optimized firstly theoretically. The structures of molecules and orbitals with HOMO and LUMO values are shown in **fig 24**.

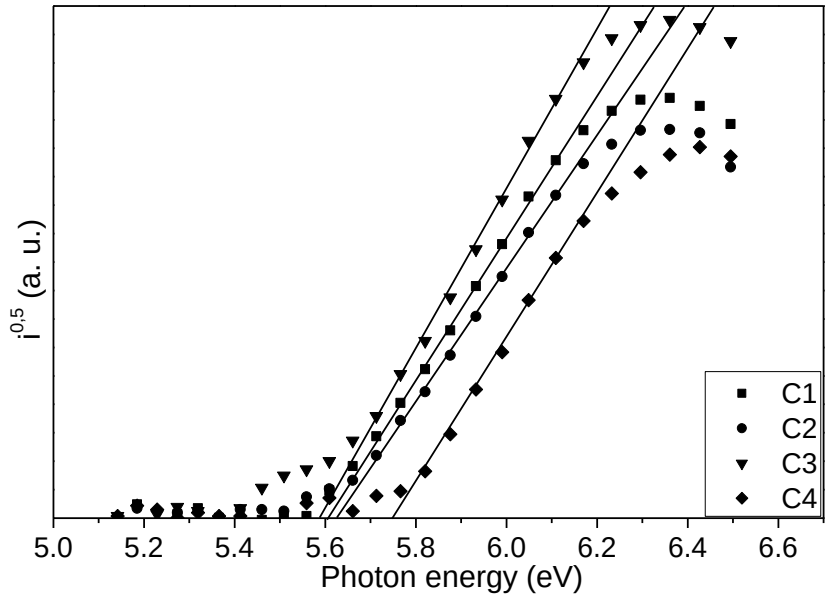

Fig. 23 Photoemission spectra of electrons

The crystal structure of **C2** (**C2a**) was investigated by X-ray diffraction analysis, and HOMO, LUMO energies were calculated according to XRD confirmed structure. The DFT calculations pointed out that HOMO are distributed mostly over the both carbazole units for **C2–C4** and over the carbazole and dicarbonitrile-diphenylamino part for **C1**. The estimated HOMO values range from -5.80 to 5.50eV. The values have shown high similarity with experimental data. The dihedral angles between carbazole chromophores of derivatives **C2–C4** were calculated to be 54–58°. These dihedral angles are insufficient for the spatial separation of the orbitals of HOMO and LUMO on the donor and acceptor parts.

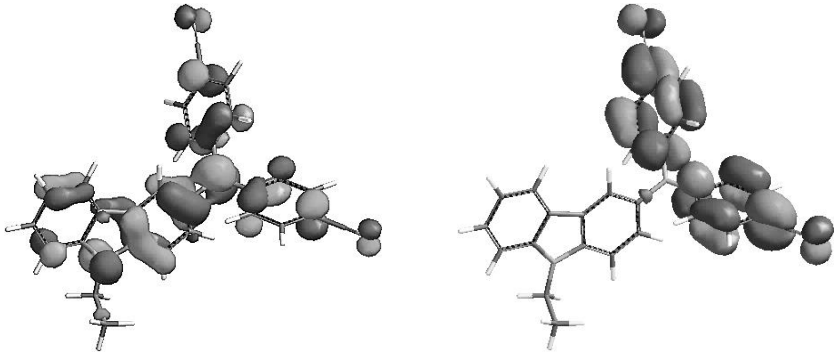

C1 HOMO = -5.50eV LUMO = -1.65eV

Fig. 24 The quantum chemistry calculations of derivatives **C1–C4**

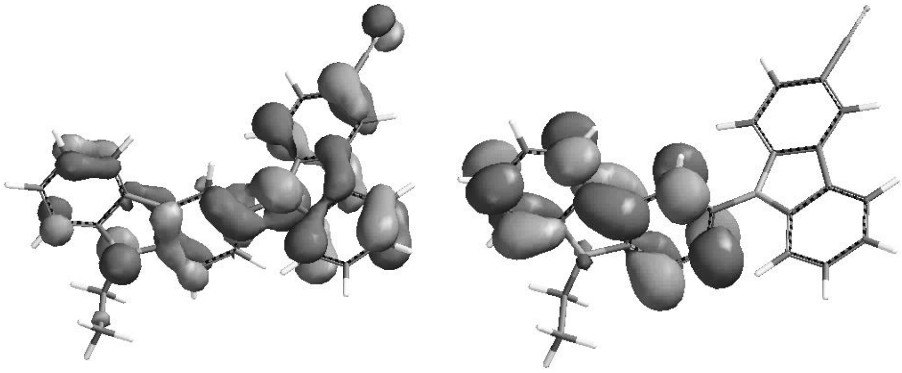

C2 HOMO = -5.56eV LUMO = -1.19eV

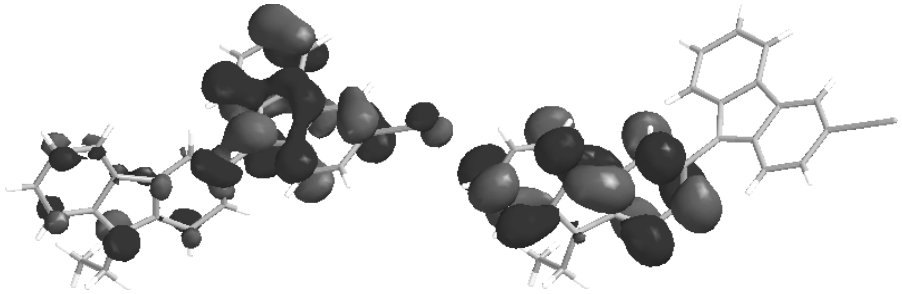

C2a HOMO = -5.60eV LUMO = -1.11eV

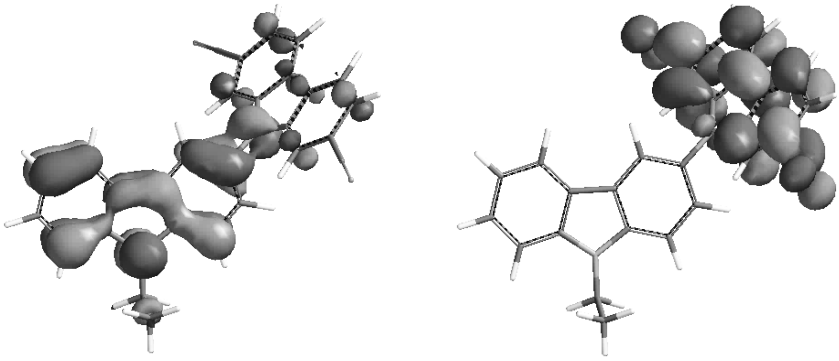

C3 HOMO = -5.80eV LUMO = -2.05eV

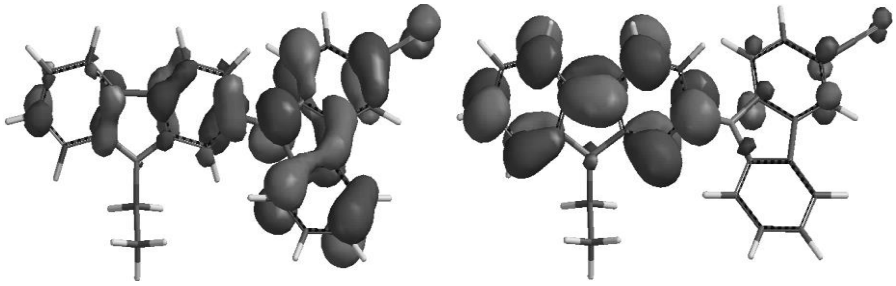

C4 HOMO = -5.66eV LUMO = -1.24eV

Fig. 24 The quantum chemistry calculations of derivatives **C1−C4** (continuous)

The photophysical characteristics of derivatives were explored by UV-vis, fluorescence, phosphorescence spectroscopies and electrons photoemission spectra (**Fig. 25**). UV-vis and fluorescence spectra were recorded from diluted solutions at THF and the thin films at ambient temperature. The low temperature luminescence spectra were recorded from diluted THF solutions that were excitated by 300nm wavelength beam at 77K temperature, and the phosphorescence maxima were found at spectra. The results of measurements are summarized in **table 11**.
Carbonitrilecarbazolyl-substituted carbazole derivatives **C2–C4** showed significant decrease of the PL quantum yield of solid sample as compared to the diluted solutions, and the PL quantum yield of solid state derivative **C1** are similar to that of the diluted solution. The dicarbonitrilediphenylamino-substituted derivative **C1** have more freedom for the rotation of C-N-C bond compared with the carbonitrilecarbazolyl-substituted compounds; hence, such PL quantum yield of **C1** in the solid state is possible to be explained by aggregation-induced emission enhancement[115]. The possibilities of TADF effect of derivatives were studied from low temperature PL spectra by Planck hypothesis. The singlet and triplet energies were determined from the onset of fluorescence and phosphorescence spectra respectively. The singlet and triplet energies of derivatives **C1–C4** and the splitting of singlet and triplet energies are shown in **table 11**. The derivatives **C1–C4** can be used for visible colours OLED's due to high triplet energies (2.76–3.02eV). TADF characteristic can be predicted for derivative **C3** due to low splitting of singlet and triplet energies (0.16eV). In order to confirm the assumption that the PL spectra were recorded from solution in THF at ambient and oxygen free conditions. The intensity of PL from degassed solution was approximately two times higher than the ambient conditions (**Fig. 25**).

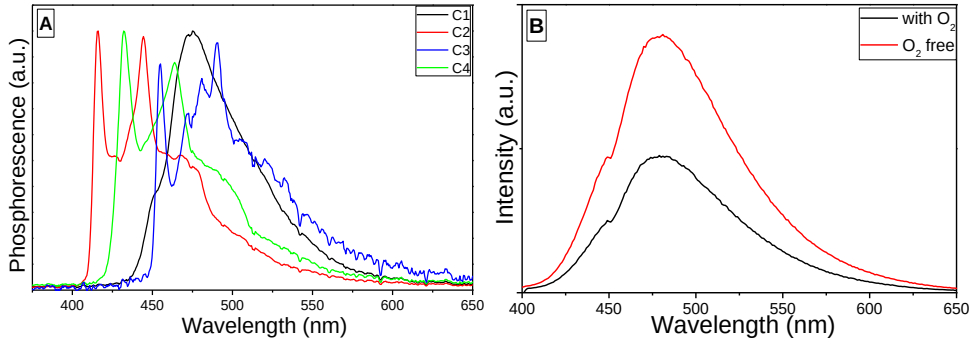

Fig. 25 A: The low temperature luminescence spectra of derivatives **C1–C4**
B: The influence of oxygen for PL intensity of derivative **C4**

The PL life-times were increased from 12.9 to 21.7ns by non-degassed and degassed conditions respectively. Despite of the increase of PL quantum yield and the life-time of luminescence, the TADF characteristic of derivative **C3** was not observed in PL life-time due to too short life-time. The increasing of intensity and longer life-time of PL of **C3** by the elimination of oxygen can be explained by a triplet-triplet annihilation that is caused by intersystem.

Table 11 Photophysical characteristics of derivatives **C1–C4**

	Solution (CH_2Cl_2)				Thin film				E_S, eV	E_T, eV	ΔE_{ST}, eV
	λ^{UV}_{onset}, nm	E_g^{opt} eV	λ^{PL}_{max}, nm	Φ_{PL}, %	λ^{UV}_{onset}, nm	E_g^{opt}, eV	λ^{PL}_{max}, nm	Φ_{PL}, %			
C1	392	3.16	480	14.8	404	3.07	457	14.3	3.26	2.79	0.47
C2	364	3.40	385	24.5	374	3.32	392	5.2	3.41	3.02	0.39
C3	357	3.47	480	49.8	362	3.43	475	26.4	2.92	2.76	0.16
C4	404	3.07	374	32.7	415	2.99	378, 494*	<1	3.49	2.93	0.56

* - shoulder;

The charge transporting properties of derivatives **C1–C4** were investigated by the time of flight (ToF) method. The dispersive holes transport was observed for the derivative **C1–C3**. The transit times for holes of derivative **C4** were not found due to the strong dispersity. Despite of donor-acceptor structures of derivatives, the electron transport properties were not confirmed for all derivatives. The properties of holes drift mobility on the square root of electric fields of derivatives **C1–C3** are shown in **fig. 26**. The dicarbonitrilecarbazolyl-substituted derivative **C3** and monocarbonitrile-substituted derivative **C2** showed two orders of magnitude higher than for the dicarbonitrilediphenylamino-substituted derivative **C1**. The holes mobility of derivative **C3** is little higher than **C2**. This observation is showing that the amount of carbonitrile substituents do not effect the mobility of holes.

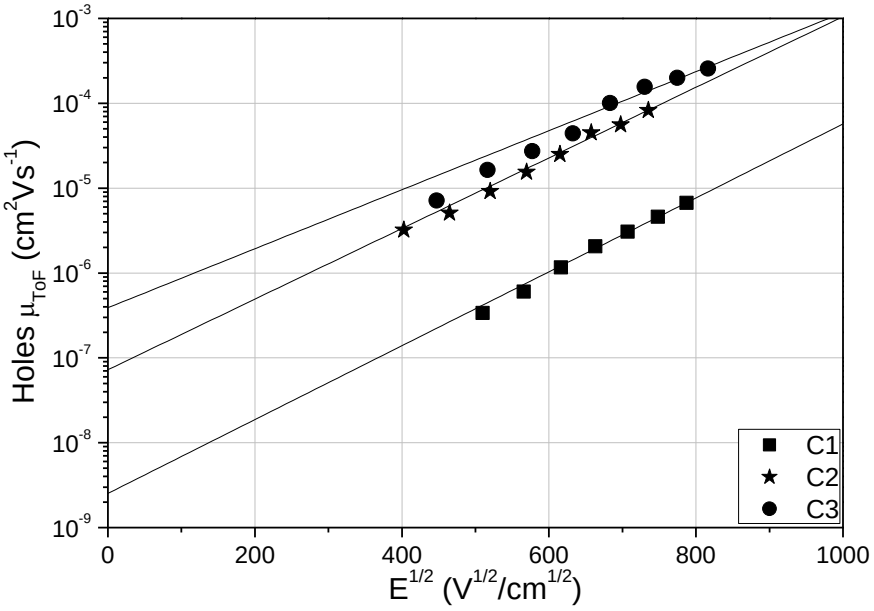

Fig. 26 The holes drift mobilities of derivatives **C1, C2** and **C3**

4.1.1. OLED investigations

Due to high enough PL quantum yield, suitable holes mobility and energy levels of compound **C3** explored that this compound could be investigated as an emitter for the application in OLEDs. The devices were made by step-by-step deposition or co-deposition of the different layers. MoO_3 or m-MTDATA was used for the preparation of hole-injecting transporting layer basing on HOMO and LUMO levels. TCTA was utilized as the host, and Bphen was used for the deposition of electron-transporting layer. The layer of indium tin oxide was used as anode, and that of Ca:Al was used as the cathode. The structures of devices A and B were: A: ITO/MoO_3/**C3**/ Bphen/Ca:Al; B: ITO/m-MTDATA/TCTA:**C3**/Bphen/Ca:Al (**Fig. 27**). Electroluminescence spectra of the devices B, C and D are depicted in **fig. 28**. The device A exhibited blue electroluminescence. The electroluminescence spectrum was very similar to the PL spectrum of the solid film of **C3**. The device A showed rather low efficiency. The reason of low efficiency of device A was a poor hole injection in the emission layer. Therefore, the hole transporting layer of m-MTDATA and TCTA as the host of emitting layer were introduced into the structure of device B. Surprisingly, this device exhibited yellow luminescence. In order to explain the experimental results, PL spectra of the layers of the molecular mixtures TCTA:**C3** and m-MTDATA:**C3** were investigated. Although the PL spectra of solid films of the pure materials **C3**, TCTA, and m-MTDATA appear in the blue region, the molecular mixtures TCTA: **C3** and m-MTDATA: **C3** exhibited sky blue and orange PL respectively. This process can be explained by the formation of exciplexes of the derivative **C3** with TCTA and m- MTDATA. Different emission colours of exciplexes TCTA: **C3** and m- MTDATA: **C3** can be explained by utilizing equation (8) for the exciplex emission maximum:

$$h\nu_{ex}^{max} = I_P^D - E_A^A - E_C \qquad (8),$$

where IP_D is the ionization potential of the donor, E_A is the electron affinity of the acceptor, and E_C is the electrone hole Coulombic attraction energy (0.35eV is a typical value for the e-h binding energy in the organic materials)[116].
Indeed, the values of $h\nu_{max}$ (TCTA:**C3**)=2:49eV and (m-MTDATA: **C3**)= 1:89eV are in good agreement with the emission maxima at 490 nm (2.53eV) and 584 nm (2.12eV) of the molecular mixtures TCTA: **C3** and m-MTDATA: **C3**. The differences between the calculated and measured values could be due the bending of HOMO, LUMO levels of the donor-acceptor interface[117] and the lack of exact e-h binding energies. As it was expected for the exciplex emission, PL decay transients for the molecular mixtures TCTA: **C3** and m-MTDATA: **C3** were observed in the range up to microseconds. Such PL decay transients cannot be attributed to the emission of 4, which was observed in the ns range (**Fig. 4C**). The PL decay curves of the solid layers of the mixtures TCTA: **C3** and m-MTDATA: **C3** could be adequately described χ^2 = 1.173 and 1.289 by the double exponential law A + $B_1exp^{(-t/t1)}$ +$B_2exp^{(-t/t2)}$. The PL lifetimes of 45 ns and 56 ns are apparently related to exciplex emission, while the lifetimes of 193 ns and 305 ns can be explained by

TADF effect of exciplexes due to RISC from singlet to triplet state[118, 119]. RISC can occur due to the small splitting of singlet and triplet energy of exciplex, which was found to be of 0.05eV for TCTA:**C3**. **Fig. 28** depicts PL spectra of the molecular mixture TCTA: **C3** at different temperatures. The curves were recorded without delays immediately after the excitation. PL decay curves of the layer of the molecular mixture TCTA: **C3** recorded at different temperatures are shown in the insert of **fig. 28**. They show two decay components displaying that PL spectrum of the TCTA: **C3** exciplex included the weak prompt fluorescence and strong phosphorescence at low temperatures, while at room temperature, the PL spectra consisted of prompt and delay fluorescence. The presence of two decay components with similar character was previously observed for the exciplexes exhibiting TADF effect[118,120]. In order to prove the assumption that the long-lived components of the PL decay curves of the layers of the mixtures TCTA: **C3** and MTDATA: **C3** appeared due to the TADF effect of the exciplexes, PL intensity dependences of the molecular mixtures TCTA: **C3** and m-MTDATA: **C3** on the laser flux were recorded (**Fig. 28**). The linear dependence with slope of ca. 1 of PL intensity on laser flux was observed for the studied mixtures TCTA: **C3** and MTDATA: **C3**. This observation shows that exciplex TADF effect is responsible for the long-lived PL components of the molecular mixtures[121]. The electroluminescence spectrum of the device B shown in **fig. 28** does not coincide with the PL spectra of the layers of the mixtures TCTA:4 and m-MTDATA: **C3**. The possible explanation of this observation could be that the electroluminescence spectrum of the device B was a combination of exciplex emissions of both TCTA: **C3** and m-MTDATA: **C3**. The exciplex emission of TCTA: **C3** (PLQY = 43.8%) was more efficient than the exciplex emission of m-MTDATA: **C3** (PLQY = 3.84%). However, the energy of electroluminescence of the device B is close to that of the exciplex PL of m-MTDATA:**C3**. This observation can apparently be explained by the energy transfer from the exciplex TCTA: **C3** to the exciplex m-MTDATA: **C3**. In order to support this assumption on the energy transfer from the bulk exciplex TCTA: **C3** to the interface exciplex m-MTDATA:**C3** in device B, there were carried out the additional experiments regarding the fabrication and characterization of exciplex-based OLEDs that were formed only with m- MTDATA: **C3** and TCTA: **C3** as emitters. The author of this dissertation has fabricated new OLEDs (devices C and D), the structures of which were as follows: ITO/m-MTDATA/TCTA/TCTA: **C3**/ **C3**/Bphen/Ca:Al (device C) and ITO/m-MTDATA/m-MTDATA: **C3**/ **C3**/Bphen/Ca:Al.

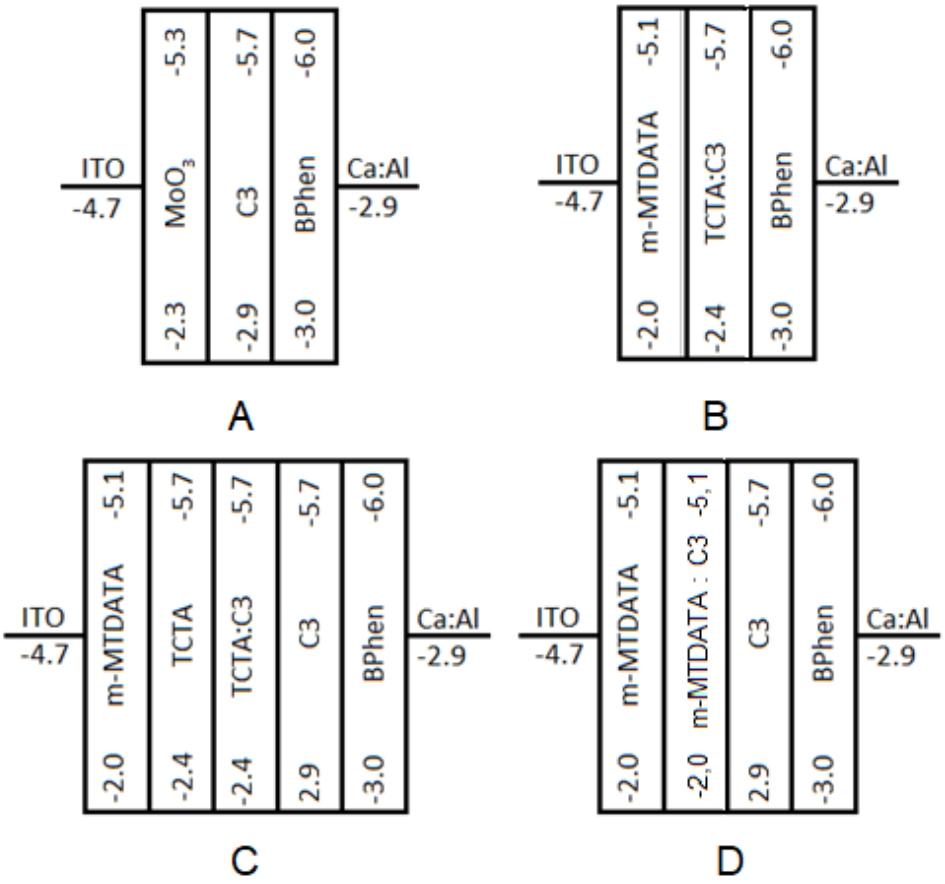

Fig. 27 The structures of OLEDs with C3 emitters

In order to avoid the formation of exciplexes, except for the needed one, non-doped layers of TCTA and/or **C3** were included in the structures of the devices C and D. **Fig. 28** shows that the electroluminescence spectra of these devices that were recorded at different applied voltages are similar to the PL spectra of the molecular mixtures TCTA: **C3** and m-MTDATA: **C3**, which exhibited sky blue and orange PL respectively.

The maximum intensity of electroluminescence spectrum for device C (at ca. 490 nm) was observed at the same wavelength as that of the PL spectrum of the molecular mixture TCTA: **C3** (**Fig. 28**). The maximum of electroluminescence spectrum that was observed for the device D at ca. 598 nm was shifted to the low energy region by 14 nm compared to that of the PL spectrum of the molecular mixture m-MTDATA: **C3** apparently due to the different excitations that were involved (optical/electrical).

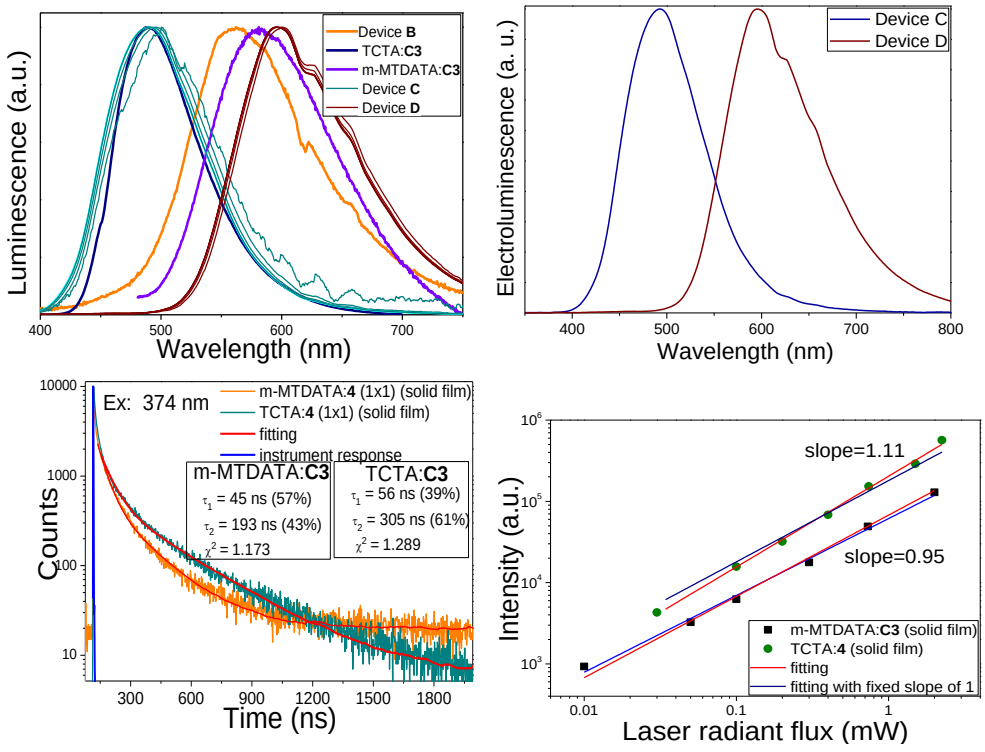

Fig. 28 Characteristics of **C3** luminescence

Table 12 Characteristics of devices **A–D**

Devices	V_{on} (V)	Max. brightness (cd/m^2)	Max. current efficiency (cd/A)	Max. power efficiency (lm/W)	Max. external quantum efficiency (%)	Rol-off efficiency (%)[a]
A	3.5	2515	7.7	5.4	2.0	28
B	4.5	6260	13.48	8.1	5.8	38
C	3.2	3600	9.9	8.8	4.2	52
D	2.5	1570	5.5	5.3	3.2	61

[a] calculated at brightness of 1000 cd/m^2

Such blue shift of electroluminescence spectrum compared to the solid-state PL spectrum of the exciplex emitter was earlier reported and was explained by the enhancement of the delayed fluorescence by the electrical excitation of the exciplex emission[22]. In contrast, the intensity maximum of electroluminescence spectrum for device B that was observed at ca. 560 nm was shifted to the high energy region by 38 nm compared to that of the device D. This observation shows that the mechanism of electroluminescence of device B is different. Most probably, it is the energy transfer from the bulk exciplex TCTA: **C3** to the interface exciplex m-MTDATA: **C3** in the device B, since the shapes of electroluminescence spectra of both devices

B and D on the m- MTDATA: **C3** exciplex are very similar as well. In addition, lower maximum external quantum efficiencies of 4.2 and 3.2% that were observed for devices C and D were lower than that for the device B (5.8%) (**Table 12**).
This result as well indicates that the energy transfer occurs in device B leading to the change of electroluminescence colour and enhancement of EQE. The output characteristics of sky blue and orange exciplex-based OLEDs are presented in **table 12**. Devices A and B exhibited low turn-on voltages of 3.5 and 4.5 V, respectively. The low turn-on voltages could be ascribed to the effective hole injection due to the suitable HOMO energy level of the derivative **C3**. **Fig. 29** and **fig. 30** as well show current density voltage luminance maxima of the devices A and B. The maximum luminance of device A did not reach 3000 cd/m^2, while that of the device B was over 6000 cd/m^2.

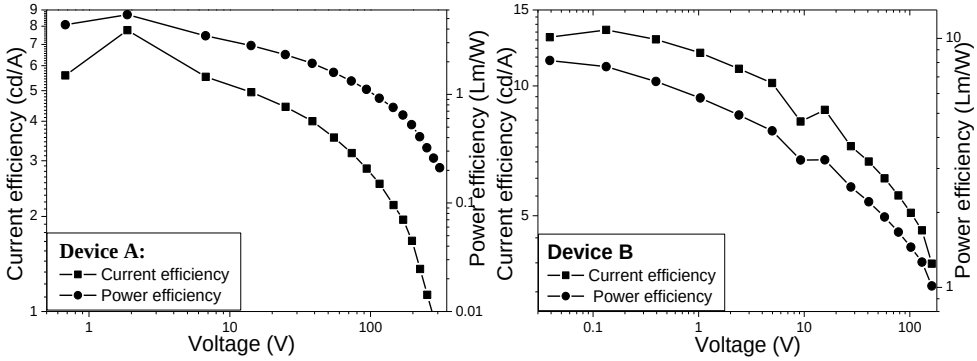

Fig. 29 The current and power efficiencies of devices A and B

The brightness of the device B was as well much higher than that of the device A. This observation can apparently be explained by the higher hole mobility of TCTA relative to that of derivative **C3**. One more reason of poor performance of device A might be the unbalanced hole and electron mobilities in the emitting layer of **C3**. The balanced hole and electron mobilities are of extreme importance for the materials of emitting layers[122].

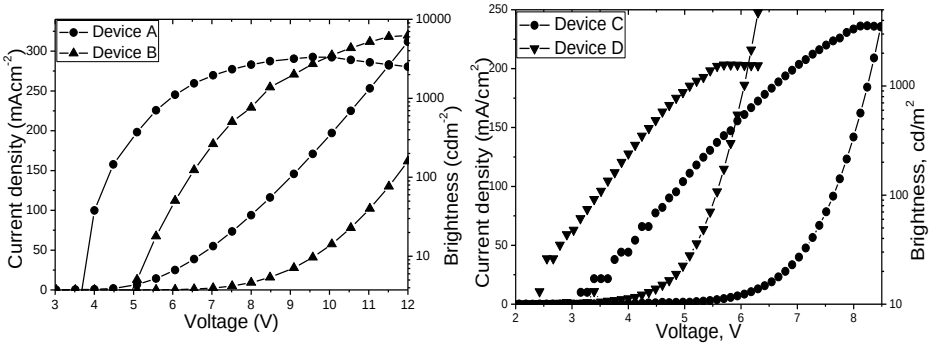

Fig. 30 The characteristics of current density and brightness of devices A–D

EQE and current density curves for OLEDs A-D are shown in **fig. 31**. The characteristics of the devices are summarized in **table 10**. The device B exhibited much higher maximum EQE than the device A at the same luminance. The maximum quantum efficiencies of 2.0 and 5.8% were observed for the devices A and B, respectively. The CIE colour coordinates were calculated to be 0.17, 0.28 and 0.40, 0.52 for devices A and B, respectively. It should be noted that triplet energy levels of **C3**, TCTA, and m-MTDATA, which could be sources of energy losses in the emitting layer, are higher than exciplex energy levels, denying the possibility of energy losses through the triplets (**Fig. 31**). The external quantum efficiencies that were observed at 1000 cd/m^2 were used to calculate the efficiency roll-offs, which were in the range from 28 to 61% for the studied devices (**Table 12**). It should be pointed out that the characteristics of OLEDs were recorded for the devices under ordinary laboratory conditions. Using variety existing materials[123, 124], the device performance could be further improved by changing the hole and electron transporting layers, optimizing the layer thicknesses, changing the concentration of **C3** in the host, varying the processing conditions.

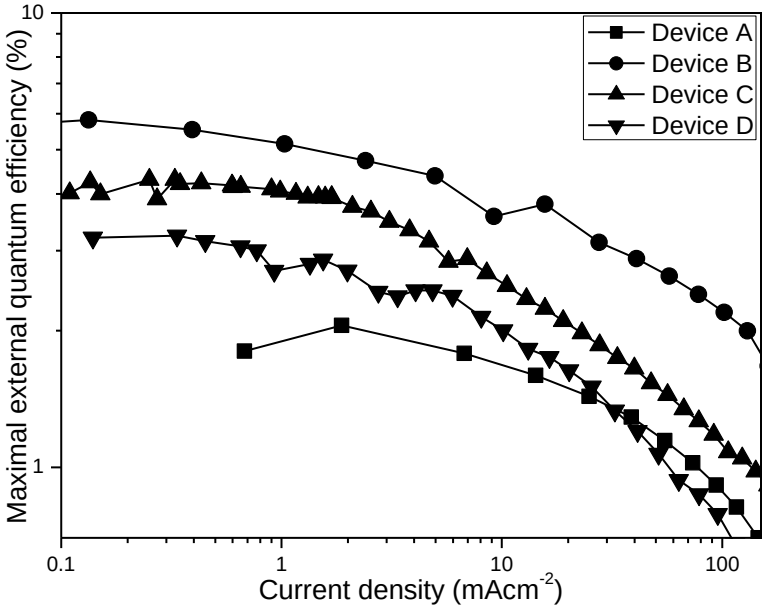

Fig. 31 The maximal external quantum efficiencies of devices A–D

4.2. Isophtalonitrile-based derivatives

The cyano-substituted benzene blocks are widely investigating with carbazole chromophores as thermally activated delayed fluorescence exhibiting materials and described in many works. However, the derivatives with other donors such as phenothiazine, phenoxazine, acridane or methoxy substituted carbazole are described purely, but they are perspective materials for the OLEDs emitters or host materials[23] due to lower ionization potentials, better charges mobilities[125, 126], lower turn on

voltages of OLEDs[127]. The methoxy-substituted carbazole derivatives are exhibiting useful properties for OLEDs applications such as lower ionization potentials, lower splitting of singlet and triplet energies[128] and improving the holes drift mobilities[129, 130].

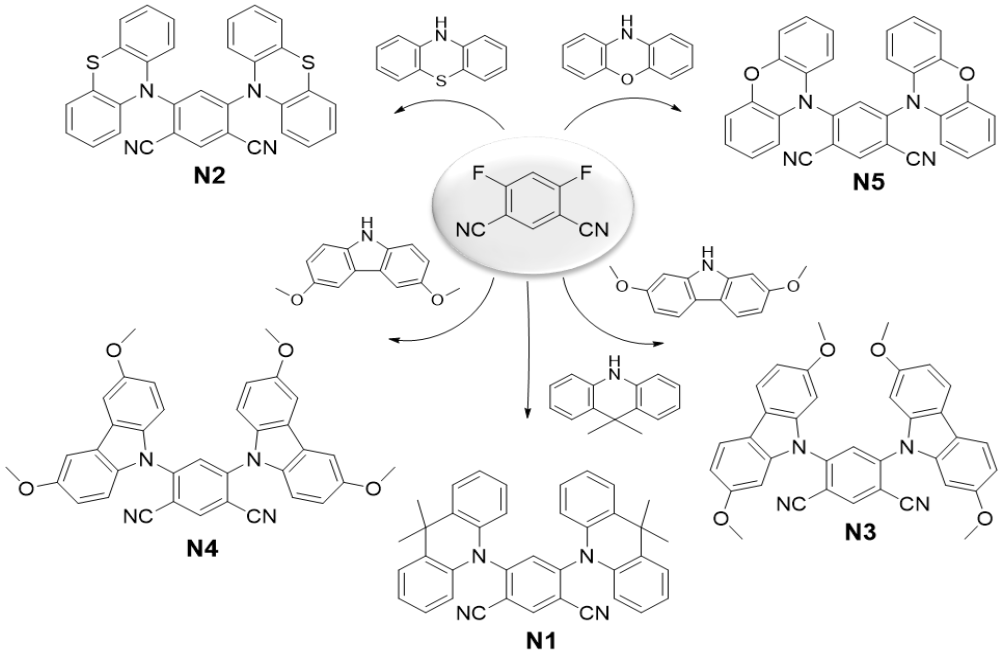

Scheme 2 Isophtalonitrile-based derivatives **N1-N5**

The isophthalonitrile-based derivatives[#] were synthesized by sodium or potassium *tert*-butoxide catalysed C-N nucleophilic coupling reaction of 1,3-dicyano-4,6-difluorobenzene with the respective chromophore (scheme **2**). The yields of synthesized products were ranging from 16% for derivatives **N2** and **N4** to 86% for derivative **N3**. All materials were obtained as yellow or red crystalline materials.
The thermal properties of derivatives were investigated by DSC and TGA methods. The DCS thermograms of derivatives **N1** and **N5** are shown in **fig. 32**.
The derivatives **N1–N5** exhibited high thermal stability, and the highest stability exhibited derivative **N3**. It could be explained by free reactive C-3 positions at carbazole, which gave lower stability. The phenothiazine-based derivative **N2** exhibited the highest thermal stability. All materials were obtained as crystalline materials, and the derivative **N3** consist of stabile molecular glass only. Other derivatives showed crystallization peaks at DSC cooling processes, and there were

[#] The synthesis and investigations of derivative **N1** were published in reference: SKUODIS, E. et al. Aggregation, thermal annealing, and hosting effects on performances of an acridan-based TADF emitter. *Organic Electronics* **2018**, *vol. 63*, 29–40; eISSN 1878-5530.

observed no glass transitions. The thermal properties of derivatives were collected in **table 13**.

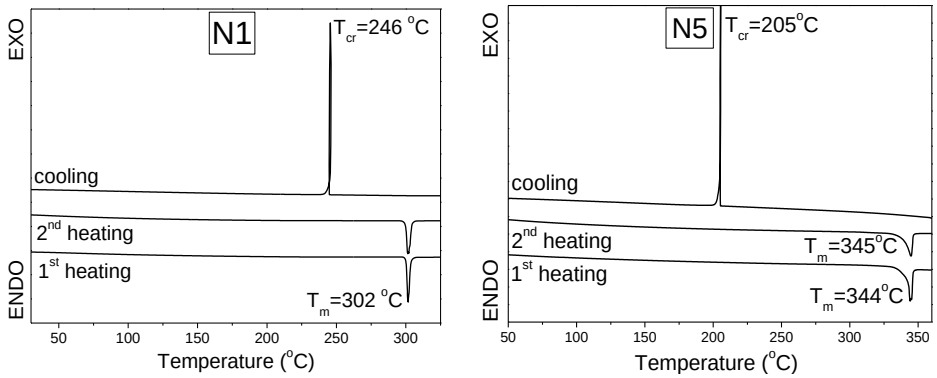

Fig. 32 The DSC curves of derivatives **N1** and **N5**

Table 13 The thermal characteristics of derivatives **N1–N6**

	T_m, °C	T_g, °C	T_{cr}, °C	$T_{-5\%}$, °C
N1	302	-	246	340
N2	303	-	281	355
N3	309	153	-	404
N4	311	148	237	376
N5	344	-	205	325

The electrochemical properties of derivatives **N1–N5** were investigated by cyclic voltammetry measurements (**Fig. 33**) in dichloromethane solution.

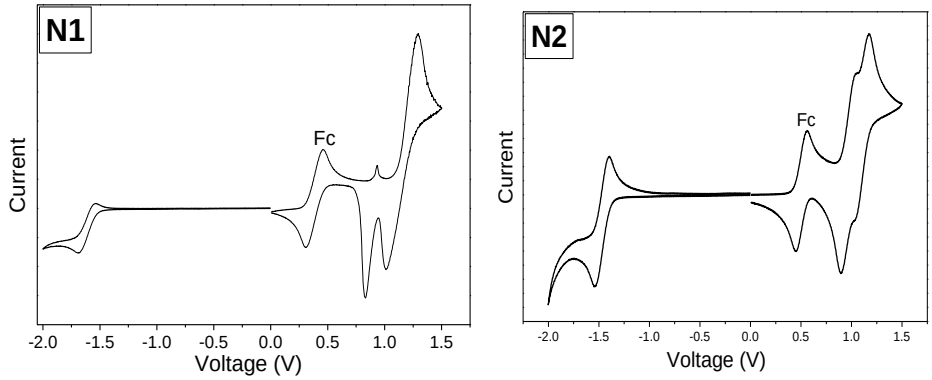

Fig. 33 The cyclic voltammetry measurements of derivatives **N1** and **N2**

The curves of measurements of derivatives **N2**, **N4** and **N5** showed reversible processes of oxidation-reduction conditions. The CV curves of derivatives **N1** and **N3** showed irreversible processes of oxidation-reduction because of free reactive spots at acridane and carbazole chromophores. The electrochemical characteristics of derivatives **N1–N5**, and the results of photoelectron spectroscopy are summarized in **table 14.** The 2,7-dimetoxicarbazolyl substituted derivative **N3** exhibited higher

electron affinity and lower ionization potential than 3,6-dimetoxicarbazolyl substituted derivative **N4**. The phenothiazinyl and phenoxazinyl substituted derivatives **N2** and **N5** exhibited the lowest ionization potentials that were measured by photoelectrons emission spectra; however, the correlation between CV and photoelectrons emissions spectra are low.

Hole and electron mobilities were calculated for the studied compounds at different electric fields having ToF current transients with recognized transit times. Electron mobility for **N3** was not obtained, since the transit times for the electrons were not observed due to the strong dispersity. Hole (h^+) and electron (e^-) mobility for the layers of **N2–N5** were found to be similar, slightly depending on the nature of donor substituents. The electron mobility of all compounds was found to be slightly higher to their hole mobility. The highest values of charge mobilities were obtained for 3,5-dicarbonitriles with attaching the methoxy-substituted carbazoles exceeding 10^{-4} cm^2/Vs at electric fields higher than ca. 6.5×10^5 V/cm.

The quantum chemistry calculations were calculated by Gaussian software[131] by the density functional theory (DFT) with the B3LYP energy functional and the 6-31G(d,p) basis set in vacuum. The theoretical HOMO and LUMO orbitals and the values of HOMO and LUMO energies are shown in **fig. 34**. The theoretical values of HOMO of derivatives **N1–N5** are lower than the experimental ionization potential, and the theoretical values of LUMO are higher than the electron affinities calculated according to the cyclic voltammetry, but the correlation between values of HOMO and LUMO and experimental values of ionization potentials and electron affinities were observed.

Table 14 Electrochemical characteristics of derivatives **N1–N5**

	I_P(CV), eV	E_A(CV), eV	I_p(Ph), eV	μ_{ToF} (max), cm^2/Vs e^-/h^+
N1	5.63	2.81	5.65	$6\times10^{-4}/10^{-3}$
N2	5.51	2.83	5.55	$4\times10^{-6}/3\times10^{-5}$
N3	5.32	2.83	5.70	8.8×10^{-5}/-
N4	5.52	2.76	5.80	$2.6\times10^{-5}/2.4\times10^{-4}$
N5	5.37	2.90	5.58	$3.2\times10^{-5}/3.6\times10^{-5}$

The photophysical characteristics were investigated by UV-vis absorption, fluorescence and phosphorescence (77K) spectroscopy. The measurements were recorded from diluted solutions (10^{-4}M) of THF or toluene. The PL spectra were recorded, and PL quantum yields were calculated from thin films as well. The optical band gaps were calculated from UV-vis spectra of neat films by Planck hypothesis. The values of band gaps were lower than 2.61eV. The fluorescence of derivatives **N1–N5** were in a range of yellow and red colours, and the shortest maxima was observed for the derivative **N1** containing acridane substituents. The PL quantum yields of derivative **N1** are 47%, but other derivatives exhibited much lower PL quantum yields that were measured in the solid state.

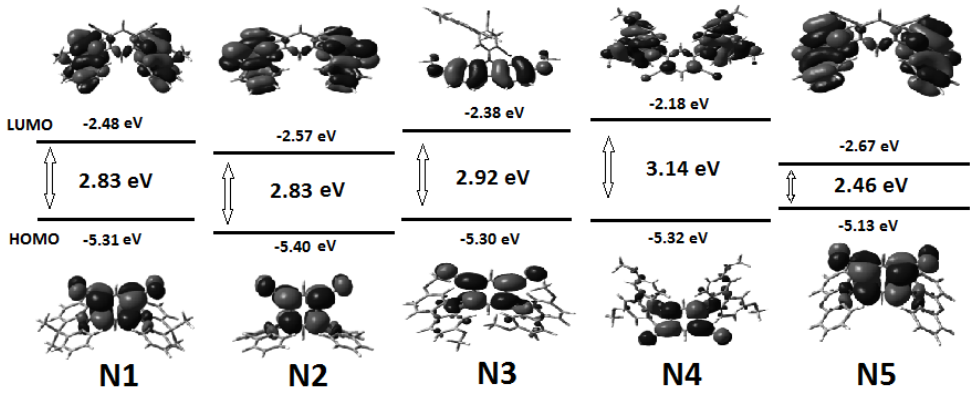

Fig. 34 The theoretical calculations of HOMO and LUMO energy levels of derivatives **N1–N5**

The splitting of singlet and triplet energies of explored derivatives are enough narrow. The derivative **N2** is showing no phosphorescence from THF solutions at 77K temperature. The photophysical characteristics of derivatives **N1–N5** were summarised in **table 15**, and the spectra of UV-vis absorption and PL are shown in **fig. 35**.

Table 15 The photophysical properties of derivatives **N1–N5**

	E_g^{opt}, eV	Pl_{max}, nm	QY, %		E_S, eV THF/mCP	E_T, eV THF/mCP	ΔE_{ST}, eV THF/mCP
			Toluene	Thin film			
N1	2.61	543	-	47	2.26/-	2.24/-	0.02/-
N2	2.58	643	1	4	2.62/2.74	-/2.69	-/0.05
N3	2.53	572	16	5	2.71/2.60	2.69/2.56	0.02/0.04
N4	2.57	575	16	7	2.73/2.63	2.71/2.59	0.02/0.04
N5	2.30	678	2	0.06	2.38/2.33	-/2.35	-/0.02

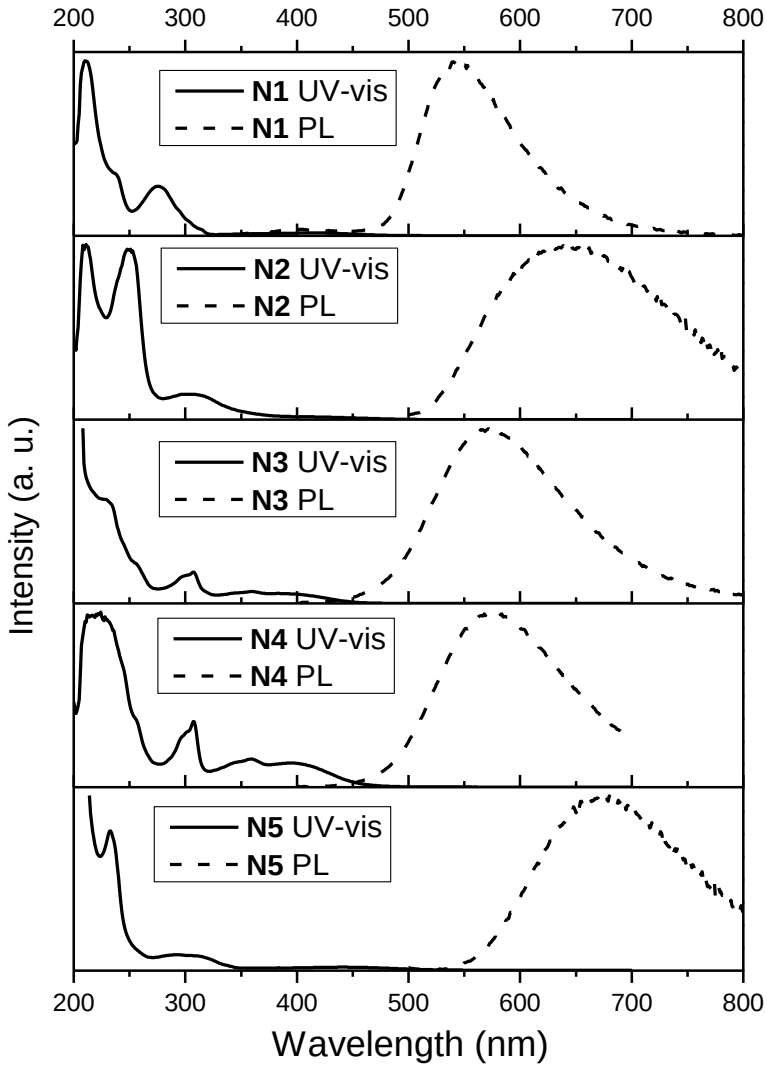

Fig. 35 The UV-vis absorption and luminescence spectra of derivatives **N1–N5**

The PL spectra were recorded from toluene solutions in ambient and oxygen free conditions. The difference of intesivity of the PL spectra were 7.3, 1.2, 1.5, 1.5 and 1.3 times of derivatives **N1–N5**, respectively. The PL decaying time spectra were recorded by using 350nm picosecond laser beam from the solutions of THF of derivative **N1** and toluene solutions of other derivatives at ambient and oxygen free conditions. The curves of PL decay times were smoothed. The influence of PL intensity by decaying time of ambient and oxygen free conditions are shown in **fig. 36**. The longest luminescence decay time of oxygen-free solutions were observed for

derivatives **N1** and **N4**. Phenothiazine and phenoxazine based derivatives **N2** and **N5** exhibited no increasing of luminescence intensity of longer decay.

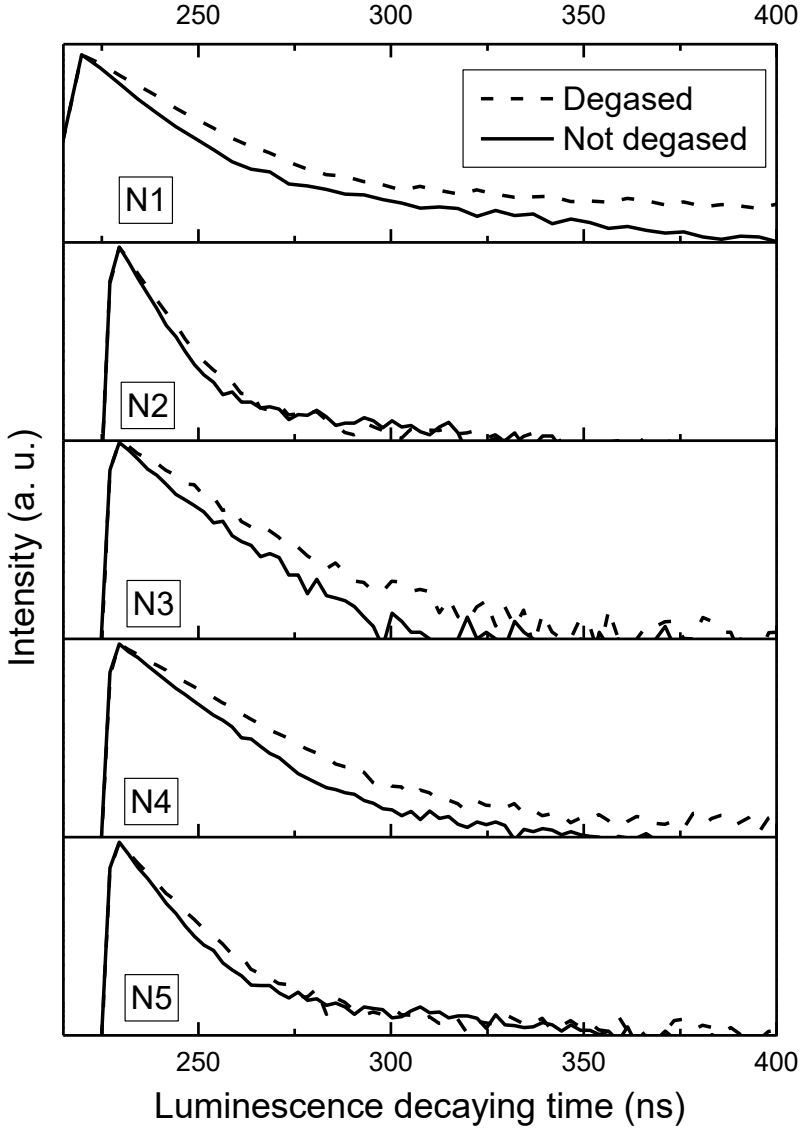

Fig. 36 The PL decaying time of derivatives **N1–N5** of solutions in ambient and oxygen-free conditions

In order to show that the formations of different aggregates are mostly related to the influences of intermolecular bonds but not to the structure properties of aggregates (i.e. amorphous or crystallinity), the PL behaviours of **N1–N5** compounds were tested in solid-state solutions by using ZEONEX host. The refractive index of

ZEONEX polymer is 1.53. The emission maxima of thin films of ZEONEX matrix were different for derivatives **N1, N2, N4** and **N5** at different concentrations of derivatives in ZEONEX matrixes, and the process of aggregation was observed slightly for the derivative **N3**. The PL maxima of derivatives were shorter measured from ZEONEX 1% solid solution; then, the maxima were measured from diluted solutions in hexane. The PL spectra of 15% **N1** in ZEONEX exhibited a double band emission profile with a left-hand shoulder situated around 494 nm (non-aggregated **N1**) and a maximum around 565 nm (pure **N1**). The same process is possible to be seen in the spectra of derivative **N5**. The smoothed PL spectra of derivatives **N1–N5** in ZEONEX matrix are shown in **fig. 37**.

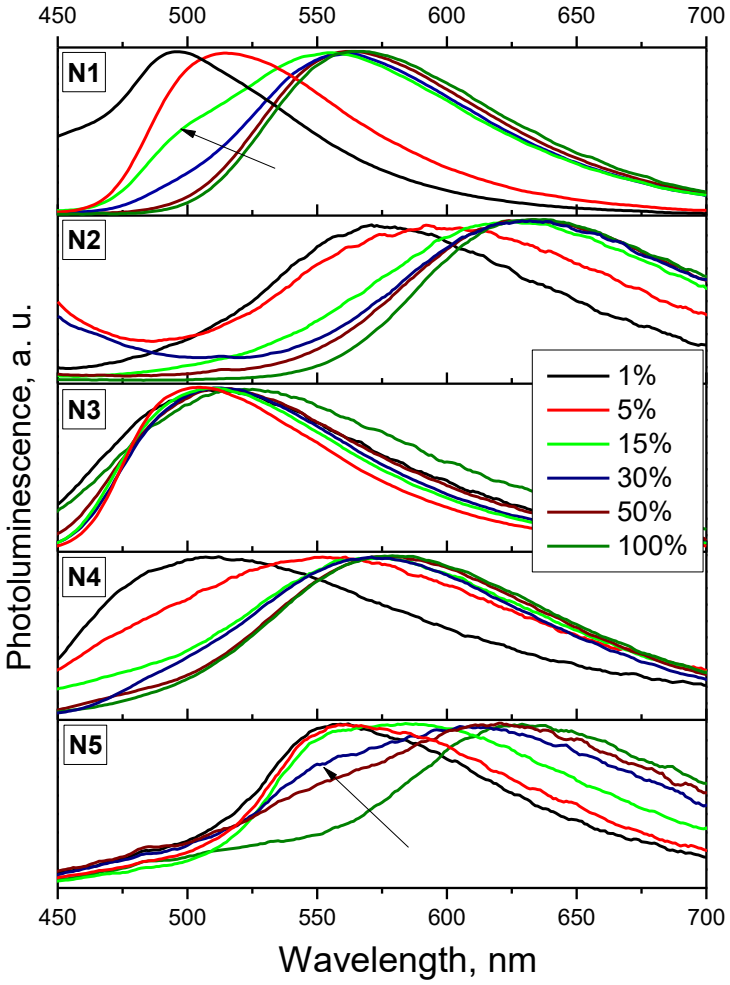

Fig. 37 The aggregation processes of derivatives **N1–N5**

The host polarity influence for the wavelength of PL of thin films and thin films with mCP matrix are shown in **fig. 38**. The wavelengths of derivatives in matrixes were 524, 591, 525, 543 and 598 for derivatives **N1–N5** respectively, which were shorter wavelengths of 33–54nm as compared with single material thin films. The intensity of PL of derivatives **N1–N5** in mCP matrix were much higher than the intensity of PL of single material thin film. The PL decaying time spectra of derivatives **N2–N5** in mCP matrixes were recorded at different temperatures from 100K to ambient temperature. The decaying time of PL were increased for all derivatives, but the characteristics of thermally activated delayed fluorescence were not observed for all the derivatives **N2–N5** in mCP matrixes**.**

The intensity of PL of thin films with derivatives **N2–N5** and mCP matrix were recorded at air conditions and vacuum. The increasing of PL of host-guest systems are explained by the better transition of energy[132]. As shown in **Fig. 39**, the intensity of PL of **N4** and mCP was increased by 9.4 times at vacuum compared with the air conditions, and other derivatives exhibited much lower increasing in intensity.

The absorption and PL spectra of the dilute solutions (10^{-5} M) and vacuum deposited solid layer of **N1** were recorded. The dilute solutions in solvents with the different polarities demonstrate similar positions (~415 nm) of the low-energy absorption bands at UV-vis absorption spectra, whereas the red-shift of low-energy absorption peak is observed for the neat film of **N1**, as compared to the spectrum of hexane solution.

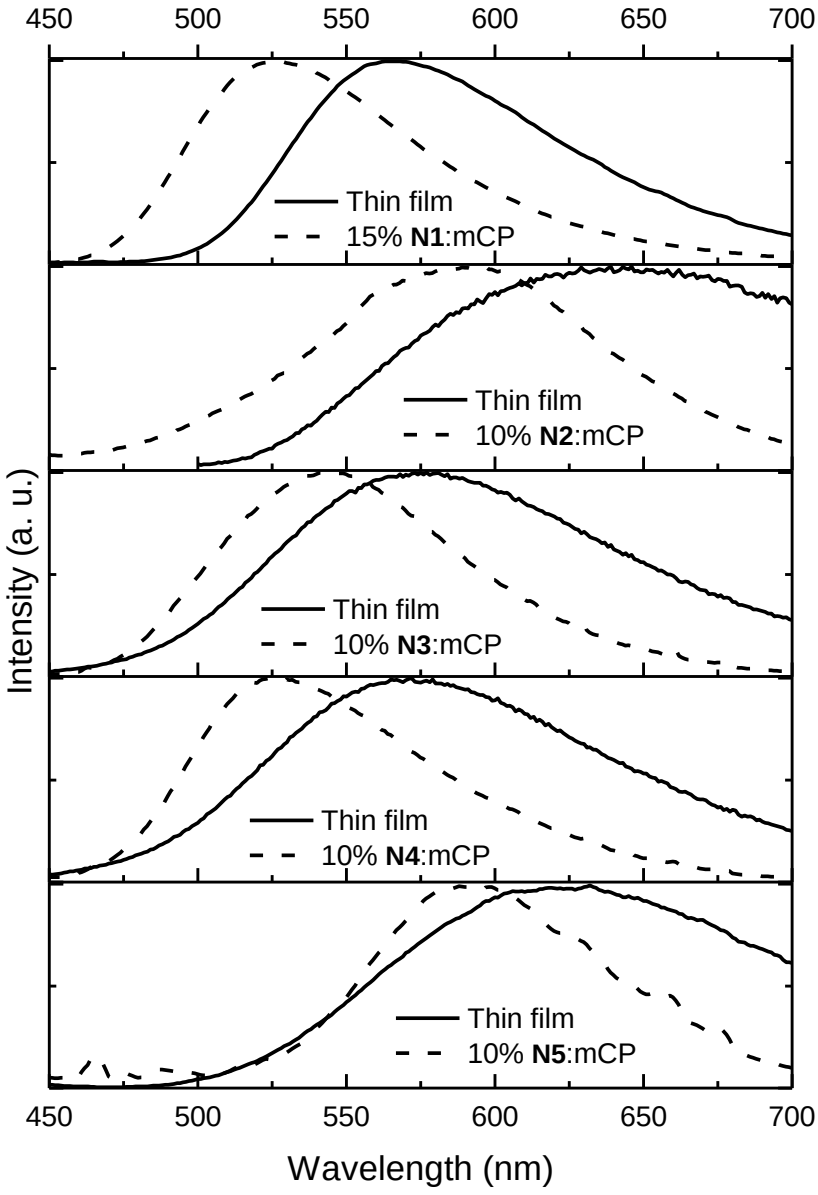

Fig. 38 The PL spectra of derivatives **N1–N5** in mCP matrixes

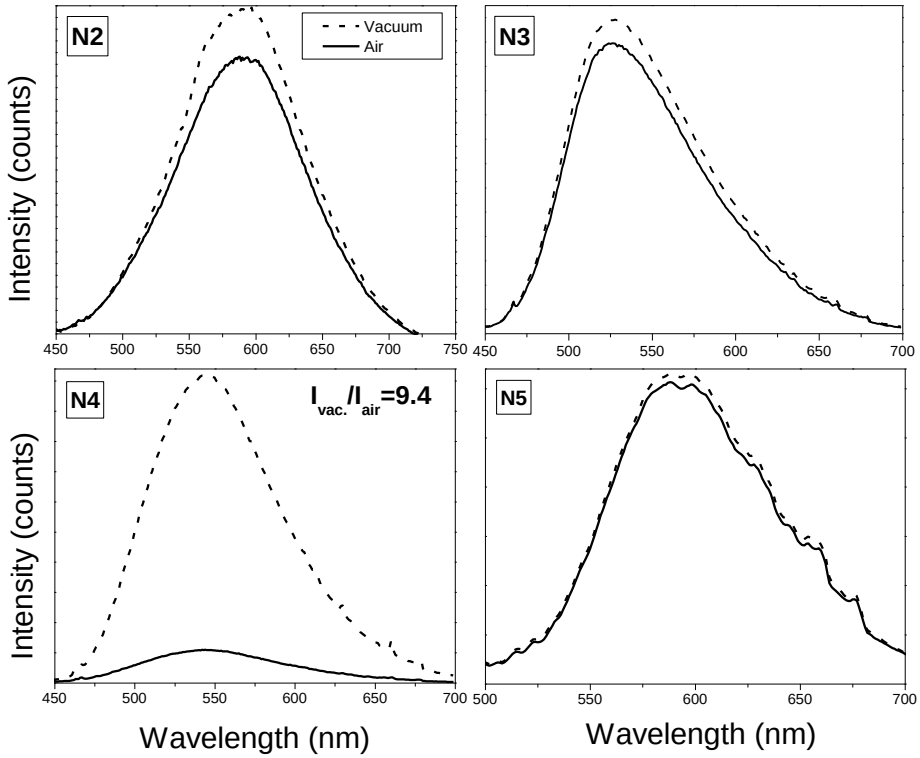

Fig. 39 The intensity of PL of thin films with **N2–N5** and mCP in air and vacuum

The PL spectra of the **N1** in solutions of increasing polarity are shown in **Fig. 40**. Strong solvatochromic effect in the PL spectra of the solutions of **N1** is detected as the polarity of the solvent increases, which is consistent with the charge transfer nature of the transitions that are contributing to this band. The bathochromic shift of PL maxima of **N1** solutions increases with increasing dielectric constant of solvents[133] in the order: hexane (ε=1.88), toluene (ε=2.38), THF (ε=7.5), dichlormethane (ε=9.1), acetone (ε=21) and *N*,*N*-dimethylformamide (ε=38), with an overall Stokes shift of 133 nm. An exception was observed for the PL spectrum of the solution of **N1** in methanol (ε=33). Despite the lower polarity as compared to that of *N*,*N*-dimethylformamide, the redshift for the solution in methanol was found to be larger due to the H-bonding potential[134], which additionally results in strong PL quenching.

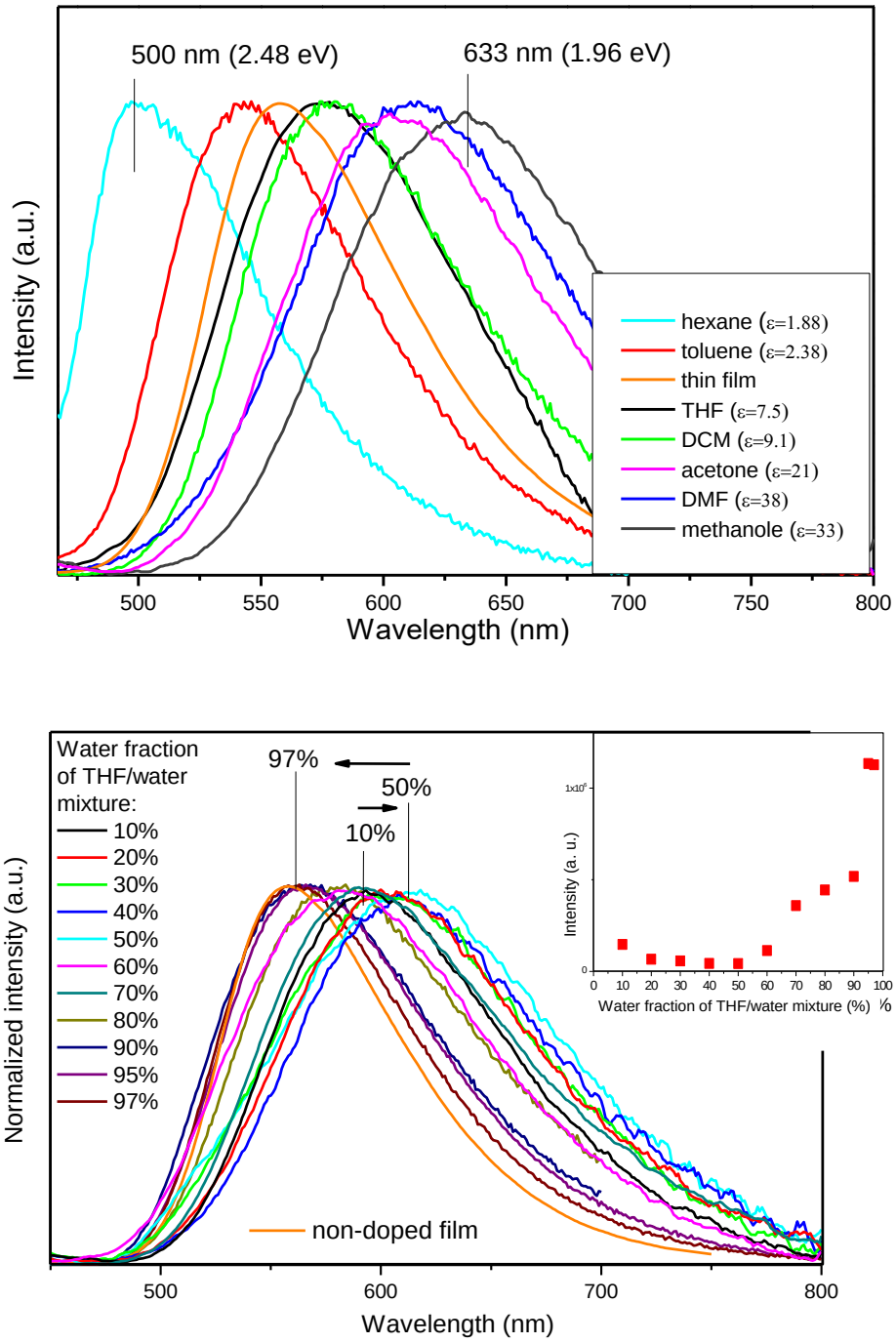

Fig. 40 The solvatochromism properties of derivative **N1**

4.2.1. TADF exploration

The excited state dynamics of **N1** dispersed in different media was investigated by recording emission decay curves at the wavelength of PL maximum (**Fig. 41**). The PL decay curve of dilute THF solution (as prepared) exhibited double exponential decay with τ_1= 14 ns and τ_2= 103 ns. The lifetimes of long-lived components τ_2 of deoxygenated THF solution and the solid film of **N1** were found to be considerably longer, i.e., 438 ns and 802 ns, respectively.

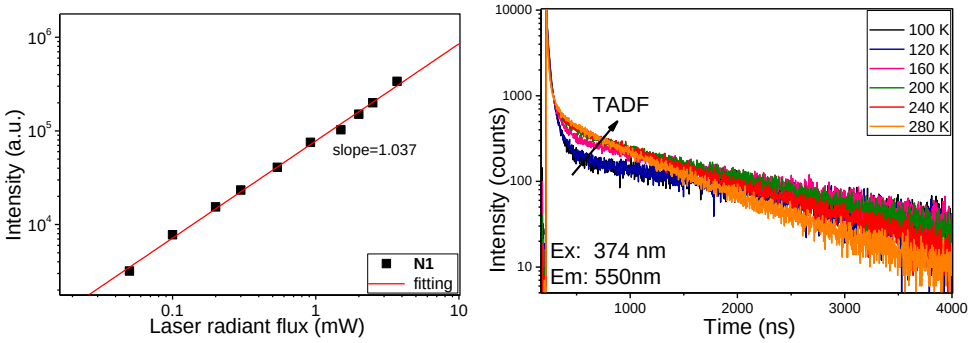

Fig. 41 The confirmation of TADF properties of **N1**

Given the strong quenching induced by oxygen, τ_2 of 103 ns could be assigned to the non-radiative decay (NRD), thus suggesting for τ_2 of 438 ns in deoxygenated THF, a radiative PL stemming from the TADF mechanism. The attribution of the long-lived component of the solid layer of **N1** to TADF was confirmed by the linear dependence of the PL intensity on laser flux with the slope of ca. 1, which is typical for TADF molecules[135] (**Fig. 41**). In addition, upon temperature increase, the increasing intensity of long-lived component related to TADF was detected by PL decay measurements of vacuum deposited layer of **N1**. The shapes of the PL spectra of the solid-state layer of **N1** were found to be similar in the range of temperatures from 100 to 300 K.
In order to investigate the emissive nature of the studied derivatives **N2–N5**, PL spectra and PL decay curves were recorded for the synthesized compounds in contained oxygen and oxygen free dilute toluene solutions. The solutions emitted light with independent PL spectra on the oxygen contents displaying fluorescence nature on emission. However, their PL decay curves clearly demonstrated two-exponential attenuation of emission, which most possibly related to prompt and delayed fluorescence **(Fig. 42 A).**

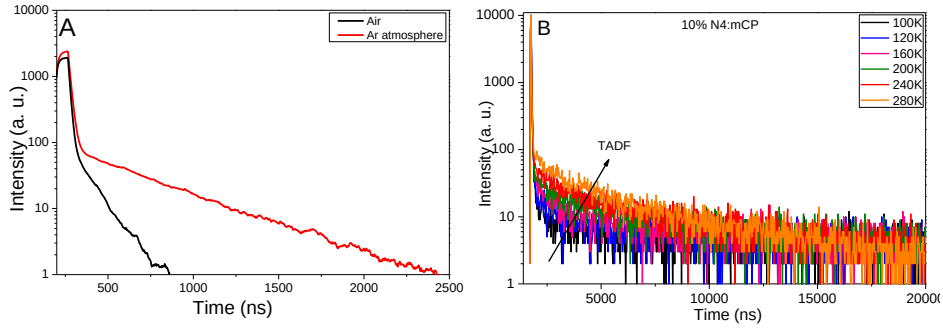

Fig. 42 The photoluminescence decay times of derivative **N4:** A – in argon and air conditions, B – in 100 and 300 K temperatures of 10% **N4** in mCP matrix

In order to find out the nature of the delayed fluorescence for the studied emitters, ΔE_{ST} values were obtained for the studied compounds **N2–N5** in dilute THF solutions and hosted films by using mCP as the low-polar host (ε=2.84) recording their PL and phosphorescence (Ph) spectra at 77K. Due to the very small ΔE_{ST} values that were obtained for **N2–N5** compounds (**Table**), the emission of studied emitters can be characterized by TADF nature. This assumption was well proved, since the intensity of the delayed fluorescence for all emitters successively increased by increasing temperature from 77 to 300 K, undoubtedly establishing distinct TADF nature of the studied compounds. The example of **N4** photoluminescence decay times is shown in **Fig. 42 B**.

4.2.2. Aggregation-induced enhanced emission characteristics

Studying PL spectra of the dispersions of compounds **N2–N5** in THF/water mixtures with different water fractions (f_w), their AIEE properties were detected.

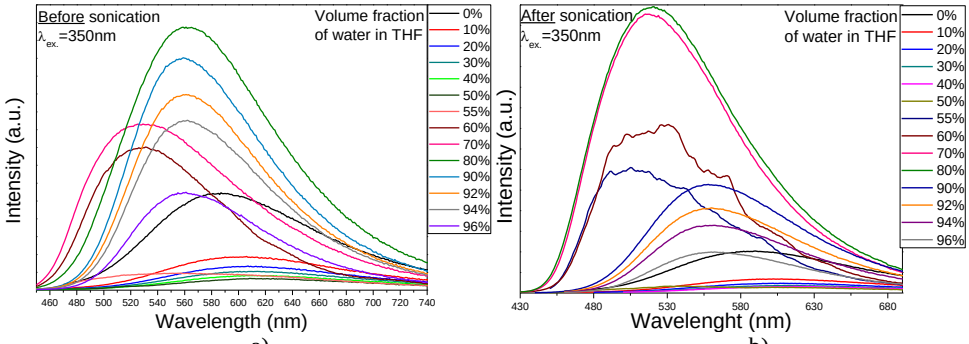

Fig. 43 PL spectra of the dispersions of N3 in THF/water mixtures with different water fractions before (a) and after (b) sonication

When the aggregates of **N2–N5** were formed at the certain f_w, a considerable increase of PL intensity of the dispersions relative to that of the THF solutions was observed, displaying AIEE effect. For example, due to the aggregation, the PL

intensity enhancement was detected for the dispersion of compound **N3** in THF/water mixture at f_w=55% (**Fig. 42**). At the highest f_w, the PL spectra of the dispersions in THF/water mixtures were very similar to the PL spectra of spin-coated films of the compounds. The PL spectra of the dispersions in THF/water mixtures as well as their intensities were quite dependent on the values of f_w. For instance, red-shifts of the PL spectra from 586 to 613 nm and the decrease of PL intensities were observed for the dispersions of **N3** in THF/water mixtures with the increasing values of f_w from 0% to 50% (**Fig. 43**). This observation can be explained by the sensitivity of **N3** emission that is characterized by ICT nature to change the dielectric constant of THF/water mixtures with the addition of water. In addition to the PL intensity enhancement, strong PL blue-sift from 613 to 527 nm was detected for the dispersion inTHF/water mixture of **N3** at higher f_w then ca. 55%, apparently due to the change of polarity of the media. This PL spectrum with the maximum at 527 nm is blue-shifted in comparison to the PL spectrum of the solid film of **N3** film with the maximum of 562 nm. This observation can apparently be explained by the formation of the first-type of **N3** aggregates with low dielectric constant. In the THF/water mixtures with higher f_w then ca. 70%, the formation of the second-type of **N3** aggregates with higher dielectric constant apparently occurred. Their PL spectra were red-shifted and being very similar to the spectra of the films of **N3**. The strongest PL intensity was observed at f_w of 80%. Further, at f_w>80%, the PL intensity continuously decreased by displaying the quenching, which was apparently induced by the interactions between different **N3** aggregates. Different values of dielectric constants for the first-type and second-type of **N3** aggregates may be explained by assuming different dihedral angles between the donor and acceptor units of **N3**, undoubtedly affecting its own polarity. The difference in dihedral angles between donor and acceptor units of TADF molecules result in their ΔE_{ST} values and TADF efficiency.

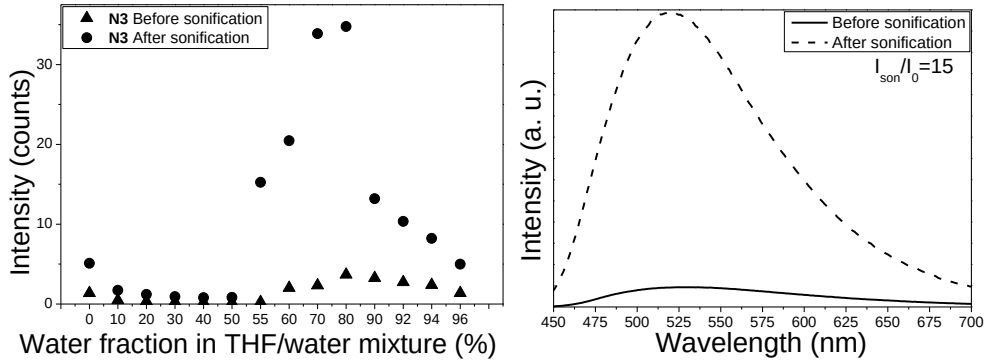

Fig. 44 PL intensities of **N3** in THF/water mixtures with different water fractions before and after sonification (a). PL intensities of **N3** in THF/water mixtures at f_w=80% before and after sonification (b).

Apparently, the second-type of **N3** aggregates were induced by intermolecular interaction (e.g., H-bonding) of **N3** molecules that are containing methoxy groups. Meanwhile, the first-type of **N3** aggregates were formed without the participation of

hydrogen bonds when aggregates are very small. It is known that H-bonds can be broken by heating or applying a sonication bath [134, 136]. Therefore, the dispersions of **N3** in THF/water mixtures were treated by sonification for the corroboration of this assumption. Indeed, the green emission of **N3** aggregates was observed instead of yellow one for the mixtures after sonification (**Fig. 44**). This observation proves that the second-type of **N3** aggregates switched to the first-type of **N3** aggregates due to the breaking of intermolecular bonds (i.e. H-bonds). Since more intensive emission was recorded after the sonification, the breaking of intermolecular bonds resulted not only in the shift of the spectrum, but in the additional AIEE ("double" AIEE) as well. The "double" AIEE can be explained by the increase of dihedral angles between the donor and acceptor units of **N3** after the sonification leading to the decrease of ΔE_{ST} and increase of TADF efficiency. The similar behaviour was observed for methoxy-substituted compound **N4**. However, small differences were observed for the dispersions in THF/water mixtures of compounds **N2** and **N3** which are not capable of hydrogen bonding.

4.2.3. OLEDs with isophthalonitrile-based emitters

In order to estimate the effect of polarity of guests on the PL efficiency of **N1**, the host-guest systems were prepared by taking p-type mCP and TCTA, n-type DPEPO and bipolar 3,6-bis(carbazol-9-yl)-9-(2-ethyl-hexyl)-9H-carbazole (TCz1) hosts for **N1** guest. The hosts were selected taking into account the HOMO and LUMO energy levels of the components of host-guest systems. Due to the triplet energy level (2.92eV), bipolar mobility, values of HOMO/LUMO levels, TCz1 was successfully utilized as the host, electron-transporting and even as the violet/blue emitting material[137, 138, 139, 140]. However, TCz1 was not used for the fabrication of TADF OLEDs up till now.
The similar profiles of the PL spectra for mCP:**N1**, TCTA:**N1**, DPEPO:**N1** and TCz1:**N1** but with the different wavelengths of PL maxima ranging from 529 to 552 nm were observed (**Table 16**). In contrast to the reported study[32], there were not observed any exciplex emission (which may explain the shifts of PL maxima) for the studied TADF host-guest systems.
Effect of host polarity. In order to obtain the insight on the impact of hosts on PL spectra of host-guest systems, the dielectric constants of **N1** and several hosts were measured (**Table 16**). It was found that the trend of PL-maxima wavelengths of mCP:**N1**, TCTA:**N1**, DPEPO:**N1** and TCz1:**N1** systems with 15 wt. % of guest does not correlate with the dielectric constants of hosts. Indeed, while mCP with lowest ε=2.84 showed PL maximum at 533 nm, TCTA with twice higher value of ε=5.61 exhibited PL maximum at shorter wavelength (529 nm). Moreover, pure layer of **N1** with relatively small ε=3.15 showed the largest bathochromic shift of the PL maximum (565 nm). Additional PL measurements of molecular mixtures mCP:N1 and TCz1:**N1** with the different concentration of **N1** support this conclusion: despite the respectively lower- and larger polarity of mCP (2.85) and TCz1 (4.85) as compared to **N1** (3.15), similar PL redshifts with increasing concentration of

N1 were observed for both guest-host systems. All these results in concert lead to the conclusion that the position of PL maxima of the guest-host systems decorrelates with the host-polarity.
Interestingly, the polarity of the hosts seems to have no effect on the singlet-triplet energy splitting of **N1**. The measurement of ΔE_{ST} of guest-hosts mixtures containing 10% of **N1** in mCP, TCz1 and TCTA exhibit identical ΔE_{ST} values of 0.016eV, despite the important differences in host dielectric constants (ε=2.84, 4.85, and 5.61 respectively).

Table 16 The host: **N1** characteristics

Host	**PL of N1:host, nm**	**ε**	**QY of N1:host, %**	**S_t, eV**	**T_t, eV**	**ΔE_{ST}, eV**	**ΔT, eV**
mCP	533	2.84	83	4.06	3.28	0.78	1.04
TCTA	529	5.61	54	3.70	3.07	0.63	0.83
DPEPO	552	6.12	60	-	-	-	-
TCz	537	4.85	73	3.63	3.15	0.49	0.90
N1	565	3.15	47	2.26	2.24	0.02	-

As the final point, It should be noted that the absence of host polarity impact on the PL maximum wavelength and ΔE_{ST} should not be considered as an absolute effect, given the strong solvatochromic effect shown in **Fig. 40**. It is suggested that inside the narrow window of the host dielectric constants tested in this study (2.85–6.12), the host-polarity effect on the charge transfer state energies varies very little, thus constituting a minor effect as compared to the dominant effect of aggregation on the dihedral angles.
The estimation of electroluminescence properties of the structure ITO/MoO_3/**N1**/LiF/Al was made. The devices with not annealed and annealed emitters were prepared. The OLEDs showed 560 and 537nm electroluminescence maxima with not annealed and annealed emitters respectively. For the estimation of electroluminescent properties of **N1** as emitter, the devices with the host were prepared by the structure of ITO/MoO_3/NPB/host:**N1**/TPBi/Ca:Al (**Fig. 45**) that were fabricated and characterized. The efficient injection and transport of holes and electrons from the ITO anode and the Ca cathode to the host:**N1** layer can be expected according to HOMO and LUMO levels of the used materials. The different hosts, i.e., mCP, DPEPO, TCTA and TCz1 were used to fabricate devices I–IV, respectively. The non-optimized concentration of 20 wt% of **N1** emitter (guest) in the host:guest emitting layer of the devices I–IV was taken. The hosts were mainly selected on the basis of their appropriate HOMO and LUMO levels for the charge injection, charge-transporting properties and high triplet-energy levels.

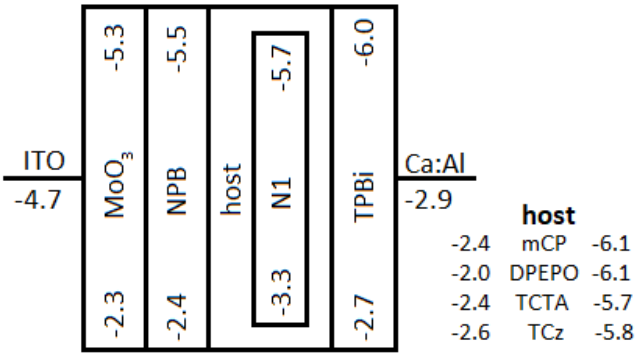

Fig. 45 The OLED structure with **N1** emitter

The output characteristics are presented in **fig 46**, and the key output parameters of devices are given in **table 17**. The EL intensity maxima of devices I–IV were found to be in the range from 521 to 540 nm. Some noises of electroluminescence of device 2 are due to the low intensity of electroluminescence on turn-on voltage. Commission Internationale de l'Eclairage (CIE 1931) chromaticity coordinates (x, y) of the devices that are presented in **table 17**. The CIE chromaticity coordinates how devices I–IV correspond to green, green/yellow, yellow colours depending on the used host. The highest values of maximum brightness and maximum EQE were obtained for the device IV, showing that the most efficient correlation between PL quantum yield and the charge balance and TADF efficiency were observed for the system TCz1:**N1**.

Table 17 Characteristics of devices with **N1** emitter

	V_{on}, V at set 10/1000 cd/m^2	Max brightness, cd/m^2	Current efficiency, cd/A	Power efficiency, lm/W	EQE, %	λ_{OLED} at 5V, nm	CIE colour coordinates at 5V (x, y)
			max/1000 cd/m^2				
1	3.4/5.2	3900	7/6.7	5.2/4.3	2.2/2	521	(0.27, 0.56)
2	3.6/6.1	4900	9.7/7.5	6/4.2	2.8/2.3	536	(0.35, 0.56)
3	3.1/4.9	8400	11/9.2	13.7/5.6	4.5/2.4	536	(0.34, 0.59)
4	4.55/7.7	34700	18/17	9.5/7	4.8/4.6	540	(0.37, 0.58)
5	3.55/6.8	35500	66.5/67	49/31	18/17.1	540	(0.36, 0.58)
6	2.3/5.7	44900	63/58	33/26	17.1/15	540	(0.36, 0.59)
7	2.4/4.2	20700	68/46	62/31	22.5/12.8	532	(0.33, 0.6)

The concentration of **N1** was additionally optimized in the light-emitting layer of device IV. Devices V–VII were fabricated with the same structure as device IV, but with the different concentrations of **N1** in TCz1: 15% (device V), 10% (device VI), and 5% (device VII). EL spectra of devices V, VI, and VII are plotted, and the CIE chromaticity coordinates that are calculated at 5V are given in **table 17**. Similar EL spectra were recorded for all the devices (V–VII) (**Fig. 46**). Only slight shift towards lower energies of the maximum of EL spectrum of device VII was observed. This

shift lead to the change of emission colour to green with CIE (0.33, 0.6) for device VII compared to the devices IV, V, VI, which emitted in the yellow region with CIE (0.37, 0.58), (0.36, 0.58), (0.36, 0.59), respectively.

The electroluminescence maxima of devices **1** and **3** were the same at the interval of voltages 4–10V. The PL spectra of device **2** were similar, but the influence of voltage for wavelength maxima were observed for device **4** and **5–7** as well. The electroluminescence spectra of devices at different voltages and the electroluminescence spectra of devices **1–4** at 5V are shown in **fig. 46**.

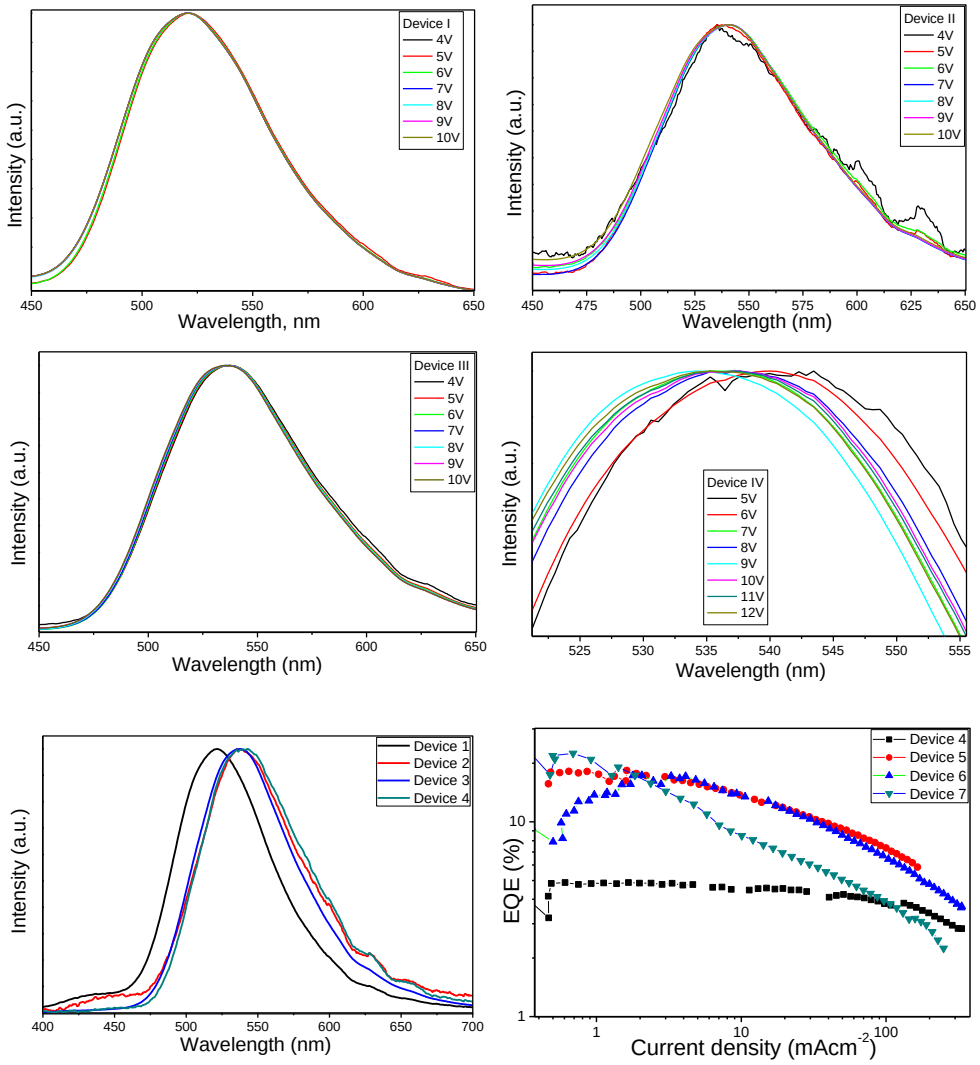

Fig. 46 Electroluminescent characteristics of devices **1-7**

The devices containing emitters **N2–N5** were prepared. Their structure was ITO/ MoO_3/ NPB/ mCP: **N2-N5**/ TSPO1/ TPBi/ Ca:Al. TCz was selected as host taking

into account its good performance in combination with emitter **N1** and due to appropriate HOMO and LUMO levels. The characteristics of OLEDs are given in **fig 47**.

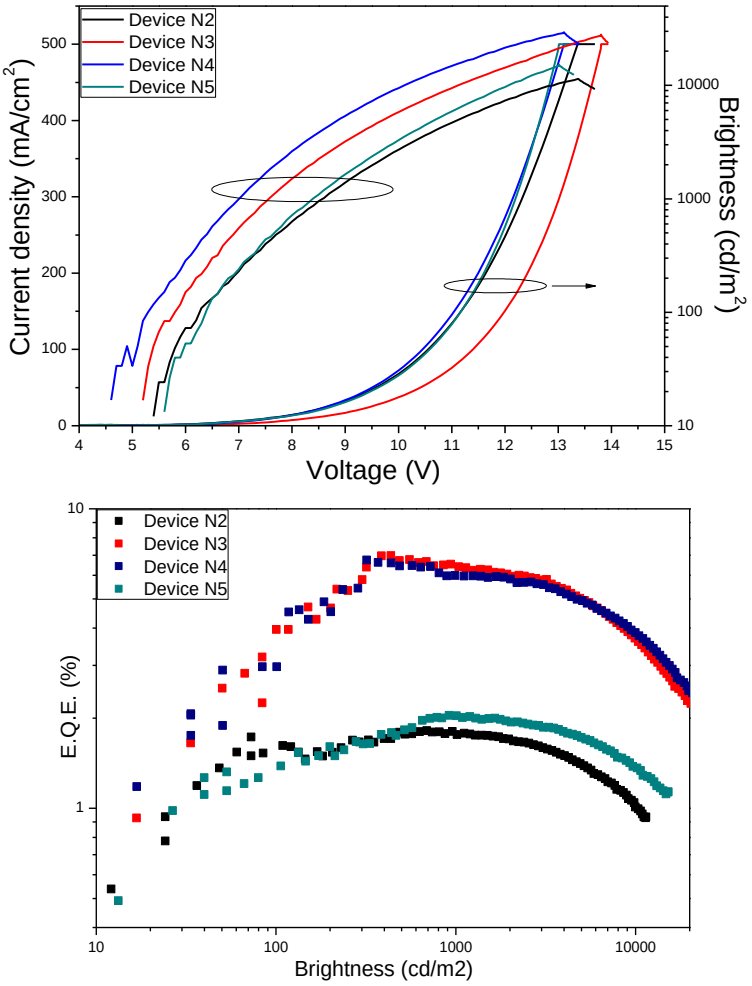

Fig. 47 Electroluminescent characteristics of OLEDS containing emitters **N2–N5**

The devices exhibited electroluminescence in green (carbazole-based derivatives) or orange (phenothiazine and phenoxazine based derivatives) spectral region. The electroluminescence intensity maxima of devices containing emitters **N2–N5** were observed at 586, 521, 528 and 580 nm, respectively. The characteristics of the devices are summarized in **table 18**. The wavelengths of electroluminescence intensity maxima of OLEDS are shorter by 47–98nm, comparing with those of the PL spectra of pure derivatives **N2–N5.** This observation can be explained by the effect of host material on electroluminescence spectra of the devices. The same phenomenon was observed for OLED with **N1** emitter. No tangible influence of the

position of metoxy substituents of carbazole moiety on the device performance was observed. The characteristics of OLEDs, containing emitters **N3** and **N4,** were found to be comparable. The devices containing emitters **N2** and **N5** were found to be rather ineffective. Thus, it is possible to conclude that phenothiazinyl and phenoxazinyl substituted isophtalonitriles are not very promising emitters for OLEDs.

Table 18 The characteristics of devices with **N2–N5** emitters

Emitter	**EQE, %**	**Max. brightness**	**Power efficiency, lmW^{-1}**	**Current efficiency, cdA^{-1}**	**CIE**
	max/ 1000 cdm^{-1}	cdm^{-1}	max/1000 cdm^{-1}	max/1000 cdm^{-1}	X; Y
N2	1.8/1.8	11400	12.7/11.6	4.45/4.30	0.49; 0.49
N3	7.0/6.5	28100	54.7/46	22.9/21.1	0.25; 0.57
N4	6.7/6.0	29000	48.3/44	22.4/19.8	0.29; 0.6
N5	2.0/2.0	15100	16.0/14.6	5.47/5.45	0.49; 0.49

4.3. Phenylpyridine dicarbonitrile-based derivatives

Pyridine, carbonitrile, sulphones and other simple electron withdrawing moieties are widely used in the design of TADF materials[27]. More complex acceptors with some electron withdrawing blocks such as pyridine carbonitriles are less explored, but more complex acceptor structures often provide desirable properties of TADF materials[141,142]. Thus, it is worth of focussing on exploration of complex acceptors. The structure of substituents on pyridine ring was selected according to the literature data with the aim to obtain compounds exhibiting PL in high-energy spectral region[32, 33, 143]. The usage of methoxy and other alcoxy substituents are widely described in literature[41, 95] and known as a tool of improving thermal and photophysical characteristics of the materials[144]. The introduction of *tert*-butoxy substituents affect photophysical properties[145], solubility and glass-forming properties of compounds[146].

The series of pyridine dicarbonitrile-based derivatives were synthesized by sodium or potassium *tert*-butoxide catalysed nucleophilic coupling reaction or Buchwald-Hartwig coupling method (**scheme 3**). The compounds were obtained in low to moderate yields ranging from 8 to 41%. The higher molecular mass substituents such as diphenylcarbazole, N,N-di(di-(*tert*-butyl)-phenyl)-amine or N-biphenyl-N-(*tert*-butyl)-phenylamine were incorporated by using Buchwald-Hartwig coupling. For example, **P1** was obtained by nucleophilic coupling reaction with the yield of 41%, while the **P6** was prepared by Buchwald-Hartwig coupling reaction with the yield of 8% . The compounds were obtained as transparent, yellow or red crystalline substances.

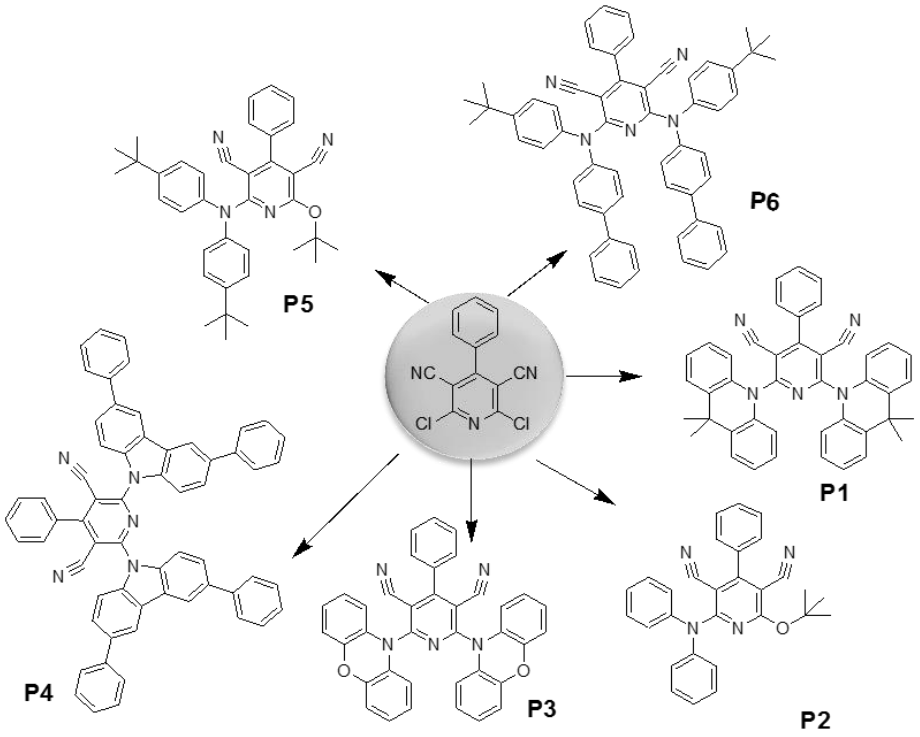

Scheme 3 Synthesis of phenylpyridine dicarbonitrile-based derivatives **P1–P6**

The thermal properties were evaluated by TGA and DSC. The characteristics are summarized in **table 19**. The examples of DSC curves are shown in **fig. 48**. The derivatives were obtained as crystalline materials and showed melting temperatures higher than 240 °C. The derivative **P2** did not form molecular glass, the crystallization peaks were observed on the DSC curve of cooling processes. The derivatives **P5** and **P6** formed unstable molecular glasses. The crystallization peaks were found in the second heating scans.

Table 19 Thermal characteristics of derivatives **P1–P6**

Derivative	T_m, °C	T_g, °C	T_{cr}, °C	$T_{-5\%}$, °C
P1	241	122	-	366
P2	318	-	266*	332
P3	267	111	-	356
P4	250	120	-	333
P5	255	128	223	350
P6	273	128	182	337

* - DSC cooling;

Thus, the derivative **P2** with diphenylamino substituent did not form molecular glass, but **P5** containing di-*tert*-butyldiphenylamino group could be transformed into

the glassy state. This observation can be explained by the presence branched aliphatic substituent on aromatic rings of **P5.**

Compounds **P1–P6** exhibited high thermal stability. Their 5% weight loss temperatures were found to be close and ranged in narrow interval from 332 to 366 °C.

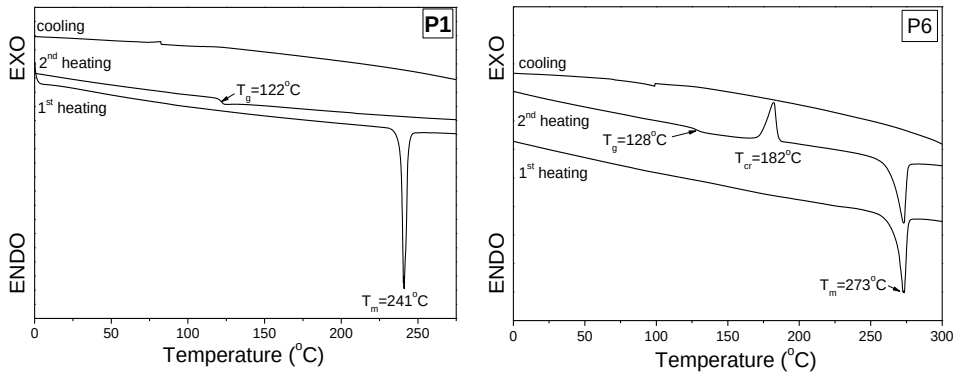

Fig. 48 The DSC thermograms of derivatives **P1** and **P6**

In order to explore electrochemical stability and energy levels of derivatives **P1–P6**, the investigations were performed by cyclic voltammetry. The measurements were recorded for the diluted solutions in dichloromethane or acetonitrile. The electrochemical characteristics of derivatives **P1–P6** are summarized in **table 20**. The ionization potentials were found to be in the range of 5.44–5.82eV. The electron affinities of the derivatives were in the range of 2.30–2.95eV. The reversible processes of oxidation-reduction were observed for derivatives **P2–P6**, and the irreversible process was recorded for derivative **P1**. *tert*-Butoxy substituted derivatives **P2** and **P5** showed lower electron affinities and higher ionization potentials than derivatives without *tert*-butoxy substituents. Phenoxazinyl-substituted derivative **P3** exhibited the lowest ionization potential among the synthesized phenylpyridine dicarbonitrile based derivatives. The reduction potential was not fixed for derivative **P6** at the used conditions.

Table 20 Electrochemical characteristics of derivatives **P1–P7**

Derivative	**I_{ox}, V**	**I_{red}, V**	**I_P(CV), eV**	**E_A(CV), eV**	**HOMO,** eV	**LUMO,** eV
P1	0.71	-1.86	5.51	2.94	-5,43	-2,10
P2	1.03	-2.33	5.82	2.47	-5.73	-1.69
P3	0.64	-1.85	5.44	2.95	-5.73	-2.49
P4	0.98	-1.85	5.78	2.95	-5.51	-2.66
P5	0.96	-2.50	5.76	2.30	-5.57	-1.50
P6	0.72	Not fixed	5.52	-	-5.63	-2.0

The HOMO and LUMO energies were calculated by using Gaussian software by the density functional theory with the B3LYP energy functional and 6-31G(d,p) basis set in vacuum. The theoretical calculations of **P2** were based on crystalline structure confirmed by X- ray analysis. The **fig. 49** is showing the crystalline structure and angles between some bonds of molecule. The volume of the molecule in crystal was found to be 2529Å^3. The distributions of HOMO and LUMO orbitals are shown in **fig. 49**. HOMO and LUMO orbitals of the derivatives are not completely separated for all the structures that were studied. The results of HOMO and LUMO energy values correlate with ionization potentials and electron affinities estimated by the CV measurements. LUMO energy levels of **P2** and **P5** were found to be lower than those of other derivatives of this family. The trends LUMO levels as well correlate with the experimental values of electron affinities that were obtained by CV. The highest LUMO levels were obtained for compounds **P2** and **P5** containing *tert*-butoxy substituents**.**

Photophysical properties of derivatives **P1–P6** were investigated by UV-vis absorption and PL spectroscopies. The experimental photophysical characteristics of the compounds are summarized in **table 21**. The values of optical band gaps, singlet and triplet energies were estimated by using Planck hypothesis. PL quantum yields of the solid films of the materials ranged from 5 to 45%. The highest PL quantum yield was observed for the film of compound **P2** containing *tert*-butoxy substituent. The solid sample of another derivative of *tert*-butoxy substituted pyridine (**P5)** showed considerably lower PL quantum yield of 27.5%. This observation can apparently be explained by the attachment of bulky *tert*-butyl substituents to diphenylamino moieties of **P5**. The films of compounds **P1** and **P4** as well showed relatively high PL quantum yields for the solid samples (20 and 28%). Interestingly, these compounds showed the lowest values of $\mathbf{\Delta E_{ST}}$. All the compounds exhibited relatively high triplet energies, which ranged from 2.71 to 2.9 eV. The highest triplet energies were observed for compounds **P2** and **P5**. Singlet energies of the compounds were found to be in the range of 1.96–3.16eV. The singlet energy of **P2** was found to be higher than **P5**, but their triplet energies were the same. Di-*tert*-butyl substituted derivative **P5** exhibited lower $\mathbf{\Delta E_{ST}}$. This observation is in agreement with the literature data, showing that the introduction of *tert*-butyl substituents results in the decrease of singlet-triplet energy splitting[46]. The diphenyl-substituted carbazole derivative **P4** exhibited lower singlet and triplet energies and much wider splitting of singlet and triplet energies than the similar compound containing unsubstituted carbazole moiety[147]. Phenoxazine substituted derivative **P3** showed no phosphorescence in THF solution at 77K. Therefore, it was impossible to estimate its triplet energy.

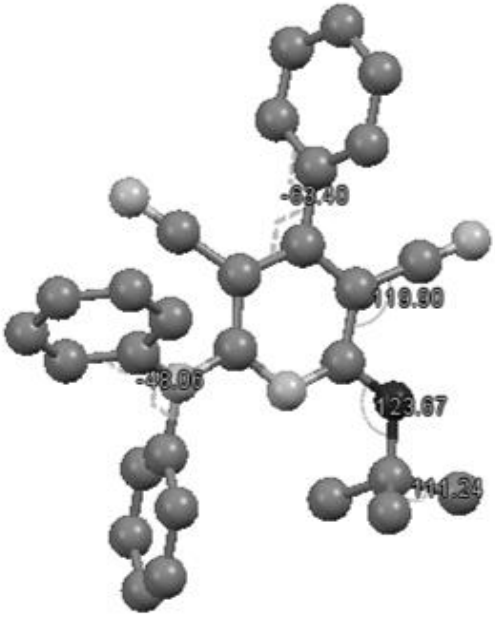

(a)

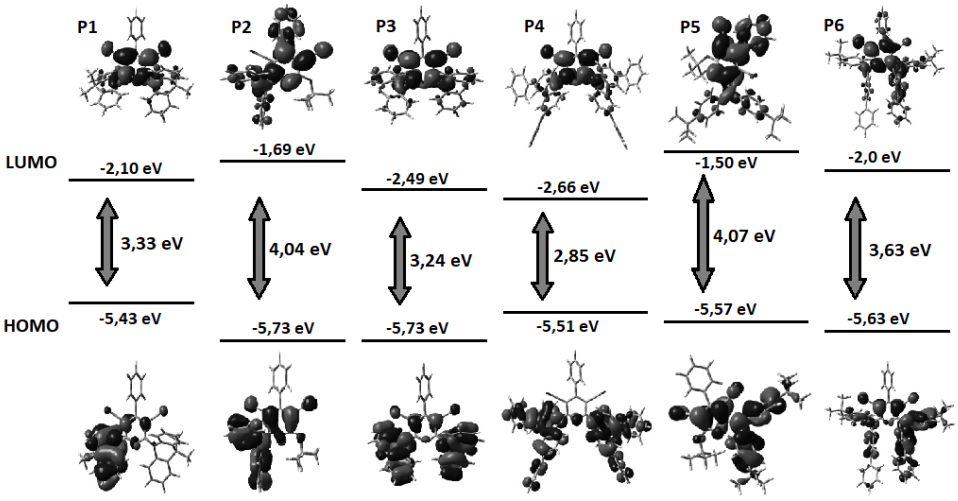

(b)

Fig. 49 (a) The crystalline structure of **P2** estimated by X ray analysis (b) Theoretical HOMO and LUMO orbitals and energies of compounds **P1**–**P6**

Table 21 The photophysical characteristics of derivatives **P1–P3**

	E_g^{opt}, eV	λ_{Pl}, nm	QY, %	λ_{Phos} (THF), nm	E_S, eV	E_T, eV	ΔE_{ST}, eV
P1	2.73	591	20	505	2.72	-	-
P2	3.01	478	45	471	3.16	2.90	0.26
P3	2.51	634	5	-	1.96	-	-
P4	2.63	547	28	515	2.81	2.71	0.10
P5	2.87	491	27.5	515	3.01	2.90	0.11
P6	2.82	513	6	518	3.05	2.72	0.33

Deoxygenation effects of the PL spectra of the compounds were investigated by purging with argon their dilute solutions. The photoluminescence were excited by 310nm wavelength light for derivative **P2** and 350 nm for others derivatives. The solution of **P3** in toluene exhibited very low PL intensity, and it was impossible to register its PL spectrum. The results of measurements are shown in **fig. 50**. The PL quantum yields of the solutions of all the derivatives increased after the deoxygenation. The PL quantum yield of the solution of **P6** rose from 10 to 78%. The oxygen-free solutions of derivatives **P1**, **P3** and **P5** exhibited noticeably lower PL quantum yields than their solid films. The PL quantum yields of deoxygenated solutions of derivatives **P2** and **P4** were found to be close to those of their solid films. This observation allows to presume that the aggregation induced emission enhancement is characteristic for compounds **P1**, **P3** and **P5.**

The PL decay curves of toluene solutions of pyridine-based derivatives were recorded by using 374 nm picosecond laser beam excitation (**Fig. 51**). The investigations were measured at ambient and oxygen-free conditions. In PL, the decay curves of deoxygenated solution of derivatives **P1**, **P4**, **P5** and **P6** intensities of longer-lived components were found to be higher than those of air equilibrated solutions. This observation indicates the participation of triplet excitons in the emission of these compounds. The PL decay curve of the solution of derivative **P2** exhibited very low intensity at the decay times longer than 150ns both at ambient and oxygen free conditions.

The processes of solvatochromizm were investigated by PL spectroscopy by using solutions of the compounds in the solvents of different polarity[133] such as hexane, toluene, chloroform, tetrahydrofurane, dichloroethane, acetone and acetonitrile. The values of PL maxima of the solutions in different solvents and dielectric constants with refractive index of solvents are given in **table 22**. Due to the insolubility of the derivatives **P1–P6** in methanol, butanol, isopropanol and dimethylsuphoxide, these highly polar solvents could not be used in the measurements of solvatochromism. The derivative **P3** exhibited no PL from solutions, and the characteristics of solvatochromism were not-explored.

Fig. 52 shows the dependence of maxima of PL and solvent polarity. All the studied compounds showed strong solvatochromic effect. The strongest red shift with the increase was observed for the derivative **P6**. Its PL maximum shifted by 75nm when dielectric constants of solvents increased from 1.9 (hexane) to 37.5 (acetonitrile).

The polarizability properties of solvents are described clearer by the orientation polarizability coefficient Δ*f* which is calculated by formula **9**[19]:

$$\Delta f = \frac{\varepsilon - 1}{2\varepsilon + 1} - \frac{{R_D}^2 - 1}{2{R_D}^2 + 1} \qquad (9),$$

where ε is the dielectric constant of solvent, R_D is the refractive index of solvent.

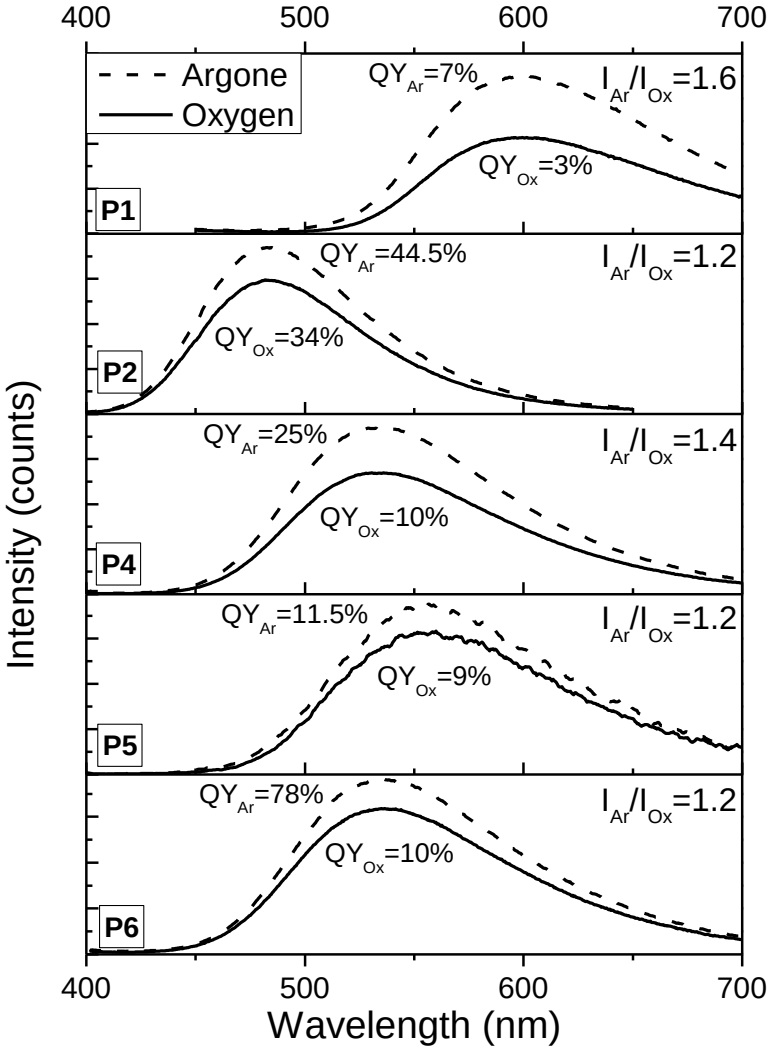

Fig. 50 Deoxygenation effects on PL intensity of the solutions derivatives **P1–P6** in toluene.

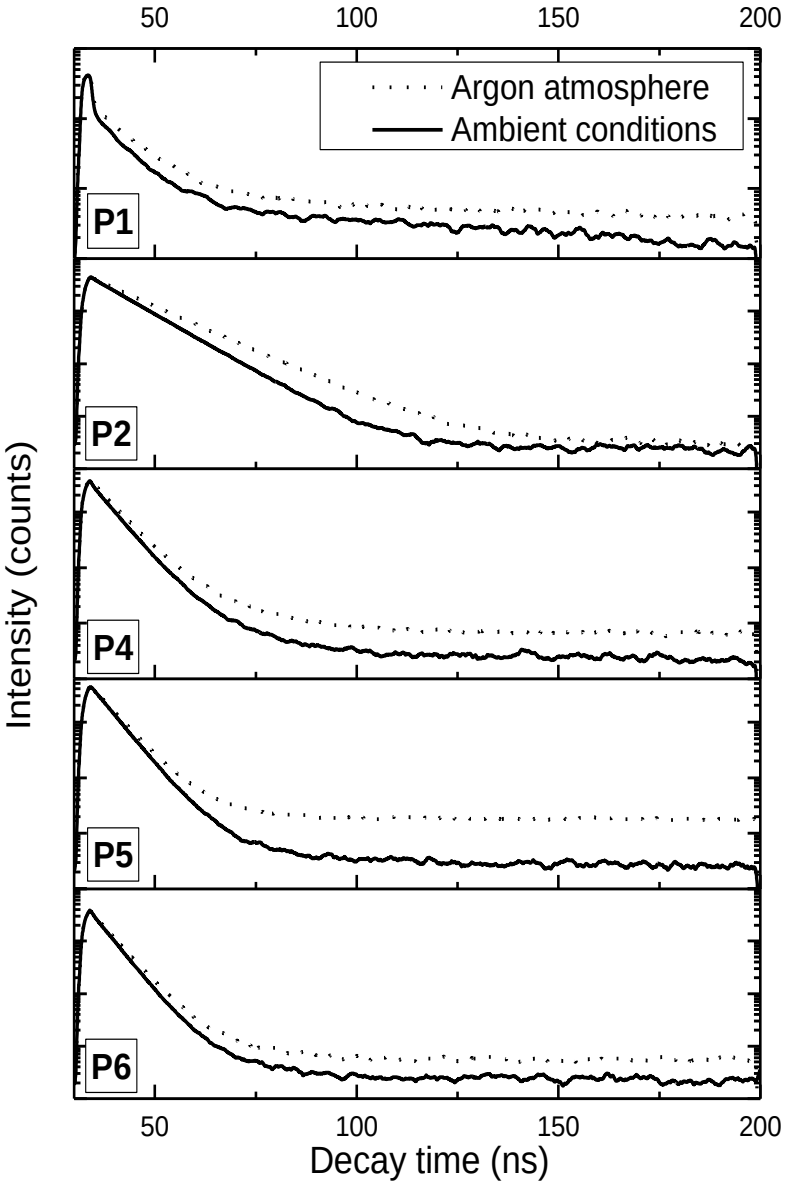

Fig. 51 PL decay curves of the solutions of **P1,P2, P4–P6**.

Table 22 Solvatochromic characteristics of compounds **P1, P2, P4–P6**

Solvent	ε^{133}	R_D^{133}	Δf	λ_{pl}, nm				
				P1	**P2**	**P4**	**P5**	**P6**
Hexane	1.9	1.89	0.001	600	476	524	520	515
Toluene	2.4	31.1	0.013	610	482	533	555	537
Chloroform	4.8	21.0	0.148	636	508	567	565	563
Tetrahydrofuran	7.6	19.9	0.210	641	516	560	569	571
Dichloroethane	10.4	21.0	0.217	652	521	574	574	574
Acetone	20.7	20.7	0.284	661	541	583	584	588
Acetonitrile	37.5	11.1	0.306	670	549	589	589	590
$\Delta\lambda_{pl}$, nm				70	73	65	69	75
λ_{pl}, nm				591	478	547	491	513

The *tert*-butyl-substituted derivative **P4** showed the lowest bathochromic shift with the increase of solvent polarity, but the maximum emission wavelength was longer for the neat film. The bathochromical shift of PL maxima was observed in hexane solutions compared with the neat film for derivatives **P1**, **P2**, **P4**, **P5** and **P6**, but the hypsochromical shift was observed for derivative **P4** as seen as the lowest bathochromical shift by increasing the polarity of solvents. The solvatochromic properties show strong intramolecular charge transfer effect.

4.4. The summary of results and discussion

The three series of compounds were synthesised and investigated. The N-bicarbazole based derivatives formed molecular glasses and exhibited blue light fluorescence. However, the splitting of singlet and triplet energies was too big to show TADF effect. The isophthalonitrile-based derivatives exhibited very low splitting of singlet and triplet energies and exhibited TADF effect, but the photoluminescence maxima wavelengths were longer and were in the range from green to red colour. The morphological characteristics were worse than N-bicarbazole based compounds. Dicyanophenylpyridine compounds exhibited worse photoluminescence quantum yields, but the high influence of chromophore was observed. The synthesis of dicyanophenylpyridine compounds were the most complicated, and the lowest yields were achieved. As seen in the results of photoluminescence characteristics, the most perspective chromophores for OLEDs emitters are carbazole and 9,9-dimethylacridane. The system of strong electrons withdrawing groups and chromophores is influencing the intermolecular charge mobility. It is possible to confirm that by solvatochromic effect.

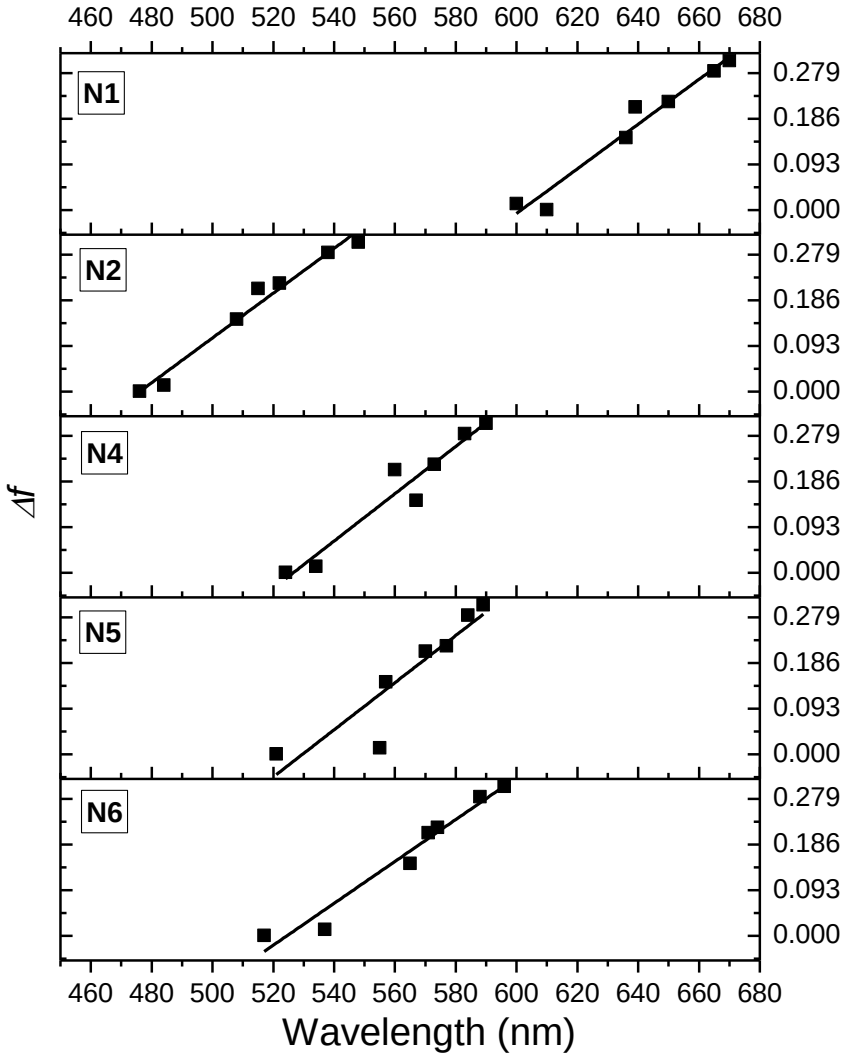

Fig. 52 Δf versus the wavelengths of PL intensity maxima of compounds **P1, P2, P4–P6**

5. CONCLUSIONS

1. The series of new cyanophenyl and cyanocarbazolyl derivatives were synthesized, and their properties were studied.
   1.1. The derivatives exhibited ability to form molecular glasses with glass transition temperatures that are in the range of 77–111 °C; they demonstrated high thermal stability with 5% weight loss temperatures exceeding 300 °C.
   1.2. The synthesised compounds emitted blue or sky-blue light with photoluminescence quantum yields in the range of 15–50%. 3-(2,7-Dicyanocarbazol-9-yl)-9-ethylcarbazole showed the highest photoluminescence quantum yield reaching 50%.
   1.3. The synthesized compounds are capable of hole transporting. The highest hole mobility, exceeding 10^{-4} cm^2/Vs at $6.4 \cdot 10^5$ V/cm electric field, was observed in the amorphous film of 3-(2,7-dicyanocarbazol-9-yl)-9-ethylcarbazole.
   1.4. A combination of cyanophenyl or cyanocarbazolyl electron acceptor moieties and electron donating core resulted in a strong intramolecular charge transfer confirmed by the solvatochromism study of emission.
   1.5. 3-(2,7-Dicyanocarbazol-9-yl)-9-ethylcarbazole was studied as exciplex-forming the emitter in OLED structures. The yellow exciplex OLED exploiting the effect of thermally activated delayed fluorescence had maximum brightness of 6260 cd/m^2 and external quantum efficiency of 5.8%. The sky-blue OLED showed the maximum brightness of 3600 cd/m^2 and maximum current efficiency of 9.9 cd/A, maximum power efficiency of 8.8 lm/W, and maximum external quantum efficiency of 4.2%.
2. The series of new isophthalonitrile-based derivatives containing different donating units were synthesized, and their properties were studied.
   2.1. The ionization potential values of the amorphous layers of the synthesized compounds do not depend on the nature of the donor.
   2.2. The synthesized compounds are capable of transporting holes and electrons.
   2.3. The studied derivatives showed strong intramolecular charge transfer and small singlet-triplet energy splitting (0.02–0.06eV).
   2.4. The synthesized compounds showed thermally activated delayed fluorescence.
   2.5. The derivatives were tested as emitters in OLEDs. 1,3-Bis-(9,9-dimethylacridan-10-yl)-4,6-dicarbonitrilebenzene showed good performance as TADF emitter in OLED with maximum brightness of 20700 cd/m^2, maximum current, power and external quantum efficiencies of 68 cd/A, 62 lm/W and 22.5%.

3. The series of new dicyanophenylpyridine-based compounds containing different electron donor units were synthesized, and their properties were studied.
    3.1. The compounds demonstrated high thermal stability with 5% weight loss temperatures ranging from 332 to 366 °C and high glass transition temperatures in the range of 111–128 °C.
    3.2. The photoluminescence quantum yields of thin films of the synthesized derivatives range from 5 to 45%. 2,6-Bis((4-*tert*-butylphenyl)-(4-biphenyl)-amino)-4-phenylpyridine-3,5-dicarbonitrile solution exhibited the highest photoluminescence quantum yield.
    3.3. The synthesized compounds showed high triplet energies in the range of 2.71–2.90eV.
    3.4. The combination of different electron donating groups with dicyanophenylpyridine electron acceptor core resulted in a strong intramolecular charge transfer that was confirmed by solvatochromism study of emission.

6. REFERENCES

1. ROUND H. J. A note of carborund. *Electr. World*, **1907**, *vol. 19*, 309–310;
2. LOSSEV O. V. Luminous carborundum detector and detection effect and oscillations with crystals. *Philosophical Magazine.* **1928**, *vol. 39*, 1024–1044;
3. BERNANOSE A. et al. Sur un nouveau mode d'émission lumineuse chez certains composés organiques. *J. Chim. Phys*. **1953**, *vol. 50*, 64–68;
4. TANG C. W and VANSLYKE S. A. Organic electroluminescent diodes. *Appl. Phys. Lett*. **1987**, *vol. 51*, 913–915 DOI: 10.1063/1.98799
5. CHO, D.-H. et al. Flexible integrated OLED substrates prepared by printing and plating process *Organic Electronics.* **2017**, *vol. 50*, 170–176. DOI: 10.1021/am501521p.
6. SHOLZ, S. et al. Degradation Mechanisms and Reactions in Organic Light-Emitting Devices. *Chem. Rev.* **2015**, *vol. 115*, 8449–8503. DOI: 10.1021/cr400704v.
7. IHN S.-G. et al. An Alternative Host Material for Long-Lifespan Blue Organic Light-Emitting Diodes Using Thermally Activated Delayed Fluorescence *Adv. Sci.* **2017**, 1600502. DOI: 10.1002/advs.201600502;
8. MÜLEN, K and U. Scherf. Organic Light Emitting Devices: Synthesis, Properties and Applications *Wiley-VCH*, Weinheim **2006** ISBN 3-527-31218-8. pp. 245–261, 338–339;
9. YOOK, K. S. et al. Organic Materials for Deep Blue Phosphorescent Organic Light-Emitting Diodes. *Adv. Mater*. **2012**, *vol. 24*, 3169–3190. DOI: 10.1002/adma.201200627
10. LIU, J. et al. Highly Efficient and Stable Electron Injection Layer for Inverted Organic Light-Emitting Diodes *Appl. Mater & Interfaces* **2015**, *vol. 7*, 6438–6443. DOI: 10.1021/am506300c.
11. ZHOU, X. et al. Very-low-operating-voltage organic light-emitting diodes using a *p*-doped amorphous hole injection layer. *Appl. Phys. Lett.* **2001**, *vol. 78*, 410–412. DOI: 10.1063/1.1343849.
12. SYMALLA, F. et.al. Charge Transport by Superexchange in Molecular Host-Guest Systems *Phys. Rev. Lett.* **2016**, *vol. 117*, 276803. DOI: 10.1103/PhysRevLett.117.276803.
13. KULKARNI, A. P. et al. Electron Transport Materials for Organic Light-Emitting Diodes. *Chem. Mater.* **2004**, *vol. 16*, 4556–4573. DOI: 10.1021/cm049473l.
14. FARCHIONI, R. and GROSSO, G. Organic Electronic materials. Conjugated Polymers and Low Molecular Weight Organic Solids. *Springer-Verlag*, Berlin Heidelberg **2001** ISBN 3-540-66721-0. pp. 215-439.
15. DIAS, F. B. et al. Photophysics of thermally activated delayed fluorescence molecules. *Methods Appl. Fluoresc.* **2017**, *vol. 5*, 012001. DOI: 10.1088/2050-6120/aa537e.
16. WONG, M. Y. et al. Purely Organic Thermally Activated Delayed Fluorescence Materials for Organic Light-Emitting Diodes. *Adv. Mater*. **2017**, *vol. 29*, 1605444. DOI: 10.1002/adma.201605444.
17. BALDO, M. A. et al. Highly efficient phosphorescent emission fromorganic electroluminescent devices. *Nature* **1998**, *vol. 395*, 151–154. DOI: 10.1038/25954.
18. ENDO, A. et al. Efficient up-conversion of triplet excitons into a singlet state and its application for organic light emitting diodes. *Appl. Phys. Lett*. **2011**, *vol*. 98, 083302. DOI: 10.1063/1.3558906.
19. VALEUR, B. Molecular Fluorescence: Principles and Aplications *Wiley-VCH*, Weinheim, **2001** e-ISBN 3-527-60024-8.

20. VALCHANOV, G. et al. Understanding the Fluorescence of TADF Light-Emitting Dyes. *J. Phys. Chem. A* **2016**, *vol. 120*, 6944–6955. DOI: 10.1021/acs.jpca.6b06680.
21. WANG, H. et al. Novel Thermally Activated Delayed Fluorescence Materials–Thioxanthone Derivatives and Their Applications for Highly Effi cient OLEDs. *Adv. Mater*. **2014**, *vol. 26*, 5198–5204. DOI: 10.1002/adma.201401393
22. GOUSHI, K. et al. Organic light-emitting diodes employing efficient reverse intersystem crossing for triplet-to-singlet state conversion. *Nature Photonics* **2012,** *vol. 6*, 253–258. DOI: 10.1038/nphoton.2012.31.
23. YANG, ZH. et al. Recent advances in organic thermally activated delayed fluorescence materials. *Chem. Soc. Rev.* **2017**, *vol. 46*, 915–1016. DOI: 10.1039/C6CS00368K.
24. JOU, Jw.-H. et al. Approaches for fabricating high efficiency organic light emitting diodes. *J. Mater. Chem. C*. **2015**, vol. 3, 2974–3002. DOI: 10.1039/c4tc02495h.
25. WU, Zh. et al. Precise Exciton Allocation for Highly Efficient White Organic Light-Emitting Diodes with Low Efficiency Roll-Off Based on Blue Thermally Activated Delayed Fluorescent Exciplex Emission. *Adv. Optical Mater.* **2017**, 1700415. DOI: 10.1002/adom.201700415.
26. QI, Y. et al. Color stable and highly efficient hybrid white organic light-emitting devices using heavily doped thermally activated delayed fluorescence and ultrathin non-doped phosphorescence layers *Organic Electronics* **2017**, *vol. 43*, 112–120. DOI: 10.1016/j.orgel.2017.01.012.
27. GODUMALA, M. et al. Thermally activated delayed fluorescence blue dopants and hosts: from the design strategy to organic light-emitting diode applications *J. Mater. Chem*. C **2016**, *vol*. 4, 11355–11381. DOI: 10.1039/C6TC04377A.
28. LIN, T. A. et al. Sky-Blue Organic Light Emitting Diode with 37% External Quantum Effi ciency Using Thermally Activated Delayed Fluorescence from Spiroacridine-Triazine Hybrid *Adv. Mater.* **2016**, *vol. 28*, 6976–6983. DOI: 10.1002/adma.201601675.
29. THOMAS, K. R. J. et al. Cyanocarbazole Derivatives for High-Performance Electroluminescent Devices *Adv. Funct. Mater***. 2004**, *vol. 14*, 387–392. DOI: 10.1002/adfm.200305144.
30. RYU, H. et al. Photo- and electroluminescent properties of cyano-substituted styryl derivatives and synthesis of CN–PPV model compounds containing an alkoxy spacer for OLEDs *Tetrahedron* **2006**, *vol*. 62, 6236–6247. DOI: 10.1016/j.tet.2006.04.051.
31. PARK, S. K. et al. High-Performance n-Type Organic Transistor with a Solution-Processed and Exfoliation-Transferred Two-Dimensional Crystalline Layered Film. *Chem. Mater.* **2012**, *vol. 24*, 3263−3268. DOI: 10.1021/cm301775c.
32. UOYAMA, H. et al. Highly efficient organic light-emitting diodes from delayed fluorescence *Nature* **2012**, *vol. 492*, 234–240 DOI:10.1038/nature11687
33. CHO, Y. J. et al. Cool and warm hybrid white organic light-emitting diode with blue delayed fluorescent emitter both as blue emitter and triplet host *Sci. Rep.* **2015**, *vol. 5*, 7859 | DOI: 10.1038/srep07859.
34. PARK, W. J. et al. Effective thermally activated delayed fluorescence emitter and its performance in OLED device *Synth. Met.* **2015**, *vol. 209*, 99–104. DOI: 10.1016/j.synthmet.2015.07.008.
35. SEREVICIUS, T. et al. Enhanced electroluminescence based on thermally activated delayed fluorescence from a carbazole–triazine derivative *Phys. Chem. Chem. Phys*. **2013**, *vol. 15*, 15850–15855. DOI: 10.1039/c3cp52255e.

36. ZHANG, D. et al. Highly efficient blue thermally activated delayed fluorescent OLEDs with record-low driving voltages utilizing high triplet energy hosts with small singlet–triplet splitting. *Chem. Sci.* **2016**, *vol. 7*, 3355–3363. DOI: 10.1039/C5SC04755B.
37. TANAKA, Y. et al. Application of wide-energy-gap material 3,4-di(9H-carbazol-9-yl) benzonitrile in organic light-emitting diodes. *Thin Solid Films* **2016**, *vol. 619*, 120–124. DOI: 10.1016/j.tsf.2016.11.016
38. CHO, Y. J. et al. The Design of Dual Emitting Cores for Green Thermally Activated Delayed Fluorescent Materials. *Angew. Chem. Int. Ed.* **2015**, vol. *54*, 5201–5204. DOI: 10.1002/anie.201412107.
39. LI, B. et al. Dicarbazolyldicyanobenzenes as Thermally Activated Delayed Fluorescence Emitters: Effect of Substitution Position on Photoluminescent and Electroluminescent Properties *Chem. Lett.* **2014**, vol. *43*, 319–321. DOI:10.1246/cl.130907.
40. KIM, M. et al. Highly efficient and color tunable thermally activated delayed fluorescent emitters using a "twin emitter" molecular design *Chem. Commun.*, **2016**, *vol. 52*, 339–342. DOI: 10.1039/C5CC07999C
41. PAN, K.-Ch. et al. Efficient and Tunable Thermally Activated Delayed Fluorescence Emitters Having Orientation-Adjustable CN-Substituted Pyridine and Pyrimidine Acceptor Units *Adv. Funct. Mater.* **2016**, *vol. 26*, 7560–7571. DOI: 10.1002/adfm.201602501.
42. CAI, X. et al. "Rate-limited effect" of reverse intersystem crossing process: the key for tuning thermally activated delayed fluorescence lifetime and efficiency roll-off of organic light emitting diodes. *Chem. Sci*., **2016**, *vol. 7*, 4264–4275. DOI: 10.1039/C6SC00542J.
43. YU, L. et al. Tuning the emission from local excited-state to charge-transfer state transition in quinoxaline-based butterfly-shaped molecules: Efficient orange OLEDs based on thermally activated delayed fluorescence emitter. *Dyes and Pigments* **2017,** *vol. 141*, 325–332. DOI: 10.1016/j.dyepig.2017.02.035.
44. GANESAN, P. et al. Functional Pyrimidine-Based Thermally Activated Delay Fluorescence Emitters: Photophysics, Mechanochromism, and Fabrication of Organic Light-Emitting Diodes *Chem. Eur. J.* **2017**, *vol. 23*, 2858 – 2866. DOI: 10.1002/chem.201604883.
45. NAKAO, K. et al. Significant Enhancement of Blue OLED Performances through Molecular Engineering of Pyrimidine-Based Emitter *Adv. Optical Mater.* **2017**, 1600843 DOI: 10.1002/adom.201600843.
46. CHA, J.-R. et al. Design of ortho-linkage carbazole-triazine structure for highefficiency blue thermally activated delayed fluorescent emitters. *Dyes and Pigments* **2016**, *vol. 134*, 562-568. DOI: 10.1016/j.dyepig.2016.08.023.
47. KIM, M. et al. Simultaneous improvement of emission color, singlet–triplet energy gap, and quantum efficiency of blue thermally activated delayed fluorescent emitters using a 1-carbazolylcarbazole based donor. *Chem. Commun.*, **2016**, *vol. 52*, 10032–10035. DOI: 10.1039/C6CC04516B
48. KIM, D. H. et al. Organic light emitting diodes with horizontally oriented thermally activated delayed fluorescence emitters. *J. Mater. Chem. C*, **2017**, *vol. 5*, 1216–1223. DOI: 10.1039/C6TC04786F
49. KIM, H. M. Et al. Blue thermally activated delayed fluorescent emitters having a bicarbazole donor moiety. *RSC Adv.*, **2016**, *vol. 6*, 64133–64139. DOI: 10.1039/C6RA13240E

50. SUN, K. et al. Highly efficient and color tunable thermally activated delayed fluorescent emitters and their applications for the solution-processed OLEDs. *Dyes&Pigments* **2017**, *vol. 139*, 326–333. DOI: 10.1016/j.dyepig.2016.12.037
51. HUANG, B. et al. Simple aggregation–induced delayed fluorescence materials based on anthraquinone derivatives for highly efficient solution–processed red OLEDs. *Journal of Luminescence* **2017**, *vol. 187*, 414–420. DOI: 10.1016/j.jlumin.2017.03.038.
52. XU, Sh. et al.An Organic Molecule with Asymmetric Structure Exhibiting Aggregation-Induced Emission, Delayed Fluorescence, and Mechanoluminescence. *Angew. Chem. Int. Ed*. **2015**, *vol. 54*, 7181–7184. DOI: 10.1002/anie.201409767.
53. LEE, I. H. High efficiency blue fluorescent organic lightemitting diodes using a conventional blue fluorescent emitter. *J. Mater. Chem.* C **2015**, *vol. 3*, 8834–8838 DOI: 10.1039/c5tc01626f
54. HIGUCHI, T. et al. High-Effi ciency White Organic Light-Emitting Diodes Based on a Blue Thermally Activated Delayed Fluorescent Emitter Combined with Green and Red Fluorescent Emitters *Adv. Mater.* **2015**, *vol. 27*, 2019–2023. DOI: 10.1002/adma.201404967.
55. JEON, S. K. et al. Highly efficient exciplex organic lightemitting diodes using thermally activated delayed fluorescent emitters as donor and acceptor materials. *Nanotechnology* **2016**, *vol. 27*, 224001 DOI:10.1088/0957-4484/27/22/224001;
56. SONG, W. et al. High efficiency fluorescent white organic light-emitting diodes having a yellow fluorescent emitter sensitized by a blue thermally activated delayed fluorescent emitter *Organic Electronics* **2015**, *vol. 23*, 138–143. DOI: 10.1016/j.orgel.2015.04.016.
57. YANG, H. et al. A Phosphanthrene Oxide Host with Close Sphere Packing for Ultralow-Voltage-Driven Efficient Blue Thermally Activated Delayed Fluorescence Diodes *Adv. Mater.* **2017**, 1700553 DOI: 10.1002/adma.201700553;
58. ZHANG, Q. et al. Design of Efficient Thermally Activated Delayed Fluorescence Materials for Pure Blue Organic Light Emitting Diodes *J. Am. Chem. Soc*. **2012**, *vol. 134*, 14706–14709; DOI: 10.1021/ja306538w.
59. LI, J. et al. Deep-blue thermally activated delayed fluorescence dendrimers with reduced singlet-triplet energy gap for low roll-off non-doped solution-processed organic light-emitting diodes *Dyes and Pigments* **2017**, *vol. 140*, 79–86. DOI: 10.1016/j.dyepig.2017.01.036.
60. SONG, W. Host Engineering for High Quantum Effi ciency Blue and White Fluorescent Organic Light-Emitting Diodes. *Adv. Mater.* **2015**, *vol. 27*, 4358–4363. DOI: 10.1002/adma.201501019.
61. ZHANG, Q. et al. Nearly 100% Internal Quantum Efficiency in Undoped Electroluminescent Devices Employing Pure Organic Emitters *Adv. Mater.* **2015**, *vol. 27*, 2096–2100. DOI: 10.1002/adma.201405474.
62. GONG, Sh. et al. Tuning emissive characteristics and singlet-triplet energy splitting of fluorescent emitters by encapsulation group modification: Yellow TADF emitter for solution-processed OLEDs with high luminance and ultraslow efficiency roll-off *Dyes and Pigments* **2017**, *vol. 139*, 593–600. DOI: 10.1016/j.dyepig.2016.12.058.
63. LIU, M et al. Blue thermally activated delayed fluorescence materials based on bis(phenylsulfonyl)benzene derivatives *Chem. Commun*. **2015**, *vol. 51*,16353–16356;
64. LIU, M. et al. Introduction of Twisted Backbone: A New Strategy to Achieve Efficient Blue Fluorescence Emitter with Delayed Emission. *Adv. Optical Mater.* **2017**, 1700334 DOI: 10.1002/adom.201700334

65. KIDO, J. et al. Aromatic-Amine-Containing Polymers for Organic Electroluminescent Devices *ACS Symp. Ser.* **1997**, *vol. 672*, 381–393. DOI: 10.1021/bk-1997-0672.ch025.
66. ALBRECHT, K. et al. Patterning Carbazole−Phenylazomethine Dendrimer Films. *Macromolecules* **2012**, *vol. 45*, 1288-1295. DOI: 10.1021/ma202485h.
67. LI, J. et al. Solution-Processible Carbazole Dendrimers as Host Materials for Highly Effi cient Phosphorescent Organic Light-Emitting Diodes. *Adv. Funct. Mater*. **2013**, *vol. 23*, 619–628. DOI: 10.1002/adfm.201201326.
68. ZHU, M. et al. Triphenylamine Dendronized Iridium(III) Complexes: Robust Synthesis, Highly Efficient Nondoped Orange Electrophosphorescence and the Structure−Property Relationship. *Chem. Mater*. **2012**, *vol. 24*, 174–180. DOI: 10.1021/cm202732j.
69. XIE, Y. et al. Thermally Activated Delayed Fluorescent Polymers. *Polym. Sci. A Polym. Chem.* **2017,** *vol. 55*, 575–584. DOI: 10.1002/pola.28448.
70. ALBRECHT, K. et al. Carbazole Dendrimers as Solution-Processable Thermally Activated Delayed-Fluorescence Materials. *Angew. Chem.* **2015**, *vol. 127*, 5769–5774. DOI: 10.1002/ange.201500203.
71. SUN, K. et al. Design strategy of yellow thermally activated delayed fluorescent dendrimers and their highly efficient non-doped solution-processed OLEDs with low driving voltage. *Organic Electronics* **2017**, *vol. 42*, 123–130. DOI: 10.1016/j.orgel.2016.12.026.
72. LI, Y.et al. Dendronized delayed fluorescence emitters for non-doped, solution-processed organic lightemitting diodes with high efficiency and low efficiency roll-off simultaneously: two parallel emissive channels. *Chem. Sci.* **2016**, *vol. 7*, 5441–5447. DOI: 10.1039/C6SC00943C.
73. LUO, J. et al. Multi-carbazole encapsulation as a simple strategy for the construction of solutionprocessed, non-doped thermally activated delayed fluorescence emitters. *J. Mater. Chem. C*, **2016**, *vol. 4*, 2442–2446. DOI: 10.1039/C6TC00418K
74. REN, Zh. et al. Pendant Homopolymer and Copolymers as Solution-Processable Thermally Activated Delayed Fluorescence Materials for Organic Light-Emitting Diodes. *Macromolecules* **2016**, *vol. 49*, 5452–5460. DOI: 10.1021/acs.macromol.6b01216.
75. NOBUYASU, R. S. et al. Rational Design of TADF Polymers Using a Donor–Acceptor Monomer with Enhanced TADF Effi ciency Induced by the Energy Alignment of Charge Transfer and Local Triplet Excited States. *Adv. Opt. Mater*. **2016**, *vol. 4*, 597–607. DOI: 10.1002/adom.201500689.
76. ZHU, Y. et al. Synthesis and Electroluminescence of a Conjugated Polymer with Thermally Activated Delayed Fluorescence. *Macromolecules* **2016**, *vol. 49*, 4373–4377. DOI: 10.1021/acs.macromol.6b00430.
77. MANSFIELD, M. and O'SULLIVAN, C. Understanding Physics. Second Edition. *John Wiley and Sons, Ltd.* Atrium **2011**. ISBN 978-0-470-74638-7;
78. Comision internationale de l'eclairage. International commision on illiumination. Internationale beleuchtungskommission. Technical report colorimetry second edition. CIE 15.2. **1986**, 1-74.
79. Origin 8.1. OriginLab Corp. One Roundhouse Plaza, Northampton, MA 01060 USA, **2010**.
80. ZILINSKAITE, V. et al. Derivatives of indandione and differently substituted triphenylamine with charge-transporting and NLO properties. *Dyes and Pigments* **2015**, *vol. 113*, 38–46. DOI: 10.1016/j.dyepig.2014.07.028
81. Mercury 3.8. The Cambridge Crystallographic Data Centre **2016**.

82. VAEZI-NEJAD, S. M. Xerographic time of flight experiment for the determination of drift mobility in high resitivity semiconductors. *International Journal of Electronics*, **1987**, *vol. 62*, 361–384. DOI: 10.1080/00207218708920988.
83. MIMAITE, V. et al. Can Hydrogen Bonds Improve the Hole-Mobility in Amorphous Organic Semiconductors? Experimental and Theoretical Insights. *J. Mater. Chem. C.* **2015**, *vol. 3*, 11660−11674. DOI: 10.1039/C5TC02534F
84. JUSKA, G., et al. Extraction of photogenerated charge carriers by linearly increasing voltage in the case of Langevin recombination. *Physical Review B* **2011**, *vol. 84*, 155202–155206. DOI: 10.1103/PhysRevB.84.155202
85. JUSKA, G., et al. Extraction Current Transients: New Method of Study of Charge Transport in Microcrystalline Silicon. *Physical Review Letters* **2000**, *vol. 84*, 4946–4949. DOI: 10.1103/PhysRevLett.84.4946
86. JUSKA, G. et al. New method of drift mobility evaluation in lc-Si:H, basic idea and comparison with time-of-light *J. Non.Cryst. Solids* **2000**, *vol. 266-269*, 331–335. DOI: 10.1016/S0022-3093(99)00720-6
87. MIYAMOTO, Y. et al. Ionization Potential or Organic Pigment Film by Atmospheric Photoelectron Emission Analisis. *Electrophotography.* **1989**, *vol. 28*, 364-370. ISSN 1880–5108;
88. KUKHTA, A. N. et al. Structure-Property Relationships of Star-Shaped Blue-Emitting Charge-Transporting 1,3,5-triphenylbenzene Derivatives. *Dyes and Pigments*. **2015**, *vol. 117*, 122–123. ISSN 0143-7208;
89. TUCKER S. H. Iodination in the Carbazole Series *J. Chem. Soc.* **1926**, *vol. 129*, 546–553; DOI: 10.1039/JR9262900546.
90. WANG, Q. et al. A mitochondria-targeted colorimetric and two-photon fluorescent probe for biological SO_2 derivatives in living cells. *Dyes and Pigments* **2016**, *vol. 134*, 297–305. DOI: 10.1016/j.dyepig.2016.07.030.
91. YANG, Y. et al. Hydrogen-Bonded Cyclic Tetramers Based on Ureidopyrimidinones Attached to a 3,6-Carbazolyl Spacer. *Organic Letters* **2011**, *vol. 13*, 3186 – 3189. DOI: 10.1021/ol200946b.
92. GUERRA, W. D., Transition-Metal-Free" Synthesis of Carbazoles by Photostimulated Reactions of 2′-Halo[1,1′-Biphenyl]-2-Amines. *J. Org. Chem.* **2015**, *vol. 80*, 928–941. DOI: 10.1021/jo5024393.
93. DIERSCHKE, F et al. Efficient synthesis of 2,7- dibromocarbazoles as components for electroactive materials. *Synthesis* **2003**, *vol. 16*, 2470–2472. DOI: 10.1055/s-2003-42418.
94. PATRIC, D. A. et al. Anti-Pneumocystis carinii pneumonia activity of dicationic carbazoles *Eur. J. Med. Chem.* **1997**, *vol. 32*, 78 l–793. DOI: 10.1016/S0223-5234(99)80064-6.
95. BUCINSKAS, A. et al. Structure-property relationship of isomeric diphenylethenyl-disubstituted dimethoxycarbazoles. *RSC Advances* **2015**, *vol. 5*, 49577–49589. DOI: 10.1039/C5RA09161F.
96. REMBIAK, A. et al. Versatile Synthesis of Symmetrical Carbazole-Based Ligand Precursors via Regioselective Aromatic Bromination. *Synthesis* **2015**, *vol. 47*, 3347–3353. DOI: 10.1055/s-0034-1378825.
97. CHO, J.-H. et al. Diversification of Carbazoles by LiCl-mediated Catalytic CuI Reaction. *Bull. Korean Chem. Soc.* **2011**, *vol. 32*, 2461–2464. DOI 10.5012/bkcs.2011.32.7.2461;

98. LUX, M. et al. Polymers with pendant carbazolyl groups, 2 Synthesis and characterization of some novel liquid crystalline polysiloxanes. *Macromol. Chem.* **1987**, *vol. 188*, 811 – 820. DOI: 10.1002/macp.1987.021880415.
99. MISRA, R. et al. Carbazole-BODIPY conjugates: design, synthesis, structure and properties. *Dalton Trans.* **2014**, *vol. 43*, 13076–13086; DOI: 10.1039/C4DT00983E.
100. LIU, X.-Y. et al. An effective host material with thermally activated delayed fluorescence formed by confined conjugation for red phosphorescent organic light-emitting diodes. *Chem. Commun.* **2016**, vol. 52, 8149–8151. DOI: 10.1039/C6CC02856J.
101. LU, Z. et al. Preparations and photophysical properties of thermally activated delayed fluorescence materials based on N-phenyl-phenothiazine-S,Sdioxide. *Tetrahedron* **2017**, vol. *73*, 21–29. DOI: 10.1016/j.tet.2016.11.037.
102. TSUCHIYA, K. et al. Synthesis of charge transporting block copolymers containing 2,7-dimethoxycarbazole units for light emitting device. *Polymer* **2010**, vol. *51*, 616–622. DOI: 10.1016/j.polymer.2009.12.024.
103. KUETHE, J. T. et al. Suzuki–Miyaura Cross-Coupling of 2-Nitroarenediazonium Tetrafluoroborates: Synthesis of Unsymmetrical 2-Nitrobiphenyls and Highly Functionalized Carbazoles. *Adv. Synth. Catal.* **2008**, *vol. 350*, 1577 – 1586. DOI: 10.1002/adsc.200800162
104. CHO, Y.-J. et al. Cool and warm hybrid white organic light-emitting diode with blue delayed fluorescent emitter both as blue emitter and triplet host *Sci. Rep.* 5:7859. DOI: 10.1038/srep07859.
105. CHIOUA, M. et al. Studies on the Acetylation of 3,6-Diamino-1Hpyrazolo[3,4-b]pyridine-5-carbonitrile Derivatives *J. Heterocyclic Chem.* **2010**, vol. 47, 861–872. DOI: 10.1002/jhet.403.
106. CHIOUA, M. et al. Synthesis and biological evaluation of 3,6-diamino-1Hpyrazolo[3,4-b]pyridine derivatives as protein kinase inhibitors *Bioorg. Med. Chem. Lett.* **2009**, vol. 19, 4566–4569. DOI: 10.1016/j.bmcl.2009.06.099.
107. SURRY, D.S. et al. Selective Palladium-Catalyzed Arylation of Ammonia: Synthesis of Anilines as Well as Symmetrical and Unsymmetrical Di- and Triarylamines. *J. Am. Chem. Soc.* **2007**, *vol. 129*, 10354–10355. DOI: 10.1021/ja074681
108. JIANG, H. et al. A Review on Synthesis of Carbazole-based Chromophores as Organic Light-emitting Materials. *Current Organic Chemistry* **2012**, *vol. 16*, 2014–2025. DOI : 10.2174/138527212803251604
109. TOMKEVICIENE, A. et al. Impact of Linking Topology on the Properties of Carbazole Trimers and Dimers. *J. Phys. Chem. C*, **2011**, *vol. 115*, 4887–4897. DOI: 10.1021/jp111333v
110. SUN, J. et al. Synthesis and characterization of heteroatom substituted carbazole derivatives: potential host materials for phosphorescent organic light-emitting diodes. NewJ.Chem., **2013**, vol. 37, 977–985. DOI: 10.1039/c2nj40900c
111. TSAI, M.-H. et al. 3-(9-Carbazolyl)carbazoles and 3,6-Di(9-carbazolyl)carbazoles as Effective Host Materials for Efficient Blue Organic Electrophosphorescence. *Adv. Mater.* **2007**, *vol. 19*, 862–866. DOI: 10.1002/adma.200600822
112. AMBROSE, J. F. et al. Anodic Oxidation Pathways of Carbazoles: I. Carbazole and N-Substituted Derivatives. *J. Electrochem. Soc.* **1968**, *vol. 115*, 1159-1164. ISSN: 0013-4651.
113. QU, J. et al. Synthesis and electro-optical properties of helical polyacetylenes carrying carbazole and triphenylamine moieties. *Polymer* **2007**, *vol. 48*, 4628–4636. DOI: 10.1016/j. polymer.2007.06.011.

114. SPARTAN'14 for Windows Version 1.1.4. 1840 Von Karman Avenue, Suite 370, Irvine, CA 92612: Wavefunction, Inc., **2013**.
115. VOLYNIUK, D. et al. Highly Efficient Blue Organic Light-Emitting Diodes Based on Intermolecular Triplet–Singlet Energy Transfer. *J. Phys. Chem. C* **2013**, *vol. 117*, 22538–22544. DOI: 10.1021/jp407397y
116. KALINOWSKY, J. Excimers and exciplexes in organic electroluminescence. *Matter. Sci. Pol.* **2009**, *vol. 27*, 735–756. ISSN: 01371339
117. NG, T.W. et al. Charge-transfer complexes and their role in exciplex emission and near-infrared photovoltaics. *Adv. Mater.* **2014**, *vol. 26*, 5569–5574. DOI: 10.1002/adma.201400563
118. ZANG, T et al. Efficient triplet application in exciplex delayed fluorescence oleds using a reverse intersystem crossing mechanism based on a DES-t of around zero. *ACS Appl Mater Interfaces* **2014**, *vol. 6*, 11907–11914. DOI: 10.1021/am501164s
119. CHERPAK, V. et al. Mixing of phosphorescent and exciplex emission in efficient organic electroluminescent devices. *ACS Appl Mater Interfaces* **2015**, *vol. 7*, 1219–1225. DOI: 10.1021/am507050g
120. DEKSNYS, T. et al. Synthesis and characterisation of a carbazole-based bipolar exciplex-forming compound for efficient and color-tunable OLEDs *New J. Chem.* **2017**, *vol. 41*, 559–568. DOI: 10.1039/C6NJ02865A.
121. JANKUS, V. et al. Deep blue exciplex organic lightemitting diodes with enhanced efficiency, P-type or e-type triplet conversion to singlet excitons? *Adv Mater* **2013**, *vol. 25*, 1455–1459. DOI: 10.1002/adma.201203615
122. JOU, J-H. et al. Approaches for fabricating high efficiency organic light emitting diodes. *J Mater. Chem C* **2015**, *vol. 3*, 2974–3002. DOI: 10.1039/C4TC02495H
123. HUANG, J. et al. The development of anthracene derivatives for organic light-emitting diodes. *J Mater Chem* **2012**, *vol. 22*, 10977–10989. DOI: 10.1039/C2JM16855C
124. GUO, Z. et al. Dicyanomethylene-4H-pyran chromophores for OLEDemitters, logic gates and optical chemosensors. *Chem Commun* **2012**, *vol. 48*, 6073-6084. DOI: 10.1039/C2CC31581E
125. VAGHASIYA, J. V. et al. Role of a phenothiazine/phenoxazine donor in solid ionic conductors for efficient solid state dye sensitized solar cells. *J. Mater. Chem. A* **2017**, *vol. 5*, 5373–5382. DOI: 10.1039/C6TA09777D
126. ZILINSKAITE, V. Synthesis and Properties of 1,3-Indandione-Disubstituted Derivatives of Carbazole, Phenothiazine, and Phenoxazine. *Molecular Crystals and Liquid Crystals* **2014**, *vol. 590*, 80–89. DOI: 10.1080/15421406.2013.873851
127. ZALECKAS, E. et al. Electroactive polymers containing pendant harmane, phenoxazine or carbazole rings as host materials for OLEDs. *Dyes and Pigments* **2014**, *vol. 108*, 121–125. DOI: 10.1016/j.dyepig.2014.04.034
128. SALLENAVE, X. et al. Sensitivity of Redox and Optical Properties of Electroactive Carbazole Derivatives to the Molecular Architecture and Methoxy Substitutions. *J. Phys. Chem. C* **2018**, *vol. 122*, 10138–10152. DOI: 10.1021/acs.jpcc.8b02148
129 SAKALYTE, A. et al. Effect of Methoxy Substituents on the Properties of the Derivatives of Carbazole and Diphenylamine *J. Phys. Chem. C* **2011**, *vol. 115*, 4856–4862. DOI: 10.1021/jp109643r
130. KERUCKAS, J. et al. Influence of methoxy groups on the properties of 1,1-bis(4-aminophenyl) cyclohexane based arylamines: experimental and theoretical approach. *J.Mater.Chem.* **2012**, *vol. 22*, 3015–3027. DOI: 10.1039/c2jm14387a
131. FRISCH, M. J. et al. **Gaussian 09**, Revision B.01, Gaussian Inc., *Wallingford CT*, **2009**.

132. LI, W. et al. Efficient solution-processed blue and white OLEDs based on a high-triplet bipolar host and a blue TADF emitter. *Org. Electron.* **2018**, *vol. 58*, 276–282. DOI: 10.1016/j.orgel.2018.04.027
133. REICHARDT, Ch. Solvents and Solvent Effects in Organic Chemistry, Third Edition. *WILEY-VCH*, Weinheim **2003** ISBN: 3-527-30618-8;
134. KUKHTA, N. A. et al. Can Fluorenone-Based Compounds Emit in the Blue Region? Impact of the Conjugation Length and the Ground-State Aggregation. *Chem. Mater*. **2017**, *vol. 29*, 1695–1707. DOI: 10.1021/acs.chemmater.6b05158
135. DIAS, F. B. et al. Triplet Harvesting with 100% Efficiency by Way of Thermally Activated Delayed Fluorescence in Charge Transfer OLED Emitters. *Adv. Mater.* **2013**, *vol. 25*, 3707–3714. DOI: 10.1002/adma.201300753
136 KUKHTA, N. A. et al. Blue *versus* yellow emission in bipolar fluorenone derivatives: the impact of aggregation and hydrogen bonding. J. Mater. Chem. C, **2018**, *vol. 6*, 1679–1692. DOI: 10.1039/C7TC05798A
137. DOS SANTOS, P. L. et al. Using Guest–Host Interactions To Optimize the Efficiency of TADF OLEDs *J. Phys. Chem. Lett.* **2016**, *vol. 7*, 3341–3346. DOI: 10.1021/acs.jpclett.6b01542
138. STAKHIRA, P. et al. Blue organic light-emitting diodes based on pyrazoline phenyl derivative. *Synth. Met.* **2012**, *vol. 162*, 352– 355. DOI: 10.1016/j.synthmet.2011.12.017
139. VOLYNIUK, D. et al. Highly Efficient Blue Organic Light-Emitting Diodes Based on Intermolecular Triplet−Singlet Energy Transfer. *J. Phys. Chem.* C **2013**, *vol. 117*, 22538−22544. DOI: 10.1021/jp407397y
140. CHERPAKA, V. V. et al. 3,6-Di(9-carbazolyl)-9-(2-ethylhexyl)carbazole based single-layer blue organic light emitting diodes. *Synth. Met.* **2011**, *vol. 161*, 1343–1346. DOI: 10.1016/j.synthmet.2011.04.035
141. CAO, X et al. Simple phenyl bridge between cyano and pyridine units to weaken the electron-withdrawing property for blue-shifted emission in efficient blue TADF OLEDs. *Org. Electron.* **2018**, *vol. 57*, 247–254. DOI: 0.1016/j.orgel.2018.03.027
142. BUI, Th. T. et al. Recent advances on organic blue thermally activated delayed fluorescence (TADF) emitters for organic light-emitting diodes (OLEDs). *Beilstein J. Org. Chem.* **2018**, *vol. 14*, 282–308. DOI: 10.3762/bjoc.14.18
143. TANG, Ch. Et al. A versatile efficient one-step approach for carbazole–pyridine hybrid molecules: highly efficient host materials for blue phosphorescent OLEDs. *Chem.Commun*. **2015**, *vol. 51*, 1650−1653. DOI: 10.1039/c4cc08335k
144. GRYBAUSKAITE-KAMINSKIENE, G. et al. Aggregation-EnhancedEmission and Thermally Activated Delayed Fluorescence of Derivativesof9-Phenyl-9H-Carbazole:Effects of Methoxyand tert-Butyl Substituents. *Chem. Eur. J.* **2018**, *vol. 24*, 9581 –9591. DOI: 10.1002/chem.201800822
145. CHALKE, Rh. M. et al. New approaches towards the synthesis and characterization of alkoxy substituted spirobifluorenes and spirosilabifluorenes for organic optoelectronics. *J. Polym. Sci. A* **2017**, *vol. 54*, 556−564. DOI: 10.1080/10601325.2017.1309249.
146. KAMIMURA, A. et al. Preparation of Hydrophobic 2-Phenylthiohydroquinone Dimers and Evaluation of Their Photophysical Properties. *Heteroatom Chemistry* **2014**, *vol. 25*, 402−409. DOI: 10.1002/hc.21169.
147. LIU, W. et al. Novel Carbazol-Pyridine-Carbonitrile Derivative as Excellent Blue Thermally Activated Delayed Fluorescence Emitter for Highly Efficient Organic Light-Emitting Devices *ACS Appl. Mat. Interfaces* **2015**, *vol. 7*, 18930−18936. DOI: 10.1021/acsami.5b05648.

7. LIST OF PUBLICATIONS ON THE SUBJECT OF THE THESIS

1. Skuodis, E.; Tomkeviciene, A.; Reghu, R. R.; Peciulyte, L.; Ivaniuk, K.; Volyniuk, D.; Bezvikonnyi, O.; Bagdziunas, G.; Gudeika, D.; Grazulevicius J. V. OLEDs based on the emission of interface and bulk exciplexes formed by cyano-substituted carbazole derivative. *Dyes and Pigments* **2017**, *vol. 139*, 795–807;
2. Skuodis, E.; Bezvikonny, O.; Tomkeviciene, A.; Volyniuk, D.; Mimaite, V.; Lazauskas, A.; Bucinskas, A.; Keruckiene, R.; Sini, G.; Grazulevicius, J. V. Aggregation, thermal annealing, and hosting effects on performances of an acridan-based TADF emitter. *Organic Electronics* **2018**, *vol. 63*, 29–40;

8. LIST OF THE PRESENTATIONS AT THE INTERNATIONAL CONFERENCES

1. Skuodis. E.; Tomkevičienė, A.; Gražulevičius, J. V. Synthesis and properties of cyano substituted carbazole derivatives. 17-Th international conference-school Advanced materials and technologies, Palanga, Lithuania. 27-31 August, 2015.

2. Skuodis. E.; Tomkevičienė, A.; Gražulevičius, J. V. Glass-forming cyano substituted carbazole derivatives for optoelectronics. Baltic polymer symposium 2015. Sigulda, Latvia, 16-18 September, 2015.

3. Skuodis. E.; Gražulevičius, J. V.Phenothiazine based derivatives for optoelectronic devices. 10Th international conference on electronic processes in organic and inorganic materials (ICEPOM-10), Ternopol, Ukraine, 23- 27 May, 2016.

4. Skuodis. E.; Tomkevičienė, A.; Volyniuk, D.; Gražulevičius, J. V. Synthesis and study of dicyanobenzene-based materials. Baltic polymer symposium 2016 : Klaipeda, Lithuania. 21-24 September, 2016.

5. Skuodis. E.; Bezvikonnyi, O.; Tomkevičienė, A.; Volyniuk, D.; Gražulevičius, J. V. Host-guest systems based on acridan derivative containing cyano groups for efficient TADF OLEDs. 14th European Conference on Molecular Electronics (ECME 2017), Dresden, Germany. 29 August - 2 September 2017.

9. ACKNOWELEDGEMENTS

Dr. A. Tomkevičienė is greatly acknowledged for the supervising, sharing experience, helpful advices and great patience.

Prof. Habil. Dr. J. V. Gražulevičius is acknowledged for the opportunity to work at the Department of Polymers Chemistry and Technology at Kaunas University of Technology, the financial facilities and helpful advices.

Dr. D. Volyniuk, A. Bezvykonyi and Dr. Kh. Ivaniuk are acknowledged for a part of photophysical measurements and making the investigations of organic light emitting diodes.

Dr. G. Ragaitė is acknowledged for the nuclear magnetic resonance spectra measurements.

Dr. J. Simokaitienė and Dr. L. Pečiulytė are acknowledged for the measurements of thermal analysis and the measurements of infrared spectroscopy.

Dr. D. Gudeika and Dr. A. Bučinskas are acknowledged for the mass spectra measurements, the quantum chemistry calculations and X-ray diffraction analysis.

All colleagues of the laboratory and research group are kindly thanked for helpful advices and good mood.

The author of this dissertation is grateful for the family support.

SL344. 2019-05-02, 12,25 leidyb. apsk. l. Tiražas 14 egz. Užsakymas 105.
Išleido Kauno technologijos universitetas, K. Donelaičio g. 73, 44249 Kaunas
Spausdino leidyklos „Technologija“ spaustuvė, Studentų g. 54, 51424 Kaunas